ORNL/SPR-2020/1851
Task Order 31310021N0002

Review of Advanced Manufacturing Techniques and Qualification Processes for Light Water Reactors – Electron Beam Welding

Kevin M. Faraone
Roger G. Miller
Zhili Feng

January 2022

OAK RIDGE National Laboratory

ORNL IS MANAGED BY UT-BATTELLE LLC FOR THE US DEPARTMENT OF ENERGY

ORNL/SPR-2020/1851
Task Order 31310021N0002

Materials Science and Technology Division

REVIEW OF ADVANCED MANUFACTURING TECHNIQUES AND QUALIFICATION PROCESSES FOR LIGHT WATER REACTORS– ELECTRON BEAM WELDING

Kevin M. Faraone
Roger G. Miller
Zhili Feng

January 2022

Prepared by
OAK RIDGE NATIONAL LABORATORY
Oak Ridge, TN 37831-6283
managed by
UT-BATTELLE LLC
for the
US DEPARTMENT OF ENERGY
under contract DE-AC05-00OR22725

TABLE OF CONTENTS

LIST OF FIGURES

LIST OF TABLES

ABBREVIATIONS

AC	alternating current
ADAMS	Agencywide Documents and Access Management System
AM	additive manufacturing
AM-IGA	air melt inert gas atomized powder
AMM	Advanced Methods for Manufacturing (DOE-NE program)
AMM	advanced manufacturing method
AMT	advanced manufacturing technologies
ASME	American Society of Mechanical Engineers
ASTM	ASTM International, formerly American Society for Testing and Materials
AWS	American Welding Society
BNL	Brookhaven National Laboratory
BOP	bead-on-plate
BPVC	Boiler & Pressure Vessel Code
CCT	continuous cooling transformation
CE	carbon equivalence
CGHAZ	coarse grain heat-affected zone
CRADA	Cooperative Research and Development Agreement
CT	computed tomography
CFR	US Code of Federal Regulations
CRP	copper-rich phase
DBTT	ductile-to-brittle transition temperature
DED	directed energy deposition
DHD	deep-hole drilling
DLC	diode laser cladding
DOE	US Department of Energy
DPI	dye penetrant inspection
EB	electron beam
EBM	electron beam melting
EBAM	electron beam additive manufacturing
EBFFF	electron beam free form fabrication
EBF^3	electron beam free form fabrication
EBO	electron beam optics
EBW	electron beam welding

EBW-HV	electron beam welding – high vacuum
EBW-MV	electron beam welding – medium vacuum
EBW-NV	electron beam welding – non-vacuum
ELO	electronic optics
EPRI	Electric Power Research Institute
EWI	Edison Welding Institute
FATT	fracture appearance transition temperature
FGHAZ	fine grain heat affected zone
FZ	fusion zone
GTAW	gas tungsten arc welding
HAZ	heat-affected zone
HED	high energy density
HI	heat input
IASCC	irradiation assisted stress corrosion cracking
ICCGHAZ	intercritically reheated coarse grain heat affected zone
ICHAZ	intercritical HAZ
iDHD	incremental deep hole drilling
IIW	International Institute of Welding
LAS	low alloy steel
LBZ	local brittle zone
LLNL	Lawrence Livermore National Laboratory
LPBF	laser powder bed fusion
MIC-EBW	modular in-chamber electron beam welding
NDE	nondestructive evaluation
NG-LBW	narrow gap laser beam welding
NG-SAW	narrow gap submerged arc welding
NG-GMAW	narrow gap gas metal arc welding
NG-GTAW	narrow gap gas tungsten arc welding
NG-LW	narrow gap laser welding
NG-TIG	narrow gap TIG
NPP	nuclear power plant
NRC	US Nuclear Regulatory Commission
Nuclear AMRC	Nuclear Advanced Manufacturing Research Center
OEM	original equipment manufacturer
ORNL	Oak Ridge National Laboratory

PAGS	prior austenite grain size
PAUT	phased array ultrasonic testing
PM-HIP	power metallurgy hot isostatic pressing
PMZ	partially melted zone
PTR	Precision Technologies Inc.
PWHT	post-weld heat treatment
PWR	pressurized water reactor
RF	radiofrequency
RPV	reactor pressure vessel
RPEB	reduced pressure electron beam
RP-EBW	reduced pressure electron beam welding
RT	radiographic examination/testing
SA	submerged arc
SAW	submerged arc welding
SCC	stress corrosion cracking
SCCGHAZ	subcritical reheated coarse grain heat affected zone
SEM	scanning electron microscopy
SF	Sheffield Forgemasters
SMA	shielded metal arc
SMAW	shielded metal arc welding
SMF	stable matrix features
SMR	small modular reactor
SSPT	solid state phase transformation
TIG	tungsten inert gas
TOFD	time-of-flight diffraction
TWI	The Welding Institute
UMD	unstable matrix defect
UT	ultrasonic examination/testing
UTS	ultimate tensile strength
VIM-IGA	vacuum induction melted inert gas atomized
YS	yield strength

EXECUTIVE SUMMARY

Advanced manufacturing technologies (AMTs), including electron beam welding (EBW), are being explored by academic, industrial, and regulatory entities for technical feasibility, cost effectiveness, and safety of fabricating components for nuclear power plant (NPP) applications. EBW is considered one of the cleanest welding processes, with fewer defects than conventional arc welding. Because of its high equipment cost, vacuum chamber, and facility requirements, EBW has been limited to high-production or high-consequence applications. To date, EBW has seen the highest usage in the automotive and aerospace industries.

EBW would typically be considered machine welding according to the American Association of Mechanical Engineers (ASME) Boiler & Pressure Vessel Code (BPVC); however, it can also be instrumented to be fully automatic. The application of EBW is typically autogenous, without filler metal additions. This requires that precise machining and joint fit-ups be designed into the welded joint. Larger gaps and large edge breaks (i.e., chamfer) contribute to higher residual stresses in the joint and have been known to cause cracks. The use of wire feeding systems can mitigate issues caused by large gaps and weld concavity at the top of the joint. The welding controller can allow operator adjustments for joint tracking and filler metal positioning during welding. The majority of published electron beam (EB) research in the nuclear power industry is primarily focused on large pressure vessel girth welds fabricated using reactor pressure vessel (RPV) steels. Development of welding systems to accommodate the welding of small modular reactor (SMR) pressure vessels is currently underway. Both local vacuum-reduced pressure and in-chamber EBW are being investigated. A reduced-pressure electron beam (RPEB) system was developed by The Welding Institute for large component fabrication, thus eliminating the need for a large vacuum chamber. This process is currently being investigated for use by Nuclear Advanced Manufacturing Research Centre (AMRC) to support the inclusion of EBW in the R6 (UK) and API 579-1/ASME FFS-1 [1] fitness-for-service procedures. Welds on SA508 Grade 3 and 4N steels were evaluated for weld metal microstructure, hardness, and residual stress. Residual stress levels of the EB welds were compared to those of arc welds and were found to be comparable in magnitude but varying in location and distribution within the weld. Arc welds contain the highest peaks of residual stress in the fusion zone at the weld reinforcement and root of the weld, whereas EB welds had peaks at mid-thickness outside the weld area in the base metal on both sides of the weld.

A separate effort to develop thick section EB welds is being sponsored by the US Department of Energy (DOE). Contracts have been placed with Electric Power Research Institute (EPRI), Nuclear AMRC, and NuScale Power to demonstrate and establish the EBW as a viable technology for use in thick-section girth welding of SMRs and advanced reactor (GEN IV) vessels. EPRI has published three yearly reports documenting the results of the EBW weld development. This work is being performed alongside other advanced processes such as power metallurgy hot isostatic pressing (PM-HIP) material, which is a potential material for the lower and/or upper head assembly. Five simulated girth welds have been produced using EBW with no significant defects or indications within the bulk of the weld [2]. Use of EBW is currently allowed per the ASME BPVC without any restrictions on base material types; therefore, no gaps were found in the use of EBW for NPP application. Further work on the welding of PM-HIP materials is ongoing, as well as the evaluation of a full solution heat treatment to homogenize the weld and base metal microstructures. Because no filler material is added to the weld, a full solution heat treatment is being sought to return the weld fusion zone to near base metal properties. This heat treatment goes beyond the ASME BPVC required PWHT for low alloy steels, therefore, it is seen as an improvement that may require regulatory input but is not seen as an impediment or gap to the use of EBW. One goal of this heat treatment is to remove the requirement for in-service inspection of these girth welds. Further development of this concept is needed, and regulatory approval will be required to forgo current in-service inspection requirements for RPV welds.

Development of EBW has progressed rapidly in the last 20 years, due in part to advances supporting additive manufacturing (AM). Improvements have been particularly notable in the area of machine vision, electronic controller capabilities, beam optics, filler metal manipulation, movable vacuum seals, and reduced-pressure EBW. Machine vision systems utilizing cameras, electron diffraction, and/or weld parameter data are used to analyze and make real-time adjustments to the weld path or the welding parameters to successfully achieve the desired weld characteristics. These advancements allow for increased opportunities to use EBW for NPP applications.

EBW with PWHT is a permitted welding process per the ASME BPVC. As in other welding processes, a PWHT is required and specified for most materials, including RPV steels. Regulator changes are required to take full advantage of EB-welded PM-HIP materials that receive full solution heat treatment after welding. The residual gas content of PM-HIP materials must be controlled to increase the base metal's fracture toughness. There are no fracture toughness tests on EBW using PM-HIP SA508 reported to date. Gaps identified include (1) vendor and equipment availability, (2) weld repair techniques, and (3) the mechanical properties of EB-welded PM-HIP materials. In addition, thermal aging (stability) and irradiation degradation of EBW PM-HIP material weldments have not been studied. A literature review—including an evaluation of current ASME BPVC requirements and code cases—is included in this document to allow for evaluation of EBW as one of the AMTs being considered for NPP use.

The NRC has developed a companion document to this report (Agencywide Documents and Access Management System Accession No. ML22143A929) that provides context to the gaps identified in this report from a regulatory perspective and highlights key technical information related to EBW-fabricated components in NPPs.

1. INTRODUCTION

Nuclear energy supplies approximately 18% of the US electrical power supply and the majority of carbon-free electricity [3] and is a critical component of reliable domestically sourced power. However, only two reactors have been brought online in the past 25 years, with an additional two reactors under construction at the time of this document's publication [4]. To lower construction and maintenance costs, multiple advanced manufacturing methods (AMMs) are being evaluated by academic, industrial, and regulatory bodies for cost effectiveness, technical feasibility, and safety [5]. The US Nuclear Regulatory Commission (NRC) is the federal agency responsible for regulating nuclear power plant (NPP) operation and ensuring public safety. Therefore, the NRC has a vested interest in surveying current scientific literature on AMMs. The NRC internally uses the term *advanced manufacturing technology* (AMT) in lieu of AMM and is pursuing technical knowledge of multiple AMMs per the NRC's AMT Action Plan (Agencywide Documents and Access Management System [ADAMS] Accession No. ML19333B980). This report documents the current state of one specific AMM, electron beam welding (EBW), with respect to material microstructures and properties relative to conventional arc welding, technical gaps in ensuring repeatability and acceptability, and standards and regulatory gaps related to machine calibration, minimum requirements, and inspection practices. This report is motivated by the potential use of EBW of assemblies for new NPPs, particularly thick section welds that make up the reactor pressure vessel (RPV). The NRC has developed a companion document to this report (ADAMS Accession No. ML22143A929) that provides context to the gaps identified in this report from a regulatory perspective and highlights key technical information related to EBW-fabricated components in NPPs.

2. ELECTRON BEAM WELDING TECHNICAL REVIEW

The following subsections represent the current state of literature on EBW and was written with an emphasis on fabrication, quality control, nondestructive evaluation (NDE), metallurgical characteristics, and regulatory certification requirements for application to NPP service. Although many alloy systems are possible for welding with electron beams, because of the NPP focus, stainless steels and low-alloy steels for RPVs are the primary focus of this report. Two primary research and development efforts are being completed by the Electric Power Research Institute (EPRI) and the Nuclear Advanced Manufacturing Research Centre (AMRC), with some aspects of research being done in collaboration with other entities. Along with industry partners, EPRI is analyzing the use of EBW on thick-section girth welds, as well as upper and lower heads of small modular reactors (SMRs), using a modular, in-chamber, EB welder. Nuclear AMRC is leading the efforts to further develop a movable seal, reduced pressure, EB welder that would not require a substantial chamber [6-10].

2.1 PRINCIPLES OF OPERATION

EBW is a considered a high energy density (HED) welding process. A fusion weld is completed by the generation of a high-energy beam of electrons focused to a spot at the weld joint. The main component of the EB welder is the electron gun, which consists of the cathode (filament), anode, and the focusing coil (lens) (discussed further in Section 2.2.2) [11]. A vacuum is required for the beam generator to generate a stable electron beam. The beam exits the gun below the deflection coils into air, reduced pressure, or vacuum (see Section 2.3.1).

Three equipment options were considered to complete the EBW girth welds: a large chamber (40+ feet long), a local vacuum (reduced pressure, see Section 2.3.3), and modular in-chamber electron beam welding (MIC-EBW) (see Section 2.3.4) [12]. MIC-EBW is being pursued and has been reported in three yearly reports from EPRI [2, 7, 8]. A 150kV triode gun (see 2.2.2) manufactured by Precision

Technologies Inc. (PTR) will be used in the horizontal position and mounted to a dedicated EBW stage [12]. A rendered drawing of the system being manufactured is shown in Figure 1.

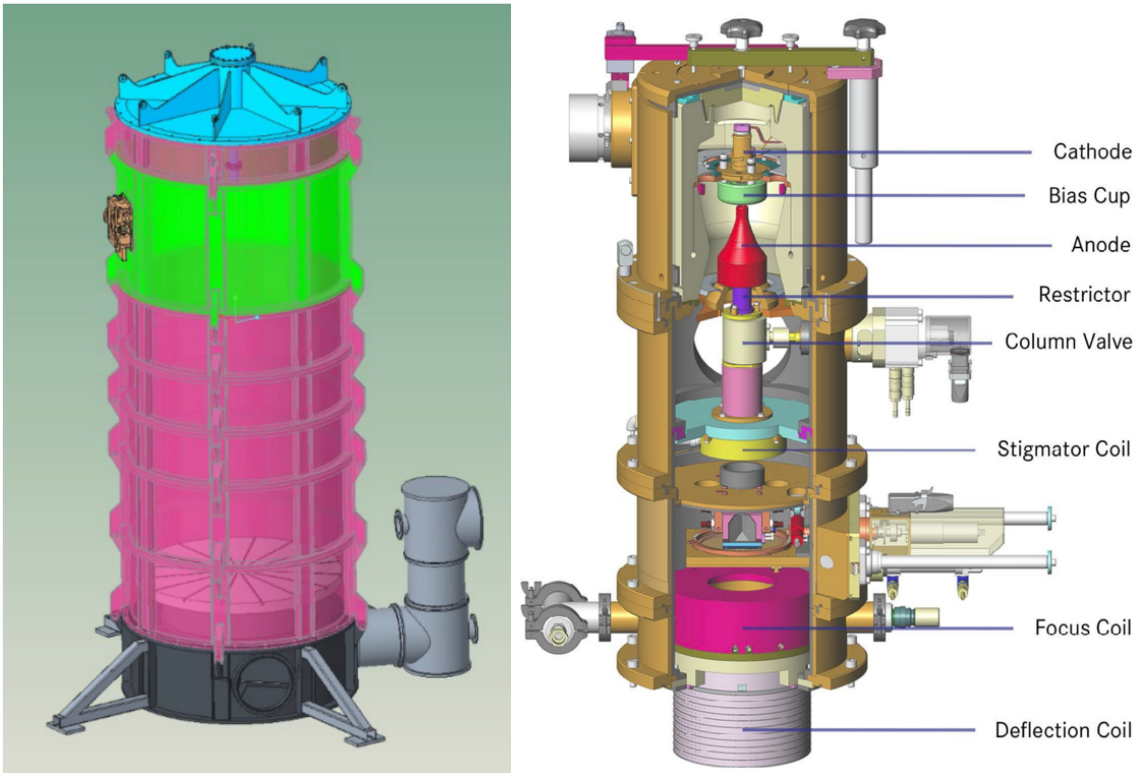

Figure 1. MIC-EBW system: components of the stages include EB gun stage (green), modular stacked rings (purple), rotation and pumping stage (gray), and lid (blue) (left) (From Gandy [12]); PTR electron beam optics (EBO) Gen Line Beam Generator, 150 kV version, to be used on MIC-EBW system (right) (From [13], courtesy of PTR-Precision Technologies).

2.2 TERMINOLOGY AND BACKGROUND

Several terms used in the EBW industry are specifically related to high-energy density welding, including *focal position*, *beam profile*, *energy density*, *beam diameter*, *keyhole*, *true focus*, and *above and below true focus*. *Focal position* is the distance between the top surface of the weld joint to a fixed position, a reference point on the electron gun to maintain a consistent position of the workpiece and beam optics. *Beam profile* refers to a digital interpretation of the EB constructed using diagnostic equipment placed in the machine and having the beam raster or sweep across the sensor. A 2D or 3D reconstruction of the *energy profile* can be created. When multiple sweeps are made across the sensor at various *focal positions*, a representative *beam profile* can be built to capture the energy density of the beam at different positions from a constant reference point (usually the internal top surface of the weld chamber). *Energy density* is the amount of energy per unit area at a position referenced at or away from the focal position of the electron beam. *Beam diameter* or *spot size* is the diameter of the beam at the focal position of the electron beam. *Keyhole* is a term used to describe the cavity created by the intense vaporization of metal at the weld pool to create the weld. When welding at sufficient energy levels, the vaporization of metal and the movement across the base material form a cavity that resembles a keyhole. *True focus* is the position of minimum beam diameter which is centered within a depth of focus, similar in theory to *optical focus*. Welding is often completed by finding the true focus position on the part through a visual brightest

spot methodology followed by a lens current offset to position the weld *above or below true focus*, if desired. Positioning the focal point above the part's surface diffuses the energy density of the beam and can soften the root of the weld to avoid root porosity as discussed in Section 2.4.16. Positioning the focal point below the part's surface also diffuses the energy density of the beam on the part's surface and aids in penetration efficiency, with the energy crossover occurring below the surface of the part.

2.2.1 History

Electron beams have a long history of use in scientific research and applied science, ranging from the study of subatomic particles to producing images on older cathode tube television sets. The EB process is based on the principles of thermionic emission of electrons in a vacuum. Upon generation of the free electrons, they can be easily collimated, focused, and energized by the use of electric and magnetic fields [3, 4]. The heating of materials caused by the impingement and conduction of electrons is the foundation of EBW. Two researchers—, Dr. Jacques André Stohr, and German physicist Dr. Karl-Heinz Steigerwald—can be credited with the advent of the EBW in the mid to late 1950s. Stohr's work on x-ray tubes and Steigerwald's work on electron microscopy led each of them to welding [5, 14].

The first customer to request an EBW machine was the Pittsburgh-based Westinghouse in 1958 [3, 14]. Two systems were eventually purchased after Steigerwald demonstrated the butt welding of two 5 mm Zircaloy plates [3]. These systems were purchased for the manufacture of fuel components for the Polaris submarine [14]. The new process was quickly adopted in the United States and spread across multiple industries because of its ability to produce high aspect ratio welds (i.e., depth to width ratio) and to join dissimilar materials, as well as difficult-to-weld materials [3, 14, 15]. EBW produces some of the highest precision and quality welds available. An estimated 3,000–3,750 EB welders are currently in operation [4, 15]. Welding speeds of 1,500 mm/min at 1 mm depth in steel and 50 mm/min at a depth of 280 mm in steel are possible [16]. Because of the high-energy densities achievable through focus of the electron beam, high-temperature materials such as tantalum and tungsten can be welded. EBW is considered a *high-energy density process*, a category shared with laser welding.

2.2.2 Electron Beam Sources

The most common type of EBW source is the triode-type EB gun [17]. Two other EB sources have been used for EBW: the diode type EB gun, and an experimental radiofrequency (RF)-excited plasma gun [17, 18]. The triode-type gun is the primary focus based on its widespread use in industry.

An EB is generally produced by the thermionic emission of electrons. This is typically achieved through the heating of a tantalum or tungsten filament enclosed in a vacuum. The internals of the beam generator—consisting of the filament (cathode), grid or bias cup, and anode—are shown in the schematic in Figure 2. A strong electrical potential is generated between the grid cup and the anode which enables the acceleration of a beam toward the workpiece. A high vacuum (HV) > 1×10^{-4} Torr is required at the electron gun to prevent breakdown of the air into a conductive medium at the high voltages used. Typical EB voltages of 60 to 200 kV are used.

The lower portions of an EB gun further manipulate the beam into a useful tool. A centering coil and a stigmator located just below the anode (not shown) refine the beam into a centered spherical beam of intensity. These two components are typically set and are not adjusted unless significant maintenance or adjustment of the gun components are made. Following the beam path further, the focusing lens and deflection coils are mounted near the bottom of the electron gun. The focusing lens is a magnetic coil that can be varied in intensity by changing the current applied to the coil to focus the electrons to a point. Electrons further away from the beam axis are closer to the focusing coil, so they are affected by a greater

force than the electrons traveling near the center of the beam axis. The resulting focal length can be tuned to obtain the beam spot size and intensity required at the material interface.

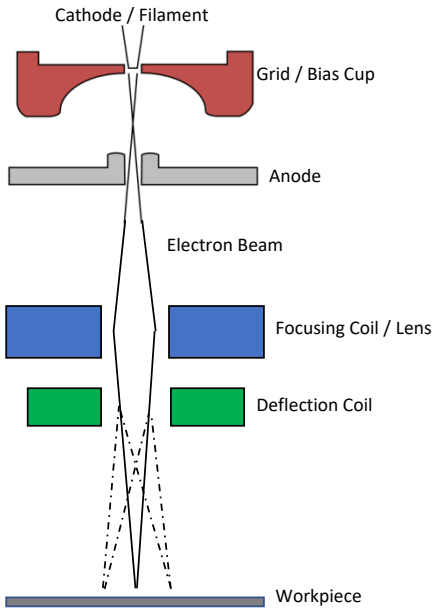

Figure 2. EB triode gun schematic.

The diode-type EB gun operates in a similar fashion, except the grid cup is held at the same voltage value as the cathode. This makes the EB gun a two-element diode EB emitter. Therefore, the diode gun controls the beam current through control of thermionic emission from the cathode itself. Several manufacturers have produced the diode-type EB guns in use today [17].

The RF-excited plasma electron gun is being developed by The Welding Institute (TWI) to address concerns of cathode life in high-use additive manufacturing EBW systems. Because the additive manufacturing process requires an always-on heat source, a non-depletable cathode was sought. This system is reported to have advantages such as no-wear, low maintenance, no beam variation, the ability to operate in a coarse vacuum, and rapid pulsing capability. This electron gun design is limited to 3.2 kW as of the most recent publication [19].

2.2.3 Safety

EBW poses more safety hazards than arc fusion processing. High voltage, vacuum, beam intensity (visible intensity), and radiation of x-rays must be considered. The American National Standards Institute (ANSI) and American Welding Society (AWS) provide safety guidance for the safety of the equipment and personnel. Important documents are listed in Table 1. X-rays are generated by the impingement of electrons on other matter through a process known as *Bremsstrahlung radiation*. This occurs when a high-energy electron interacts with the nucleus of an atom, resulting in the electron slowing down or stopping as a result of the electromotive forces. The intensity of the resulting x-ray is dependent upon the energy of the incoming electron and the mass of the nucleus it has impinged upon. High beam voltage, beam current, and the atomic number of the atom in the collision pair affect the intensity of the resulting x-ray. The x-rays produced by EBW systems can be soft or hard (i.e., low- or high-energy x-rays, respectively), so appropriate shielding must be in place to protect the operator. The electron energy level is highly dependent upon the voltage level used. Low kV systems generally do not require significant lead

shielding. Viewports must be made of leaded glass, and the chamber is required to maintain integrity at HV, which is sufficient to stop low-energy soft x-rays. High kV systems require additional lead shielding in the chamber walls and leaded glass for viewports. Radiation testing of the MIC-EBW system developed by PTR resulted in a measured value of 0.3mR/hr 3 in. from the chamber wall while at full power (150 kV, 400 mA, 60 kW) without any lead shielding; therefore, limited precautions are necessary [15].

Table 1. Recommended safety documents

ANSI Z49.1	Safety in Welding, Cutting, and Allied Processes [20]
ANSI N43.3	American national standard for general radiation safety : installation using non-medical x-ray and sealed gamma-ray sources, energies up to 10MeV [21]
AWS C7.1	Recommended Practices for Electron Beam Welding and Allied Processes
	Equipment manufacturer fact sheets

2.2.4 Advantages of EBW over Traditional Arc Welding

EBW has many benefits over traditional arc welding. Because of the nature of the electrical circuitry and mechanized control of the process, a reliable, repeatable process can be achieved. The basic advantages of EBW are captured in Table 2. Cottrell reported a heat input that was 5–10 times lower than that of arc welding, with a corresponding transverse shrinkage of less than 10% than that seen during manual or submerged arc welding [15, 22-26].

Table 2. Advantages of EBW over traditional arc welding

General process advantages	Potential NPP advantages (additional)
Single-pass deep penetrating welds [15]	Step change in productivity [27]
Low energy / heat input (< 5 J/mm – 20 kJ / mm) [11, 15, 26, 27]	Fewer defects [22]
High aspect ratio welds [5, 15, 26]	Low hydrogen contents [22]
Ability to weld high conductivity / difficult materials [15, 26]	No slag defects (no flux) [22]
Ability to weld dissimilar materials [15]	No inter-run imperfections [22]
No beam reflectivity problems [15]	Single start / stop [22]
Elimination of oxygen and hydrogen pickup from atmosphere [15]	Matching weld and base metal composition (no filler metal or flux) [22]
Reduced distortion [11, 22, 26]	
High energy transfer efficiency (80–90%) [11, 26, 27]	
Non-contact / improved joint access [11]	
Reduced / no consumable costs [11]	
Narrow (smaller) heat affected zone [11, 26]	
High welding speeds can be attained [26]	
Variable working distance to allow for easier access to joint [5]	
Reduced joint complexity [5, 22]	
Ability to weld thickness less than 0.5 mm and up to 300 mm in steel and 590 mm aluminum [23]	

Data acquisition / monitoring / control of welding parameters possible [5]	
Welding parameters are highly reproducible and consistent, improving the quality of welds [5, 22]	

When compared to arc welding, EBW bests the energy density by two orders of magnitude (10^4 W * mm^2 vs. 10^2 W * mm^2). This is feasible because of arc welding's reliance upon the heating and melting of material with the intent of coalescence through surface tension effects. The strengths of EBW result from the EB's fundamental different high-energy density. By focusing the EB, a tight spot can be placed on the weld joint, thus creating a condition called *keyhole welding*. In this mode, a vapor cavity is created in which metal is vaporized on the leading edge of the weld and deposited on the back surface. The weld is stabilized by a combination of surface tension, hydrostatic, and vapor pressure forces [28]. A keyhole mode weld is shown in Figure 3, illustrating the elliptical shape of a weld made as the EB is traversed across a joint. This is achievable by the high-energy density of the focused spot reaching estimates greater than 10^6 W × cm^{-2} [3, 29]. EBW is very sensitive to the overall heat input and energy density of the beam, so as intensity increases, the depth of penetration can also dramatically increase [30].

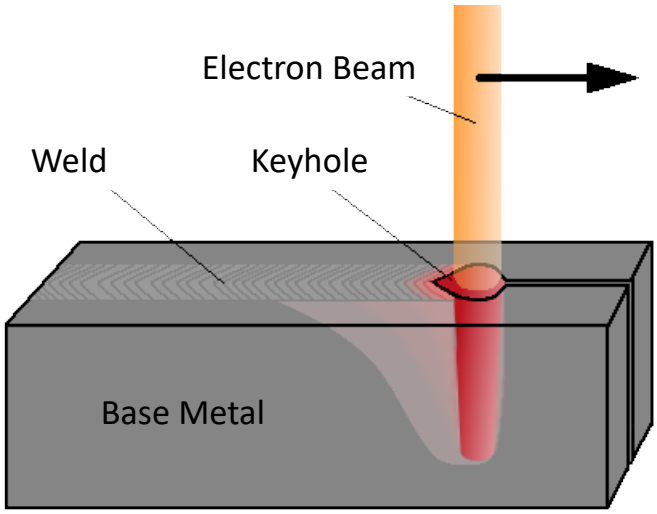

Figure 3. Formation of a keyhole during welding

To understand the differences between arc welding and EBW, some examples and demonstration pieces have been made by manufacturers of EB welders. ProBeam has demonstrated a bronze-to-steel EB weld that is not possible by any arc welding processes, as shown in Figure 4 [31].

Figure 4. Dissimilar joining of bronze to steel, 30 mm thickness (From Clauß [31], Courtesy of Pro-Beam)

2.2.5 Limitations and Disadvantages of EBW over Traditional Arc Welding

Limitations of EBW should be considered for each application. As in all manufacturing, time and money are significant inputs into the selection of the processing of components. AWS lists several limitations in their recommended practices for EBW. These limitations include cost, precision machining, precision tooling, precise setup, evacuation time, and the need for x-ray shielding and monitoring. AWS also lists issues when welding magnetic materials or fixtures that may cause the beam to deflect unexpectedly [15]. Partial penetration welds may be prone to root porosity due to instabilities of the keyhole and/or melt pool. In a review of EBW, Cottrell discusses the need for close tolerances, with the potential for a weld to fall through the joint (i.e., the molten metal flows out of the weld joint) because of small gaps at the joint [26]. Cottrell also discusses a concern that metal vapor expelled from the weld can cause arcing in the electron gun [26] when welding aluminum. This is a problem when welding materials contain elements with low vapor pressures. The metal vapor coats exposed surfaces in the weld chamber, including optics, and it may deposit on nearby surfaces of the part being welded. Therefore, the optics, chamber walls, and parts, are sometimes shielded.

The viewing optics of the chamber can be coated by the metal vapor as a result of their proximity to the beam axis. Various manufacturers use a cover slide or film to protect the optical viewing and/or camera lenses. The chamber wall is typically shielded using thin foils such as aluminum foil to reduce the amount of cleaning, grinding, and polishing needed to remove the metal vapor deposition. Parts are also affected by the deposition of metal vapor. A shield or metal cover can be used to prevent buildup in undesirable areas. Arcing in the electron gun can occur if metal buildup accumulates to sufficient thicknesses on the gun components. Periodic maintenance as recommended by the original equipment manufacturer (OEM) is adequate to reduce the potential for arcing conditions. More frequent cleaning may be required for some materials such as aluminum [3, 32, 33].

The use of EBW has been limited because of the complexity and cost of the equipment. Expertise in precision machining, high vacuum systems, high voltage, electrical controls, and feedback, as well as expertise in materials and welding engineering, are all required for a sustained, controlled EBW process. Very few universities teach EBW, and even fewer have the equipment to provide hands-on training. EBW requires a skilled workforce trained by the equipment manufacturers and those with experience applying the technology. EBW is a specialized process that is widely accepted and utilized in manufacturing across the medical, automotive, aerospace, power generation, and defense industry sectors, with capabilities exceeding those of traditional welding processes. Currently there is no US vendor with the equipment on hand to complete all the girth welds required for the RPV. However, there are some vendors and equipment that can further prove feasibility on ring sections of the RPV to further advance this technology.

When compared to arc welding technologies, EBW has some disadvantages. EBW is not forgiving in terms of joint fit-up or cleanliness. A traditional arc welding process can accommodate variations in the bevel angle or gaps in the joint better than an EB welding process. When arc welding, the welder can modify the torch weave or reposition the weld bead based on the visual feedback and skill level. EBW does not have this level of flexibility. This limitation partly caused by the single-pass nature of EBW. Surface defects such as solidification cracking are often difficult to repair by EBW. Restraint conditions and weld material chemistry cannot be adjusted without adding filler wire. Heat input can be modified by adjusting the weld parameters to reweld the cracked area, and the technique has had limited success. Subsurface defects such as pores are also difficult to repair. An EB re-weld tends to modify the size, location, and quantity of pores, but it does not typically eliminate pores. Traditional arc welding repairs are completed by mechanically removing material down to the defect or pore to remove it, and then arc welding with filler metal is performed to complete the repair. In some cases with EBW, a local arc weld repair may be the best option. Many of these limitations can be overcome through the careful engineering of the manufacturing process and correct application of the technology. EBW is an advanced manufacturing process that should be planned for as early as possible during weldment design [4, 34].

Table 3. EB Disadvantages

General process disadvantages	Potential NPP disadvantages (additional)
Good joint fit-up with minimal gap required	No filler material*
Difficulty with weld repair	Less flexible manufacturing process
Equipment cost	Limited repairs (may require arc welding)
X-ray shielding and monitoring required	Need to establish vendor capability
Need for precision fixtures and tools	
Precision machining is required	
Limited technical expertise available	
Limited job shops available	
Time to achieve required vacuum level	

*No filler material has been listed as an advantage because of the matching material chemistry of the weld and base material. This can be disadvantageous for repairs and overall flexibility of manufacturing.

2.2.6 EBW Pros and Cons vs. other AMTs

EBW has been grouped with AMTs and termed an advanced process based on its limited use in the nuclear industry. Processes such as EB free-form fabrication (EBFFF, or EBF^3), EB additive manufacturing (EBAM), and EB melting (EBM) are widely used in aerospace and automotive industries and are best discussed along with powder bed AM and direct energy deposition (DED) [35, 36]. EBFFF and EBAM are wire-fed EB processes in which a part is made through the deposition of multiple layers of welds with wire addition [35]. *EBM* refers to a powder bed process in which the melting of a metallic powder is completed over many layers to form the final product [37]. All these processes are based on the EB generator, and the application methodology defines them more accurately. *EBW* is a term used when joining any two materials together. The two materials may be wrought materials or AM-produced parts in a traditional joint fabrication design.

EBW's primary advantage over other AMTs for application in the nuclear industry is that the process may be applied to materials already used in the industry with known properties and weaknesses. This is a benefit of EBW, because the bulk material is procured through the already-established system of ingot or plate fabrication. Welding-based AMT processes such as laser powder bed fusion (LPBF) and DED, fabricate the bulk materials as part of the process. These processes bypass the need to order castings or

plates in specific sizes and thicknesses, which may significantly reduce lead times for procurement. Instead, a wire or powder is used to fabricate the part in its entirety. Because of the nature of the AM processes, each weld pass or layer will undergo a series of thermal cycles, much like a multi-pass weld. As a result, bulk chemistry and mechanical properties are determined as part of process and parameter development. Inspections and validations of the material properties would therefore be concerned with the entirety of the component, because that is the first opportunity to inspect the bulk material properties. Implementation of the EBW process would be less disruptive to the traditional process than other AMTs which have less of a learning curve for the fabricator and inspectors.

As discussed in this report, EBW is based on the traditional manufacturing method of joining two workpieces to make an assembly. In this respect, EBW is at a disadvantage to other AMTs because it relies on the traditional wrought material fabrication methods and lead times. Large forgings such as those for an RPV require multiple years of planning to procure, produce, and deliver the materials needed to start the EBW process. For a successful weld to be completed, EBW also relies upon the machining tolerances of the joint and the joint cleanliness to avoid defects. EBW does not have the flexibility when welding autogenously (without wire) to fill a joint. An assembly with large joint gaps may cause the EB weld to have excessive concavity, or the joint may not be fused together at all. Other AMTs such as additive manufacturing methods have more flexibility because they build upon the last deposited layer with essentially zero gap.

2.3 MANUFACTURING METHOD

2.3.1 High Vacuum, Medium Vacuum, and Non-Vacuum

In terms of beam fidelity, a HV produces the smallest producible focal spot. If air molecules are in the path of the beam, they are sufficient to disturb the finely columnated and focused electrons, diffusing the intensity through electron scattering. Most EB welds are performed in a HV environment where the EB gun and workpiece are within a chamber and evacuated to less than 10^{-4} Torr pressure. Medium vacuum (MV) and non-vacuum (NV) EBW processes have been developed with equipment specific to the associated vacuum level (Table 4). AWS C7.1M, "Recommended Practices for Electron Beam Welding and Allied Processes," defines the modes of EBW as described below and as illustrated in Figure 5.

Table 4. AWS-recognized EB modes of operation

Process abbreviation	Process	Vacuum level of part
EBW-HV	High-vacuum EBW	1.3×10^{-1} Pascal [1.0×10^{-3} Torr] or lower
EBW-MV	Medium-vacuum EBW	1.3×10^{-1} to 3.3×10^{-1} Pascal [1.0×10^{-3} to 2.5×10^{-3} Torr]
EBW-NV	Non-vacuum EBW	Atmospheric

All EBW modes require the electron gun to be held at high vacuum for electron emission. Placement of the workpiece in a similar high or low vacuum delineates the mode of welding. In the MV or NV modes, the HV gun must be separated from the work chamber or workpiece to maintain the vacuum in the gun for process stability. A modern HV system incorporates a column valve to separate the vacuum chambers so that a clean HV can be maintained on the gun components while a new part is cycled into the work chamber. A MV system incorporates a vacuum divider to allow the two vacuum levels to be maintained during welding. An NV system incorporates a series of vacuum dividers between the gun and the workpiece [15].

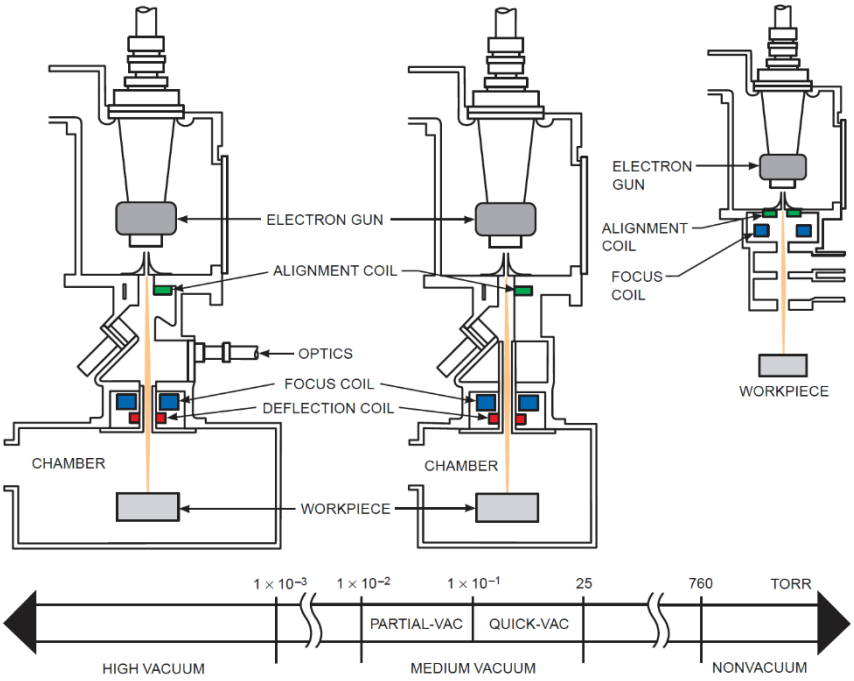

Figure 5. EBW: high vacuum (EBW-HV), medium vacuum (EBW-MV), and non vacuum (EBW-NV) (From Kautz et al. [33], reprinted with permission of American Welding Society).

The vacuum level also reduces the amount of potential contamination to the component. Because a shielding gas is not used for EBW, a clean environment is created through the absence of gaseous contamination. The Welding Handbook [33] compares the ppm levels of contamination in shielding gases to various vacuum levels used during EB as shown in Table 5 [33].

Table 5. Gaseous ppm contents at various pressures(Adapted from Powers [32])

Argon shielding	
Purity grade	Contamination level (ppm)
99.95%	500
99.995%	50
Gas molecules as function of pressure (Air)	
Pressure, Torr	Contamination level (ppm)
380×10^{-3}	500
100×10^{-3}	132
38×10^{-3}	50
10×10^{-3}	13.2
1×10^{-3}	1.3
1.0×10^{-4}	0.1

2.3.2 Plasma Window and Plasma Shield (EBW-NV)

Through a cooperative research and development agreement (CRADA), Hershcovitch from Brookhaven National Laboratory (BNL) worked with Acceleron to develop a plasma window, and later a plasma shield, for non-chamber EBW (EBW-NV). Acceleron envisioned a robotic head unit to allow for use of this technology in the automotive sector. Hershcovitch investigated the process of using a plasma arc to create a vacuum interface between the bottom of the electron gun and the part to be welded. This process had the added benefit of focusing the EB as a result of the Lorentz forces, resulting in a 3× factor of improvement in contamination prevention over in-air welds. The plasma shield was developed using a vortex-stabilized arc, thus allowing the process to function in air or liquid environments. The vortex is comprised of a sacrificial gas or liquid, resulting in a process with a claimed efficiency improvement of 41.5 to 47.4% over traditional EBW-HV. Several systems were sold, but the need for further development of the robotic arm unit and increased operational longevity were noted by the author. Figure 6 shows the beam propagation in atmosphere when using a 2 mm argon–helium plasma window [38-40].

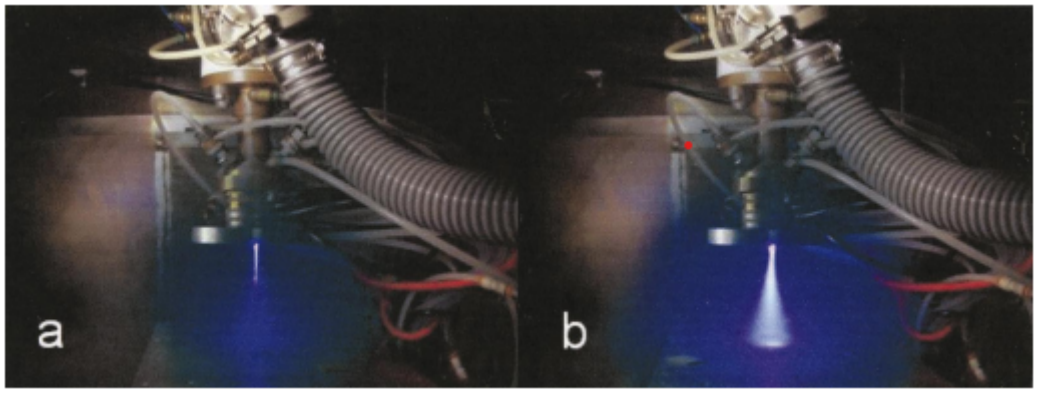

Figure 6. Plasma window (Ar-He) developed for out-of-chamber EBW: 9 mA (a), 25 mA (b) (From Hershcovitch [38], reprinted with permission from AIP Publishing).

2.3.3 Reduced Pressure Electron Beam (RPEB)

TWI developed an EBW process without a chamber. In collaboration with CVE, TWI, U-Battery, and Cammel Laird, the Ebflow system is being developed by the EBManPower project to weld large-scale power generation infrastructure components [41]. The process uses much of the same technology as traditional EBW without the large vacuum chamber. In lieu of a large vacuum chamber, the Ebflow system uses a local sealing interface surrounding the location to be welded. The sealing surface of the gun and backside of a pipe weld can be seen in Figure 7. Removal of the required chamber allows immediate improvements in application to large structures and reduces the size of the pumps needed to provide the local vacuum around the weld area. A significant reduction in energy and time used to pump down a large chamber can be realized [41]. A gliding seal is then used to maintain the coarse vacuum needed for the weld. During RPEB welding, the part can be rotated with a fixed EB gun position, or for large components, the EB gun can be rotated around the part [41]. The coarse vacuum level required at the workpiece is approximately 1 mbar (0.75 Torr), which is significantly lower than the HV (10^{-4} Torr) needed in a conventional EBW system. Comparison of 150 mm thick steel section welding by Ebflow and submerged arc welding showed that RPEB was 20–30 times faster, and as much as 75% less energy was consumed to make the weld [42] while maintaining weld quality. Results of the research performed using RPEB are contained in Section 2.8.1 [1, 8, 22-24, 43, 44].

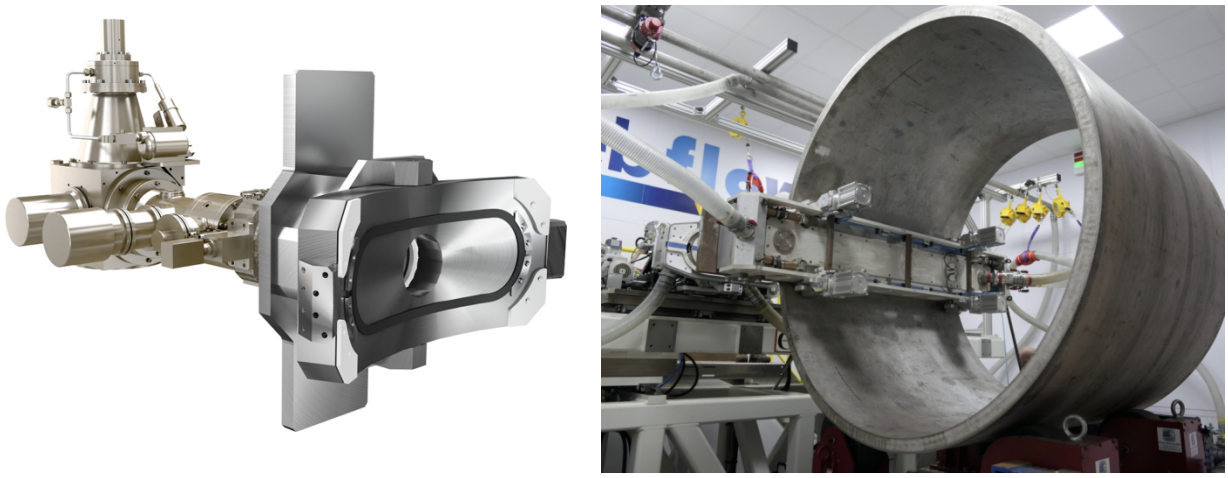

Figure 7. RPEB (Ebflow) system gun and sliding seal (left) [45], box seal on backside of weld (right) (courtesy of Cambridge Vacuum Engineering).

2.3.4 Modular In-Chamber Electron Beam Welding (MIC-EBW)

EPRI and Nuclear AMRC are collaborating to demonstrate advanced manufacturing and fabrication technologies for SMR vessels. Modular in-chamber electron beam welding (MIC-EBW) was proposed after discussing the limitations of the traditional large-vacuum EBW systems and the complexities of the RPEB process. The US Department of Energy (DOE) has contracted with EPRI and Nuclear AMRC to develop a modular in-chamber electron beam welder [8]. A conventional EBW-HV of sufficient size to weld a RPV was estimated to be over 40 feet long to accomplish the welds needed for the SMR [12]. EPRI and Nuclear AMRC seek to demonstrate the feasibility of welding thick section components, specifically RPV girth welds. Initial welds were completed at the Nuclear AMRC using a low voltage (60kV) Pro-Beam welding system, which is currently being used to demonstrate the EBW of thick sections of SA508 Grade 3 Class 1 and 2 materials [7, 8, 10].

A traditional weld chamber built to perform all the girth welds along the length of an RPV would necessitate a gun axis of approximately 35 feet, to be able to access all the weld joints in an SMR vessel or to reinstall the head assembly at specific gun locations inside the chamber. A traditional chamber dedicated to welding SMR circumferential welds is estimated to cost $20 M. A MIC-EBW system is estimated to reduce this cost by more than 50%. A model of the system can be seen in Figure 8. This model shows the critical components of the system, the manipulator (rotary) and pumping system, the gun and slide stage, spacer rings, and the lid. Numerous spacer rings could be assembled above and below the gun and slide stage to place the welder at the correct location on the assembled RPV. Once assembled and leak tight, the system would function like a traditional fixed welding chamber system. A fully stacked system is shown in Figure 9. PTR was chosen to manufacture the welding equipment, including the electron gun, the gun slide, the power supply, the CNC controller, the operator console, and the cradle lifting device [8].

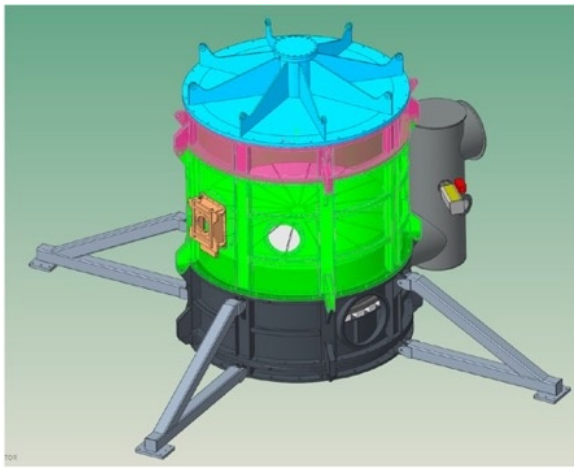

Color	Description
Gray	Rotary manipulator and pumping stage
Green	EB gun and slide stage
Magenta	Modular spacer ring stage
Cyan	Lid or cap

Figure 8 Modular in-chamber EBW system design (From Gandy [8], reprinted with permission from Electric Power Research Institute).

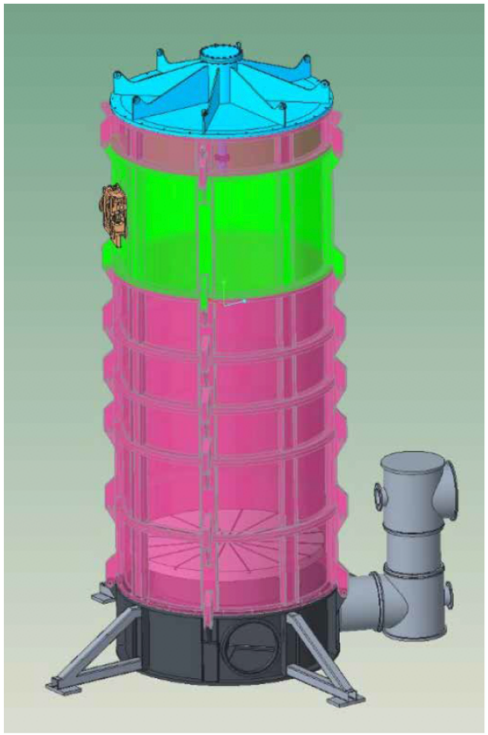

Figure 9 Fully stacked model of the MIC-EBW system (From Gandy [9], reprinted with permission from Electric Power Research Institute).

The EB gun (generator) being used in the MIC-EBW system is a triode gun design (see Section 2.2.2 for additional discussion) capable of operating up to 150 kV and 400 mA (60 kW) [8]. The EB gun will be positioned on a gun slide, a small linear axis that allows for small adjustments of the position. The EB generator and slide attachment are shown in Figure 10. The MIC-EBW system will also incorporate the EB optics (EBO) and viewing package, allowing for the use of the electron optics to view the weld and the CCD camera. The EBO package allows for the system to have seam tracking, advanced viewing, and advanced beam control. The advanced beam control allows the beam to be manipulated through fast electrical deflections to control four positions simultaneously. Figure 11 shows the available options for

the EBO optics. EPRI is currently developing the welding parameters for the thick section RPV welds, which is covered later in Section 2.8.2 [8, 9].

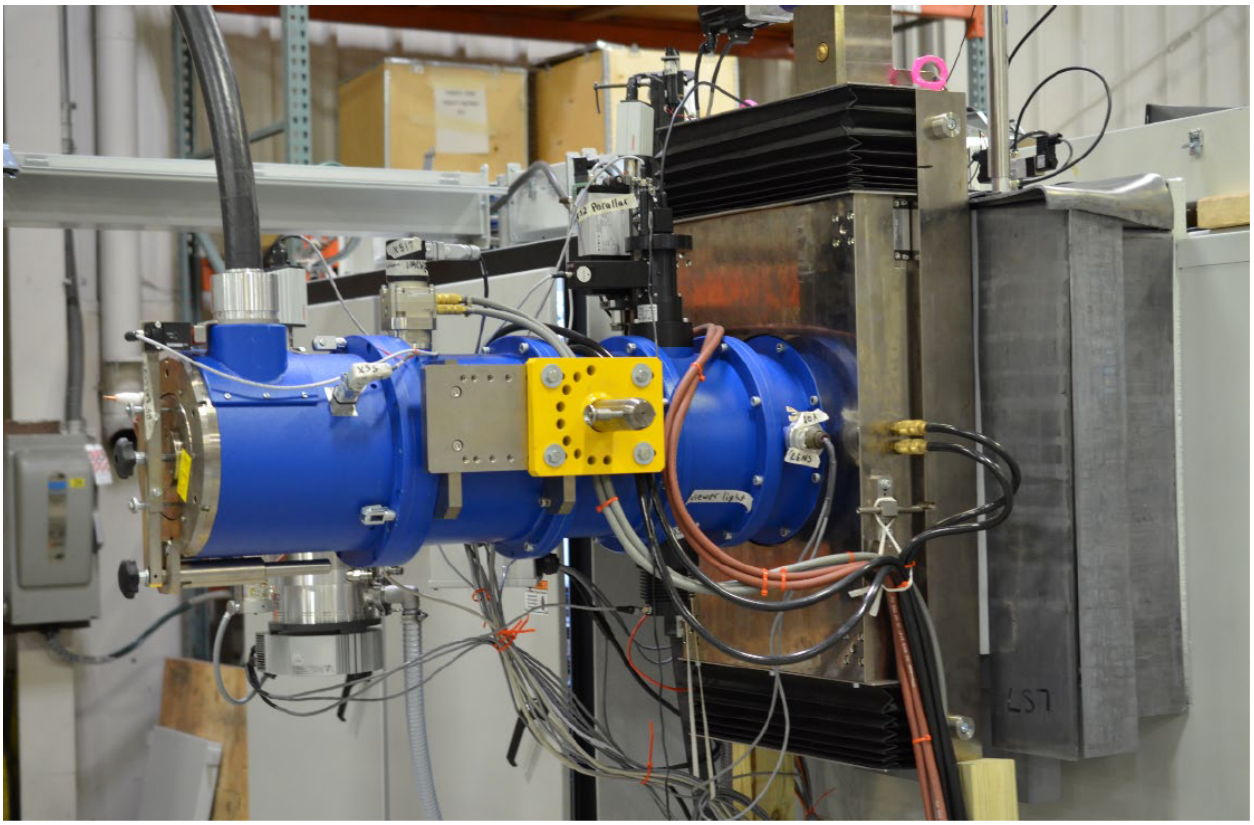

Figure 10. EB generator capable of 150 kV, 400 mA (60 kW) attached to gun slide (From Gandy [8], reprinted with permission from Electric Power Research Institute).

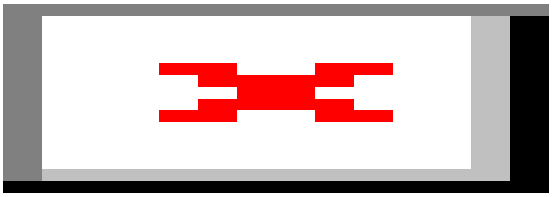

Figure 11. EBO system capabilities (From Gandy [8], reprinted with permission from Electric Power Research Institute)..

2.3.5 EB with Filler Metal Additions

Filler metals can be used with EB using two methods, as discussed by Barreda [46]: (1) the use of a wire fed assembly, or (2) preplacement of filler material between the parts to be welded. Barreda investigated

the use of a filler material with Ti6Al4V plates to improve fracture toughness, corrosion resistance, and porosity levels in the weld. Barreda noted that the wire addition method "needs adjustment of a great number of variables and proves to be very difficult," preferring to use the preplaced filler metal method, as shown in Figure 12. Preplacement of the filler metal between the two pieces to be welded simplifies the weld process and minimizes the setup for a successful result, but it increases the setup needed prior to welding and may not be feasible in all joints [46].

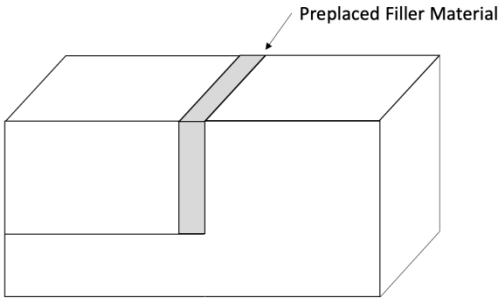

Figure 12. Preplaced filler material at joint interface.

Successful wire-fed EB welds have made between components. Research on EBW with wire additions is limited. References to conference proceedings were found from the 1970s mentioning wire addition, but these proceedings were not located. Additional research into dissimilar welding was found from the 1990s in which authors such as Sun discussed an overview of EB dissimilar welding [29]. Sun discussed the benefits when welding austenitic stainless steels to ferritic steels using a nickel filler metal. Conventional arc fusion processes also use this filler metal, but they do not benefit from the low total heat input of EBW. Sun notes that when using EBW with wire addition, a narrow heat-affected zone (HAZ) width and low residual stresses results in less distortion. Sun references a conference proceeding by Ruge in which a 60 mm thick 304L austenitic stainless steel was welded to 2¼Cr-1Mo ferritic steel in 4 passes [47]. Jones successfully developed a wire-fed EB process for the joining an ITER vacuum vessel made of stainless steel. In this report, a 60 mm thick weld with a root gap of 2 mm was successfully welded with a 1 mm or 0.5 mm circular beam oscillation. A thick or thin weld resulted, depending upon the oscillation used, with less distortion in the 0.5 mm oscillated weld. Welding time and distortions were reported to be improved over comparable processes of narrow gap tungsten inert gas (NG-TIG), laser, and laser hybrid by a factor greater than 2 [48].

Schuchardt published a paper in 2019 investigating the use of EB with filler wire for the repair of die casting dies. As in other filler metal efforts, Schuchardt used beam oscillation during wire feeding. A reported lower hardness gradient throughout the weld metal was reported when welding H11 hot work steel with EB compared to arc fusion processes. A test setup and resulting weld buildups are shown in Figure 13.

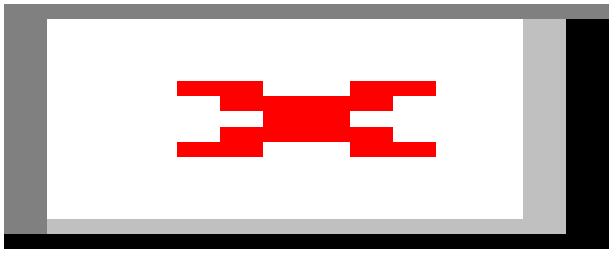

Figure 13. EBW with wire addition, (a), and weld buildups using wire (b) (From Schuchardt [49], reprinted with permission from Springer Nature).

2.4 PROCESSING CONTROLS

2.4.1 Welding Parameters

ASME BPVC Section IX defines Essential Variables for EBW procedure and performance qualification. The essential variable list for procedure qualification includes all settings upon which a change would affect the mechanical properties excluding weld toughness. Therefore, the essential variables for performance qualification are listed to describe the variables affecting the weld operator's ability to create a sound joint [50]. A subset of the essential variables is adjusted primarily during weld development. The subset includes beam current, accelerating voltage, focal spot size, and welding speed. These parameters define the energy density of the beam impinging upon the part. Beam current, accelerating voltage, and welding speed can be readily calibrated and are easily controlled through the microprocessors running the equipment. The focal spot size that effectively sets the energy density on the workpiece is not generally a directly measured parameter, but it can be calculated or measured through the use of spatial profilers. Pro-beam, TWI, and Lawrence Livermore National Laboratory have developed spatial profilers that can accurately measure spot size, but most production systems in use today do not have this capability or expertise. Focal spot size and spatial profiling are discussed further in Sections 2.4.4 and 2.4.5, respectively. In practice, the spot size is controlled by setting the gun to work distance and focusing the lens current, both of which are essential variables. In weld development, the gun-to-work distance may be limited by the physical dimensions of the part, and access to the weld joint may require that a certain distance be used. The beam current, arc voltage, lens current, and travel speed are adjusted to achieve the desired weld penetration and weld profile required for the weld joint. Beam parameters such as beam oscillation pattern, oscillation frequency, or beam current pulsing are finely tuned for the application, or they are adapted based on previous experience [31, 51, 52].

Transition points before and after steady-state welding are of higher concern than arc welding, especially when welding in the keyhole mode as discussed in Section 2.2.4. The transition from conduction mode to keyhole is quick once an energy density threshold is reached. Penetration rapidly increases because of vaporization of the parent material, and deep welding occurs. Slope-in and slope-out settings must be appropriately developed to minimize or eliminate defects at the start and stop locations.

Table 6. Primary Weld Development Parameters

Weld development parameters	Method of control
• **Beam current (mA)**	Calibration
• **Accelerating voltage (kV)**	Calibration
• **Welding speed (ipm or mm/sec)**	Calibration
• **Focal spot size** o Distance from electron gun to workpiece o Focusing / lens current	Tooling / tooling aides to properly set distance calibration of lens current

2.4.2 High kV and Low kV EBW

EBWs can be categorized as either high kV or low kV systems. Low kV systems are those operating at or around 60 kV. Low kV systems have the advantage of producing less energetic x-rays, so less shielding is required to safely protect the weld operator. The electron guns are also more compact, allowing the gun to be placed in the chamber with the workpiece and manipulated through multiple axes for complex joint tracking [15].

High kV systems range up to 200kV, can be focused to smaller spot sizes, and can be more tightly constrained to reach into deeper cavities. Non-vacuum EB welders are always high voltage machines because of the initial higher beam fidelity [15].

The type of system used is a function of part size, weld joint access, and length requirements, as well as the aspect ratio of the weld required. A high-quality weld is achieved using either process. EB manufacturers advertise systems up to 60 kW, and higher-powered custom systems are available.

2.4.3 Process Controls

Because the interaction of the beam and part are repeatable without a gas environment to interrupt the weld, the process is easily controlled through the input variables. Many of the factors essential for creating a good weld can be digitally controlled to extreme accuracies. The variability in EBW has traditionally been in the fixturing of components and the functions requiring operator input such as positioning of the gun components during filament changes. The largest influential factors dictated by the operator are the determination of focal position and tracking of the seam.

2.4.4 Focal Position

The focal position of an electron optic system is controlled through magnetic focusing of coils near the bottom of the EB gun. This round coil constricts the electrons using magnetic fields to a focal spot size. Like optical systems, a focal depth exists because of the repelling forces of electrons as they near one another. A convergence of electrons results at a distance away from the gun, resembling the shape of an hour glass (Figure 14). This figure illustrates the power distribution of the beam through the focal position at different planes through the focal cone. Like optical focus, the minimum beam diameter at the highest intensity is considered to be at focus. The center of the focal depth is referred to as *sharp focus*.

A standard procedure that is used to determine the sharp focus position is to place a sacrificial piece of metal under the beam at the same height as the weld to be performed. A tungsten alloy is typically used to avoid melting. At low power, a few mA of beam current, and at the weld voltage to be used, the operator varies the lens current to find sharp focus. Through the viewing optics or camera system, the operator watches for the brightest spot and centers it within that range. Sharp focus is then set. Stigmatism and

beam centering are recommended to be checked and adjusted after changing the filament or performing maintenance on the electron gun components. New systems may come with profiling equipment and focusing systems to automate the procedures. A representation of the beam focusing, centering and stigmatization is shown in Figure 14. In lieu of automated focusing equipment, the weld operator checks for beam alignment by placing a low power beam on a test block similar to that used to find focus, and then the weld operator adjusts the lens current above and below the true focus position. This effectively moves the beam into the hourglass portions above or below the focus position. As the weld operator adjusts the lens current, the spot should stay centered in the crosshairs and should vary in size only. The weld operator can adjust the alignment coils for any movement laterally from the true focus position and any elongation of the spot.

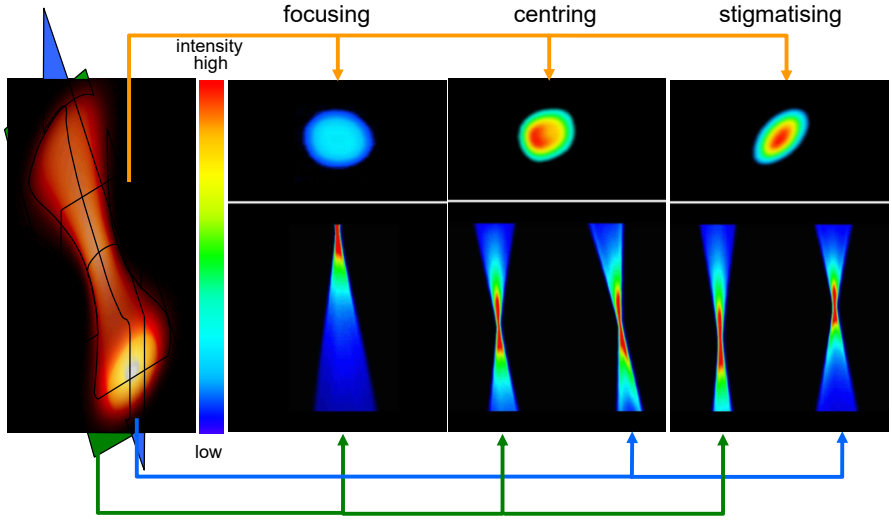

Figure 14. Illustration of beam focus, centering, and stigmatizing provided by Pro-Beam (From Sebastiano et al. [31], reprinted with permission from Springer Nature).

When new welders are being trained, it is common to compare focal set points between multiple operators to verify that they can set sharp focus within several mA of one another. Setting the focal position manually can vary because of the weld operator vision. The illustration provided by Volker qualitatively demonstrates the difference between average and experienced operators' ability to accurately set the lens current / focal position at the ideal setting (Figure 15). Gauge repeatability and reproducibility studies have shown that the highest variability occurs when using newly trained (average) operators, and less variability occurs when using experienced operators [53]. Because the EB has a focal depth in which the smallest beam diameter is relatively unchanged for small changes in lens current, the variation in setting lens current between operators typically is not a significant factor. This is particularly true of large or deep EB welds.

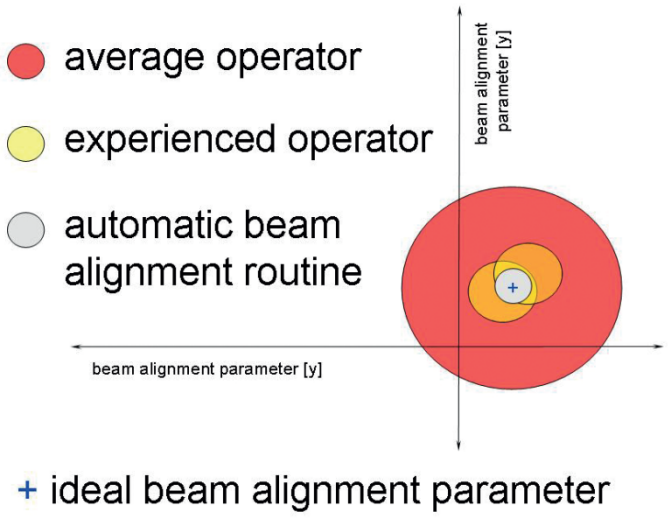

Figure 15. Qualitative representation of focus determination variability by operator and equipment (From Adam et al. [4], reprinted with permission from Pro-Beam).

2.4.5 Beam Spatial Profiling

Researchers and institutions have developed diagnostic equipment to measure and construct 3D representations of the beam [51, 52, 54-56]. Multiple methodologies exist in the equipment design of the tool. However, all of them construct the beam through an electrical signal produced by movement of the beam over a filament. Multiple orientations and focal settings are required to create a 3D model of the beam. Elmer at Lawrence Livermore National Laboratory used a profiler named the *enhanced modified Faraday cup* to measure the beam on one system for transfer of the weld schedule across country to be reproduced for welding on a different EB welder [56]. With a captured representation of the beam used to produce acceptable welds, future troubleshooting of welds in noncompliance could benefit [55].

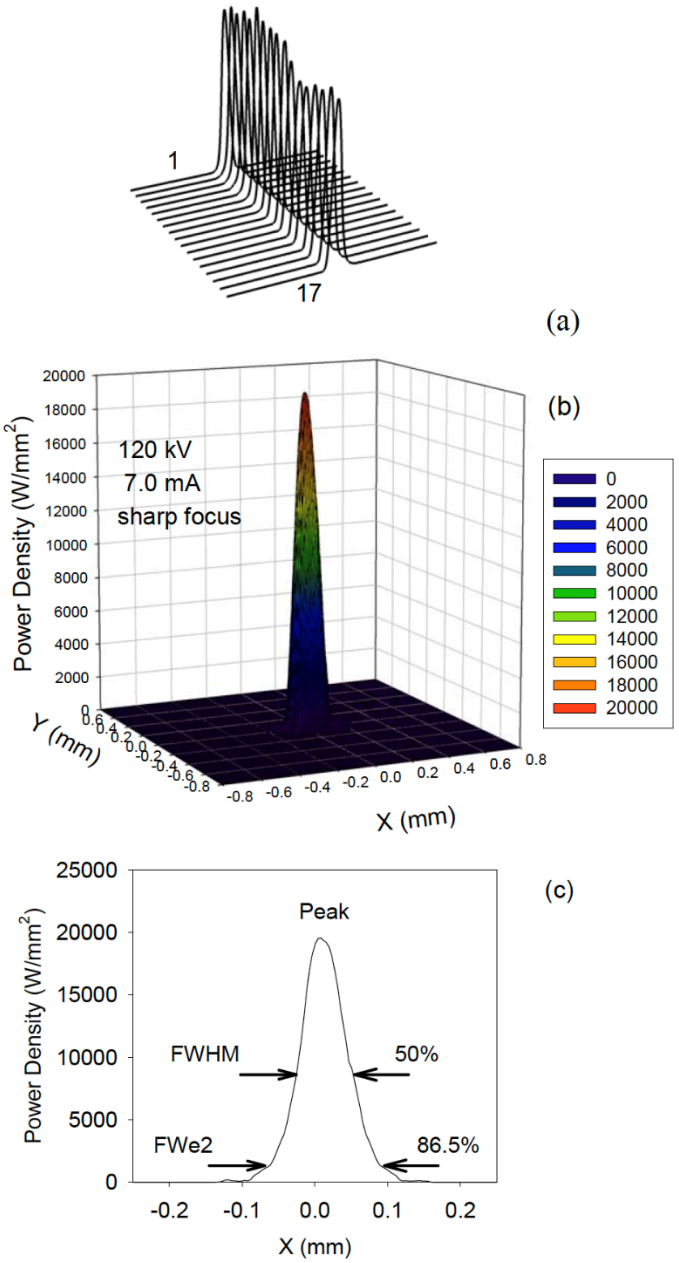

Figure 16. LLNL enhanced modified Faraday cup results showing beam profiler composition: profiles seen by each of 17 slits (a), Reconstructed power density distribution (b), and central profile (c). (From Elmer [57])

2.4.6 Data Acquisition

Data acquisition systems are available for EB welders to take advantage of the electrical signals and controls inherent in the process. The acquisition of data during welding can support quality programs like Six Sigma and can provide verification of parameter / program performance. Monitoring accelerating voltage and beam current are the two primary variables to ascertain weld joint quality. An acquisition system capable of detecting millisecond changes in accelerating voltage or beam current can identify areas of the weld for further evaluation. Common causes of these fluctuations are weld spatter impinging upon the beam optics, vapor buildup in the gun, or power supply spikes. New voltage power sources have improved the capability to detect a malfunction and can quickly recover without shutting off the beam or

leaving a hole defect. The analysis of accelerating voltage and beam current has been used for further validation of the welding process. Because the resulting penetration correlates with the incoming parameters more directly than traditional arc welding, it can provide further proof of the weld quality. However, this does not guarantee penetration, and proper inspection of the weld is necessary.

2.4.7 Seam Tracking

Automatic seam tracking has been used for many welding processes. Most systems use light optical systems in which a camera image is processed before or during welding to find and track the joint. In addition to the light optical image, EB welders can use the EB's backscattered electrons to image the part. This is accomplished by using a low power and/or quickly scanned beam to raster across the part and record the number of backscattered electrons. This is similar to a scanning electron microscope [4]. This approach has several advantages: the electrons provide a very high contrast ratio of 1:15,000 as reported by Pro-Beam, and reflection issues are negated [31]. Metallic parts that are highly reflective to photons are easily imaged by electrons. This can be seen in Figure 17 and Figure 18. Figure 18 also shows a joint line created by the difference in two different metal alloys. Because the backscatter intensity is different between the two alloys, the materials and joint line can easily be distinguished [4].

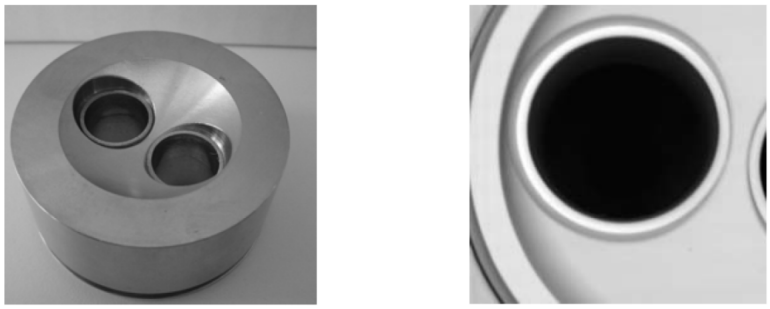

Figure 17. Light optical image (left), electron optical image (right) (From Clauß [58], courtesy of Pro-Beam).

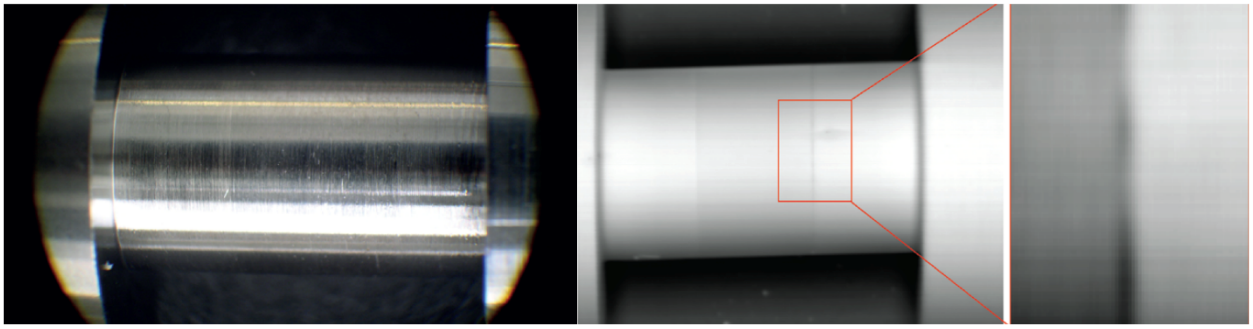

Figure 18. Electron-optical monitoring: light optical image (left), electron optical image (right) (From Adam et al. [4], courtesy of Pro-Beam).

2.4.8 Parameter Effects on Penetration and Cosmetic Passes

Beam current and energy density are the primary factors influencing the penetrating characteristic of EB welders. Other factors such as travel speed have an impact on the penetration depth, as shown by Schultz [3]. The relationship between power, travel speed, and weld thickness (penetration) can be seen in Figure 19, the shaded area represents the operating window. Although this plot is not linear, it can be seen that EB weld penetration is far more predictable than in arc welding.

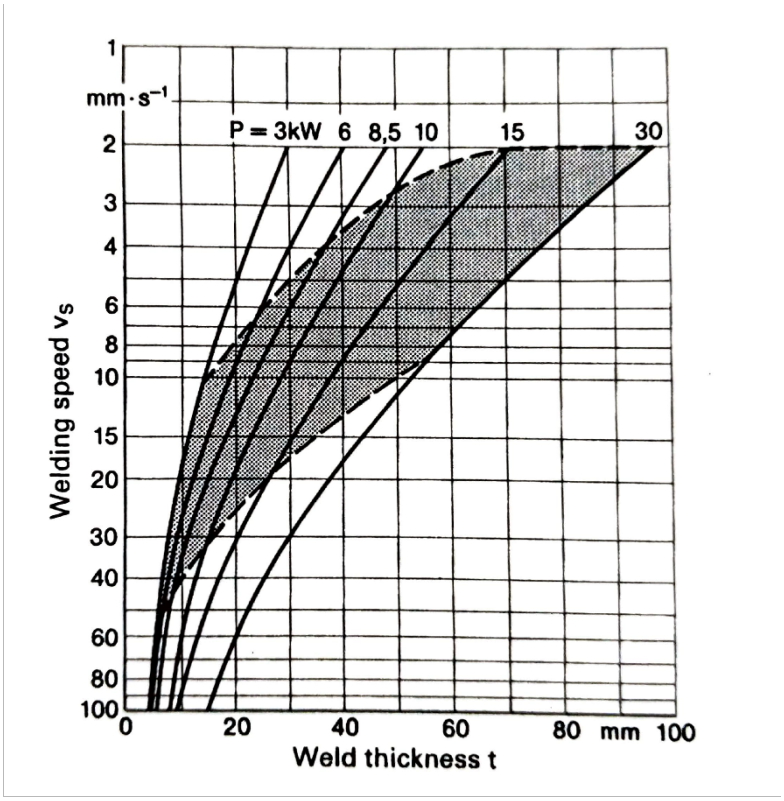

Figure 19. Welding penetration in steel as a function of beam power and welding speed (From Schultz [3]).

By defocusing or lowering of the energy input, the EB can weld in a conductive heat mode similar to arc welding. This is most commonly used for cosmetic or cover passes to smooth the exterior surface of the penetrating weld pass. Reversing the weld direction of the cosmetic weld opposite that of the penetrating weld has proven to help create a smooth surface. This can eliminate undercutting at the weld toe or lessen excessive weld reinforcement at the center of the weld. Conductive mode EBW can handle larger joint gaps and accommodate larger variances in machining tolerance. Welds of RF generators or niobium superconducting cavities, for example, benefit from the intentional ripple-free welds that are made possible through conductive mode welding. Therefore, the EB process can be tuned to produce the desired weld profile by consideration of the beam energy and spot size. Because the heat source can be controlled precisely, the beam can be focused to achieve cutting or drilling, or it can be defocused for applications such as heat treating with no melting of the material [49, 54]. Figure 20 shows operating modes based on absorbed power and beam diameter.

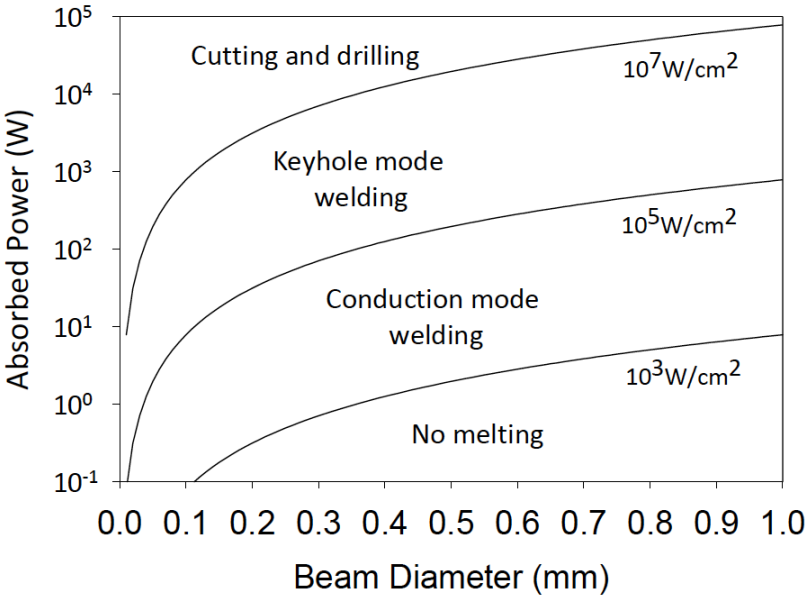

Figure 20. Operating modes dependency on absorbed power and beam diameter (From Elmer et al. [54]).

2.4.9 Weld Initiation, Termination, and Transition Segment Concerns

Parameter development of the weld initiation, transition, and termination are not commonly shared or reported. This is partly due to the confidentiality of industry process development reports. Transitions mid weld are usually completed with a linear ramp of beam current and/or beam voltage and are generally free of trouble if keyhole stability is maintained. It is important to remember the spatial profile of the weld as discussed in Section 2.4.5. The beam impinging upon the part can be considered a 2D circular area of heat input. Linearly ramping parameters will change the diameter of the impinging spot through a parabolic relationship. This is a simplistic view of the beam interaction on the material because the actual interaction dynamics are very complex, including a Gaussian distribution of energy from the EB and changes in absorption from conduction or keyhole mode welding. Changes in parameters during full penetration welding are generally easier to maintain, because the weld can be overpowered without detriment to the results. Travel speed, beam current, and focal position can be ramped while fully penetrating the material if energy input and density are sufficiently high.

Partial penetration welding is more susceptible to changes during welding. The partial penetration vapor cavity is a result of the focus, beam current, travel speed, and beam oscillation parameters. The penetration depth will vary with changes to these parameters as a result of their impact on the energy density impinging upon the material. For a partial penetration weld, a sharp root is not desired because of the possible formation of spiking defects. Focal position, travel speed, and beam current are developed to achieve a duller energy density profile to achieve a weld with a rounded root.

The weld termination must achieve a transition from a partial penetrating weld to a conduction weld. A keyhole is typically present in partial penetrating EB welds and must be closed so that termination of the weld does not leave a void or hole. This is sometimes difficult because of the sudden transition from keyhole to conduction mode. If the transition is too quick, then a keyhole will remain, a slow transition will result in underfill, and a sufficient transition will result in a small weld reinforcement in the tapered profile of the weld.

Therefore, a full penetration weld must transition from a full penetrating weld to a partial penetrating weld, and finally to a conduction mode weld. Control of the energy density during weld termination is

key to provide a stable keyhole throughout the transition until the keyhole can be collapsed and the weld ramped out. Weld initiation and termination locations are more difficult because of the transition between keyhole mode and conduction mode welding. This transition is abrupt, which can cause a keyhole to collapse onto itself, creating a pore or void in the weld metal. Deeper welds are more difficult, requiring additional development effort to be made at these transition points.

2.4.10 Additional Variables for Dissimilar Welding

Dissimilar welding between two different alloy systems is possible with EB, as discussed above. Dissimilar welds have many challenges because of the inherent differences in melting temperatures, coefficients of thermal expansion leading to high residual stresses, formation of brittle phases, and segregation of high and low melting temperature phases. According to Sun, variables such as "beam alignment relative to joint centerline, and the focal beam spot size" are dominating factors [29]. Sun refers to a joint made between copper and titanium that was successfully welded by locating the beam preferentially on the copper side of the joint. Preferentially offsetting the beam position onto the materials of higher conductivity or melting temperature helps balance the heat for each material [29].

Schuchardt included the wire positioning variables of distance and pitch as shown in Figure 21. The primary influence of the variables was reported to be bead appearance and geometry [49]. Schuchardt and Sun do not specifically mention the beam oscillation parameters. Because the EB can be narrow, an oscillating beam widens the heat source and allows for small variations in the position of the wire from imperfect wire straightening from the feeding assembly. Oscillation frequency, shape, and intensity of the oscillation are important variables to be considered. A circular oscillation is commonly used when the weld joint orientation to the beam changes, such as during a circular weld. In linear welds, a Y deflection as depicted in Figure 21 may be all that is required.

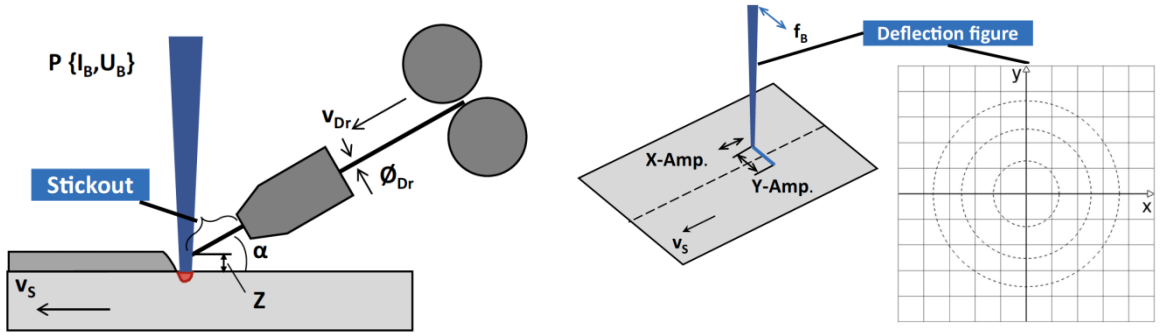

Figure 21. Distance (Z) and pitch (α) for wire-fed applications (left) and deflection orientations (right) (From Schuchardt [49], reprinted with permission from Springer Nature).

2.4.11 Joint Designs

The joint design for an EB weld is simpler in design to machine than a J or U groove arc weld joint. However, certain considerations must be made to ensure that a good joint can be welded. High precision is required to minimize the gap at the weld interface to ensure the weld has sufficient cap reinforcement. Because no filler metal is added, a larger gap may result in concavity on the surface, which may not meet requirements of the weld. Typical weld joints are shown in Figure 22. Weld joints must be designed to accommodate the high energy density EBW process. Although joint preparations are simpler, tolerances of the joining pieces must be held to precise dimensions because of the lack of filler metal for most EB welds. Like arc welding, initial thermal expansion of the material and subsequent plastic deformation from the high stresses formed when welding causes the assembly to axially shrink due to the expansion

and contraction stresses on the joint. This requires precise machining, and in the case of small components, the weld engineer may request that the joining surfaces not be deburred. Another consideration specific to high-energy density welds is the potential for spatter from the underbead upon full penetration of the joint. The intense vaporization of the weld puddle will cause spatter to be expelled from the bottom of the weld if the weld breaks that surface. The resulting spatter may stick to the opposing walls of the component, or it may solidify as BBs in the component or scattered in the EB chamber. When it is possible to access the inside of the component during welding, sacrificial spatter shields can be used to protect the component's surfaces. Spatter can be difficult to control, so partial penetration weld joints with material backing are often used when spatter is not acceptable. A gap size up to 0.15 mm (0.006 in.) can be tolerated in most steels for welds up to 6.35 mm (0.250 in.) penetration depth with moderate increases in gap size for deeper penetration welds. Wire-fed systems are available and can help significantly with gaps. Gaps equaling 10% of the penetration may cause the weld to form below the top surface of the joint [53].

The addition of a wire feeder to the EB welder, as discussed in Section 2.3.5, allows for gaps in the mating materials to be filled, thus reducing the amount of residual stress on the completed weld. This may be of particular interest for very thick welds or for welds in which a preferential filler alloy is beneficial for its metallurgical or corrosion resistance properties.

Off-axis welding can be performed using an EB welder. Off-axis joint configurations are shown in Figure 22. The most common off-axis orientation is the horizontal 2G position. Smaller welds using EBW may be indiscernible from welds using the flat position, 1G. The effects of using an off-axis weld depend upon the material being welded, as molten pool fluidity has a great effect on the surface tension of the pool and the ability to create a weld without losing molten material because of the combination of surface tension, gravity, and fluid flow. Therefore, larger welds are more susceptible to a fluid material loss. Support bars, drip trays, and run-on and run-off tabs have been used to help prevent a fluid puddle from falling out of the joint. These supports can be used on the outer and inner surfaces of the weld, depending on internal access and weld parameter settings. A "hotter" weld parameter set resulting in higher heat input to the weld will increase the molten volume of the weld and contribute to fluidity issues. A thick-walled EBW of SA508 Class 1 steel created by EPRI required supports to prevent the loss of welding material when welding in the 2G position [10].

Joint type	Assembled joint configuration	Welded joint
Square groove butt joint	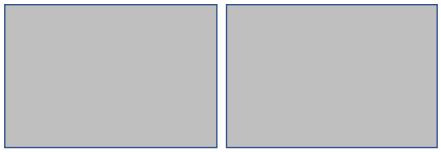	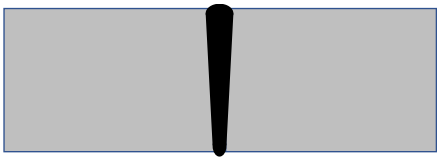
Step joint		
Step with backing		
Lap joint (low strength)		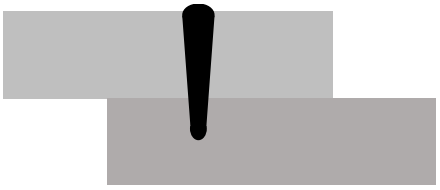
T-joint (low strength)		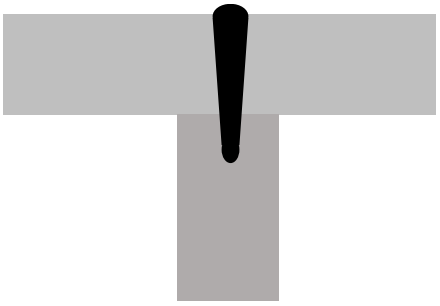

Figure 22. Typical joint configurations.

Joint type	Assembled joint configuration	Welded joint
Off-axis horizontal welding **Support bar / tab added** **Exterior position only**		
Off-axis horizontal welding **Support bar / drip tray** **Exterior and interior**		
Off-axis horizontal welding **Integral machined support** **Exterior only**		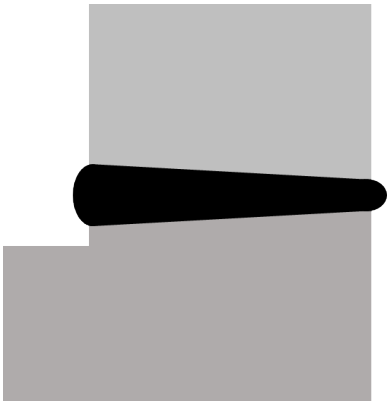
Off-axis horizontal welding **Integral support** **Exterior and interior**	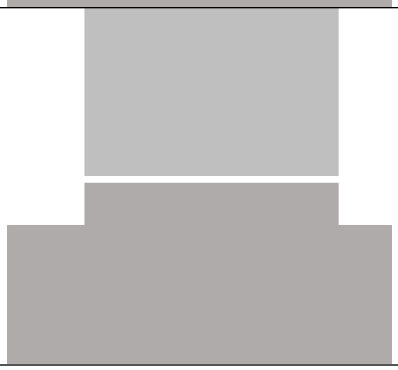	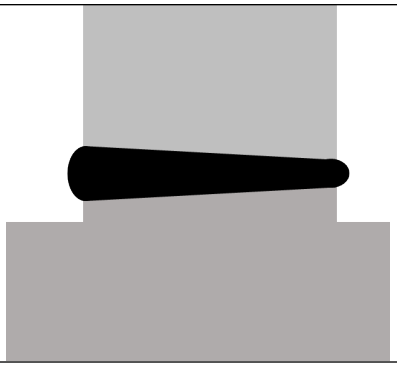

Figure 23. Off axis joint configurations (integral support used by EPRI and Nuclear AMRC).

2.4.12 Restraint Conditions

EB welds will have high stresses because their high thermal gradients during welding and deep penetrating welds. Restraining the part through fixturing or joint design can cause cracking to occur if not properly addressed. Through weld development, Wiednig determined that cracking could be caused by placing consecutive welds near one another on an otherwise weldable alloy [59]; the first weld would be completed without cracks, but subsequent welds placed nearby would form centerline cracks because of the shrinkage stresses of the neighboring weld, as shown in Figure 24 [59].

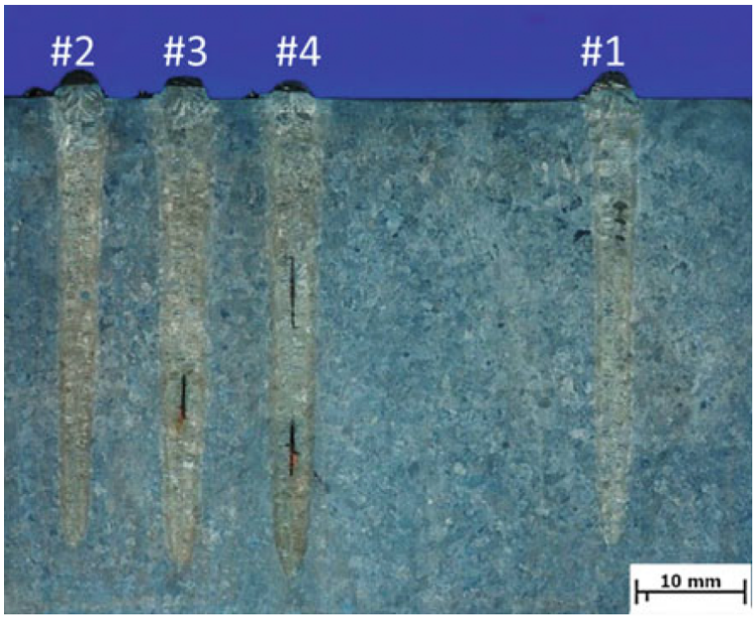

Figure 24. Solidification cracks resulting from the residual stress of neighboring welds (From Wiednig et al. [59], reprinted with permission from Springer).

Small diameter EB welds, such a plug welded into a plate, require precautions to avoid this scenario. This has been seen in small stainless steel welds on the scale of 5–10 mm diameter [53]. A small-diameter EB weld can impart stresses on the opposite side of the circular weld because the weld is completed creating a crack. This is in essence a small circular patch test. To minimize the stress levels, the joint can be designed with features to allow additional ductility in the region of the weld. A butt weld joint with relief and a standing edge butt joint are two popular joint designs (see Figure 25) that are used to minimize weld restraint on the EB weld during solidification. It has also been suggested by Kannengiesser that a zero gap weld joint may be more prone to cracking because of its inability to move with the shrinkage forces [60]. Although gaps encourage penetration of the joint, too much of a gap will allow the weld to form with either excessive concavity or completely below the top surface of the joint. Therefore, precise control of the penetration will be a function of the gap, as well as parameter variations.

Figure 25. Standing butt joint (left) and butt joint with relief (right).

2.4.13 Magnetism and Undesirable Beam Deflection

One unavoidable characteristic of EBW is the influence of magnetic fields on the beam. Due to the use of electrons as the energy source, magnetic fields have a significant influence and are necessary to produce the confined beam. However, a magnetic field generated by the parts to be welded, fixturing, or nearby sources can have a deleterious effect on the weld [61-64]. According to Blakeley, the resulting deflection of the beam for welds less than 3 mm in depth are unlikely to cause problems. Deeper welds have the potential to miss the bottom of the joint, resulting in a lack of penetration [61]. Tomita, who investigated welding of carbon steels for pressurized water reactors (PWR), recommends a residual magnetism level of less than 50 G, whereas Ayres sought to reduce magnetism to less than 5 G, and a limit of 2 was used by EPRI [2, 22, 65]. It is best to avoid magnetic materials in the tooling when possible and to minimize the amount of magnetism as much as possible near the weld joint [61].

Blakeley [61] performed a detailed study of magnetism and its effect on EB welds. The report states that residual magnetism can occur in ferromagnetic materials containing iron, nickel, or cobalt, which may be magnetized by (a) magnetic lifting devices, (b) welding processes involving high currents, (c) operations involving magnetic tables or clamps, (d) mechanical shock in the presence of a weak magnetic field, and (e) incorporation of a magnet in the assembly being welded [61]. For many materials, a local demagnetization near a slowly decreasing alternating current (AC) magnetic field can be effective immediately prior to EBW [61, 62]. A thermoelectric effect can also cause a missed joint condition in which a magnetic field is generated by the interaction of the beam with materials of different thermal potentials. Much like a thermocouple, materials of >10 mV thermal potential can cause electromagnetic fields that are capable of deflecting the beam [61]. This electric potential is known as the *Seebeck effect*. A model of the EB and dissimilar metal combinations is well explained, calculated, and analyzed by Wei [64]. Blakeley points out that the resistivity of the materials is not a cause of the deflection, but it will influence the severity of it, and that highly conductive materials such as copper, silver, and aluminum will be affected to a greater extent. Examples of beam deflection causing a lack of penetration defect can be seen in Figure 26 [61, 62].

The most obvious form of beam deflection is in the direction tangential to the joint direction causing a missed joint, as shown above. It is possible for the flux lines to be perpendicular to both the joint and the beam, thus resulting in a deflection along the joint line. Blakeley notes that this is less severe, but it did result in porosity problems [61].

Adjusting process parameters to use the higher kV input accelerates the electrons to faster speeds, thus minimizing the time that each electron is affected by the magnetic field [62]. This can reduce the magnetic influence on the beam. Demagnetization techniques are provided by Blakeley: (1) use of a slowly decreasing AC magnetic field, (2) use of a magnetic shield, and (3) preheating above the curie temperature (i.e., the temperature above which certain materials lose their permanent magnetic properties, e.g., 770°C for iron). Method 1 is most commonly used to demagnetize fixtures and components before they enter the EB chamber. This method is most effective in steels 1–2 mm thick. Method 2 may be effective for protecting the beam on transit to the material, but it will not provide protection throughout the process or through the thickness of the weld. Method 3, preheating above the curie temperature, is not an easily obtainable condition: it requires the entire component to be preheated to extreme temperatures before and during EBW [61].

Advancements in EB controls have allowed for a fourth option. The beam deflection systems in modern EBW equipment are capable of beam deflections in many different patterns at extremely fast rates. According to Rugh, welds under 25 mm in penetration depth are weldable with minimal problems,

whereas deeper welds require additional tuning through adjustment of the impingement angle of the beam to counteract the pull of the magnetic field [62]. Rugh mentions a technique of producing two simultaneous keyhole welds to counteract the magnetic influence of the part [62].

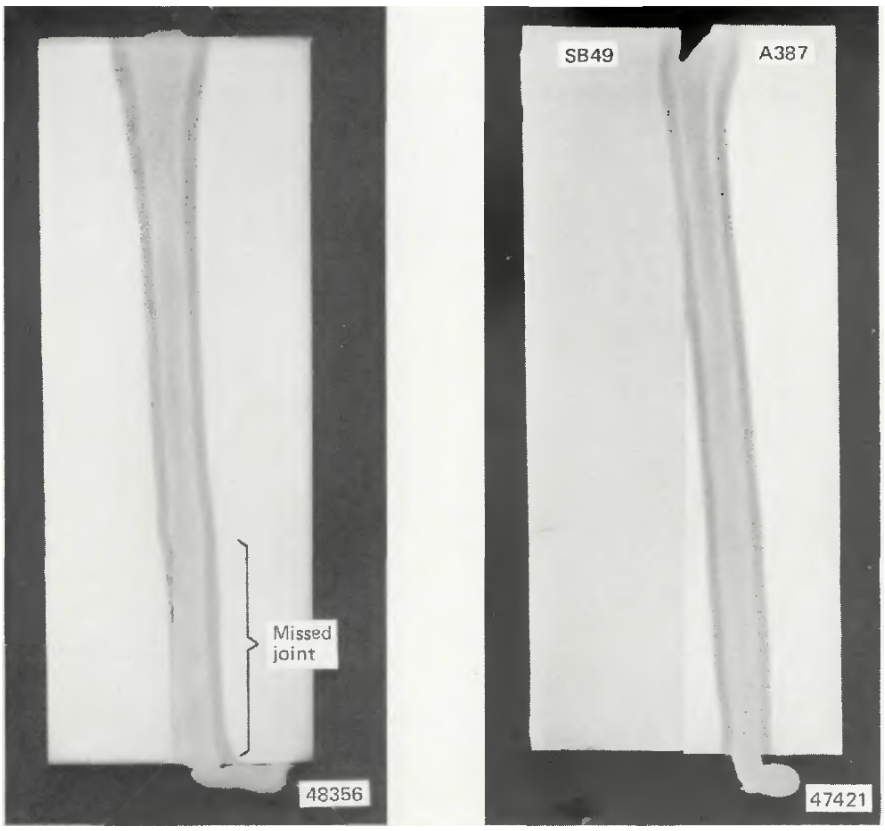

Figure 26. EB weld in 150 mm thick A387 (2¼ Cr-1Mo steel) with 3.5 G parallel to the joint (left), and dissimilar metal EB weld in 150 mm SB49 (C-Mn) steel and A387 (2 ¼ Cr-1Mo) steel (right) (From Blakeley [61], reprinted with permission from American Welding Society).

Large components such as the deep-penetrating EB welds for upper and lower reactor vessel welds being evaluated by EPRI were demagnetized using an AC magnetic field. Although EPRI took precautions to avoid magnetizing the assembly, such as not using magnetic lifting equipment, the assembly was found to have a 3–4 G magnetic field near the weld joint after welding and subsequent processing [2]. Neither the weld type and location nor the subsequent processing was detailed in EPRI's report. Unlike small components that can be carried or lifted through an AC magnetic field, the EPRI shell-to-flange assembly was demagnetized by wrapping the leads from the Maurer Magnetics demagnetizer around the unit and varying the magnetic field, as shown in Figure 27. A magnetism level below 2 G was achieved.

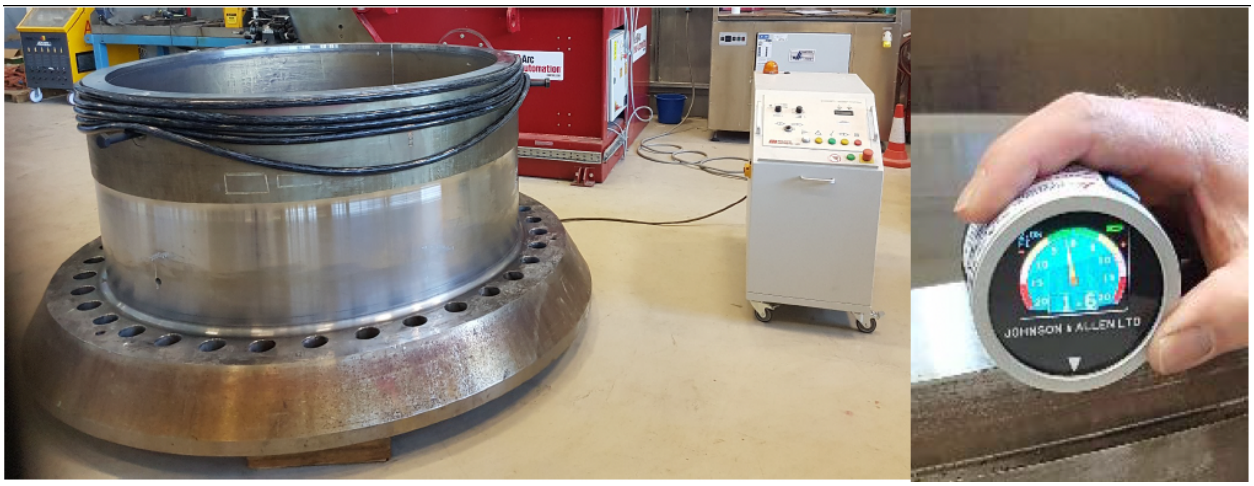

Figure 27. Demagnitization of a shell-to-flange mockup created by EPRI (From Gandy [2], reprinted with permission from Electric Power Research Institute).

2.4.14 Weld Profile and Parameter Effects on Solidification Cracking Susceptibility

Welding parameters affect the susceptibility of solidification cracking as a result of changes in the temperature gradient as seen within the solidification temperature range and the grain orientation during solidification. This thermal gradient affects the microstructural evolution and localized stresses and strains at the solidifying surface [66]. The thermal profile / stress profile can be affected by changes in the welding parameters. Speeding up or slowing down will change the rate of solidification, thereby affecting the stresses that form. A study by Lacki to model stress levels of EB welds at different travel speeds resulted in higher measured transverse and longitudinal stresses at faster travel speeds in chrome nickel steel [67]. The highest tensile and compressive strains coincide with the fastest travel speed [67].
The morphology of the solidified region can also affect the solidification cracking susceptibility. A high-speed EB weld will form a tear-drop shape weld pool, extending the weld pool further behind the impinging EB. This tear-drop shape converges to a near point with a linear fusion boundary. Grain growth rates along the solidification zone are very high, and there is a large amount of similarly oriented grains. Through competitive growth, grains orientated along the maximum heat-flow direction are preferred and dominate the solidification boundary. This allows for many similarly oriented grains to converge, forming a linear segment of high strain on the last-to-solidify metal. This last-to-solidify liquid film accumulates the remaining lower temperature segregates and impurities. The large grains and lower temperature segregates increase the crack susceptibility of the material, forming a crack during solidification or in the partially melted zone (PMZ) [59, 66, 68-74].

In a paper on welding of unique and advanced alloys, David and Vitek discuss how a method of arc oscillation can be applied during GTAW that can help randomize the grain orientations [68]. This technique can be used by EB welders through deflection of the beam to interrupt the solidification boundary of an otherwise teardrop-shaped weld to reorient the solidification front. System manufacturers have default shapes that may be used, or a fully customizable pattern can be programmed. Some examples can be seen in Figure 28. The paper does not address whether these shapes were developed for specific applications or to demonstrate the capability.

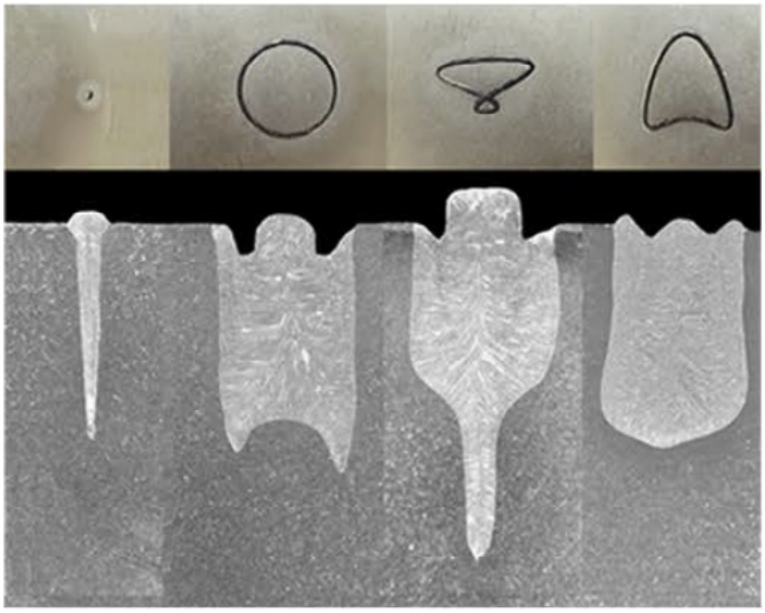

Figure 28. Beam raster patterns (From [13], reprinted with permission from PTR-Precision Technologies).

2.4.15 Post-Weld Heat Treatment and Multiple Beam Processing

Electron manufacturers have developed advanced beam control systems with very fast scanning speeds. Pro-Beam demonstrated the use of this technology in *multibeam processing*. Figure 29 shows three welds occurring at the same time on a planar surface. This is accomplished by positioning one beam to three different positions at extremely fast intervals. The frequency of switching from one weld to the next occurs quickly enough to maintain the molten pool at each weld location for the duration of the weld. This approach can be applied as shown to reduce distortion around the joint by symmetrically welding around the part.

The multibeam technology can also be used to perform preheat and post weld heat treatment during the weld operation. The beam in this case is shared by three or more zones. For preheat, the beam is rastered ahead of the advancing weld to heat up the material prior to the fusion pass. A scan behind the fusion pass can be performed to post-weld heat-treat the steel. This methodology can be used during fusion welding, or it may be programmed to raster across the weld in a more traditional PWHT method. Chen investigated the use of EB local post-weld heat-treatment on a 30CrMnSiNi2A steel. Improvements to the fusion and HAZ microstructure were achieved, increasing the fracture toughness and fatigue crack resistance [75].

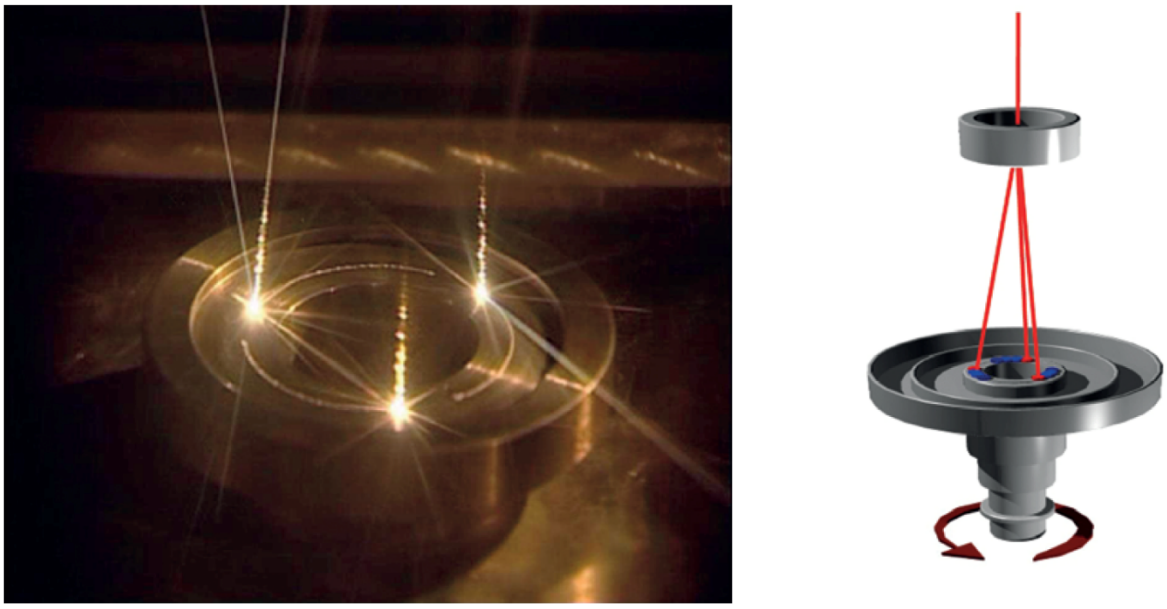

Figure 29. Multi-pool welding (From Adam et al. [4], reprinted with permission from Pro-Beam).

PWHTs completed using the EB were investigated by Sebastiano when welding SA508 to 316L. Sheets of 10 mm thickness were EB welded using a 60kV accelerating voltage, 120 mA beam current, and 1 m/min travel speed. The weld was allowed to cool to room temperature and then underwent PWHT by oscillating the beam in a rectangular pattern over the weld of 30 × 14 mm (transverse × longitudinal). A beam current of 85 mA and a travel speed of 0.10 m/min was used to reach a temperature of 560°C at a depth of 5 mm. A reduction in the weld metal hardness was achieved through EB PWHT, as shown in Figure 30.

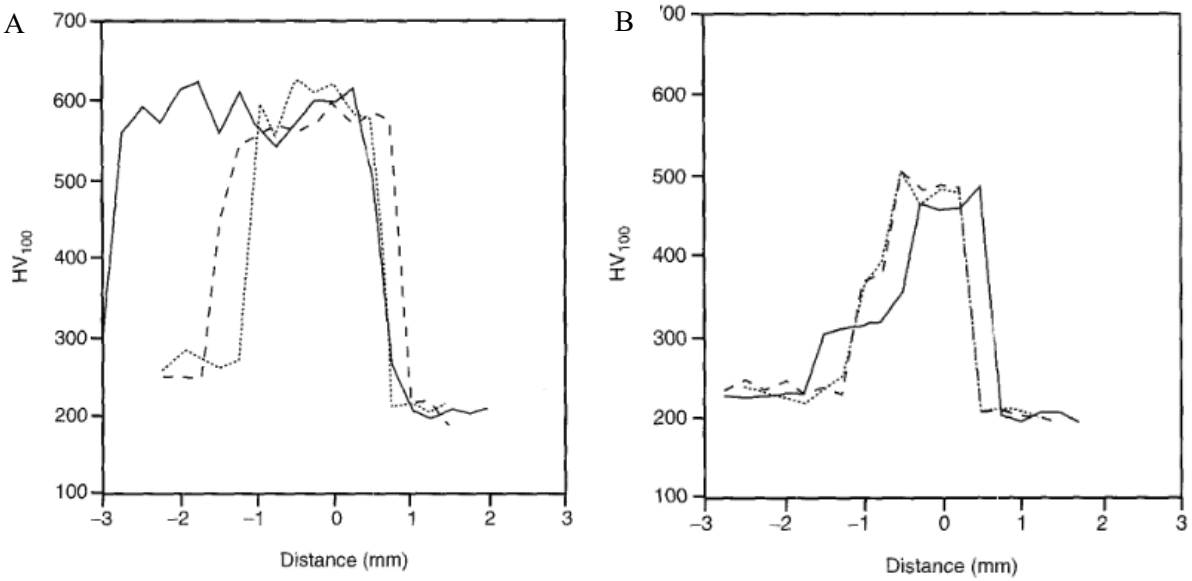

Figure 30. Hardness traces of SA508 to 316L EB weld as welded (A), and after PWHT by EB (B): solid line, 2 mm depth; dashed line, 5 mm depth; dotted line, 8 mm depth (From Sebastiano et al. [76], reprinted with permission from Springer Nature).

2.4.16 Porosity

Welding in a vacuum environment helps eliminate the formation of porosity. However, porosity can occur as a result of process development, material, or loss of cleanliness of the piece parts. Full penetration EB welds have the least incidence of porosity because the keyhole penetration goes through the entire thickness of the weld joint. A partial penetration weld is more likely to form pores in the weld from the entrapment of gas and/or turbulence of the molten pool at the root of the weld [3]. Porosity formation has been studied extensively in laser welding. Because of the common high-energy density of EBW much of the physics involved are shared. Two main forms of porosity formation have been characterized: root porosity, and uniform porosity [77]. These forms of porosity formation much more commonly studied in laser beam welding, where atmospheric pressure and shield gases are used. The mechanisms are similar for EBW in that a sharp root penetration may collapse during welding, folding the molten weld metal over the root and creating a pore. The vacuum environment used in EBW eliminates uniform porosity in welds when materials are clean and free from entrapped gasses. Tack welding of components by arc welding must be sufficiently shielded prior to EBW to reduce porosity and oxygen pickup in the EB weld. Porosity in EB welds have been traced back to inadequately shielded tack welds. Entrapped oxygen and nitrogen in steels can contribute to porosity formation. An oxygen and nitrogen content of less than 150 ppm in steels was recommended to prevent porosity [65]. Supplemental material requirements are sometimes needed for materials to be EB weldable without forming pores. Fast cooling rates and the absence of deoxidizers common in filler materials for arc welding limit the ability of the weld pool to outgas and cause porosity.

To overcome the root porosity that may form through a turbulent weld pool, the weld schedule can be defocused to lessen the sharp intensity of the beam impingement area. Unlike laser welding, EB reflection at varying intensities is not significant. A slight decrease in depth of penetration occurs with a more rounded root of the weld. An example of this is shown in Figure 31 [55].

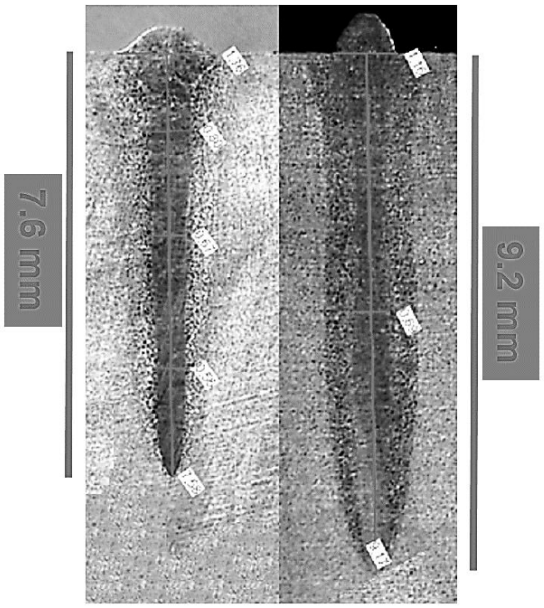

Figure 31. Welds performed at different spot sizes with same energy input (From Liebig et al. [55], reprinted with permission from Electrotechnica & Electronic).

2.4.17 Cleanliness of the Material

Cleanliness of the material being welded is very important for EBW. The fast speeds of welding and the high-temperature profiles may cause organics and other contaminants to react strongly to the beam and cause a volatile reaction. This may entrap pores or cause variations in the weld, thus leading to a defect. Dirtier materials such as plain carbon steels may release entrapped gases in the material as a result of the lower vapor pressure of the substance and vacuum during welding. This release of entrapped gases can cause momentary spikes in the gun which can terminate the weld [23, 62]. Newer switch mode power supplies can rapidly drop the voltage, subdue the arc, and continue welding, thus making it easier to weld non-vacuum refined materials [62].

Standard cleanliness procedures are required to maintain high quality welds in steels and stainless steels. Cleaning with alcohol and lint-free rags before welding, as well as handling with gloves, is typically adequate.

Aluminums may require additional cleaning because of the tenacious oxide layer. The weld joint is often scraped to minimize the porosity formation in the weld. Acid cleaning prior to welding is a best practice process, but it is not always feasible or practical.

2.4.18 Stress Corrosion Cracking

Low alloy steels (LASs) are generally considered resistant to stress corrosion cracking (SCC) under normal operating conditions for light water reactors [78]. Most occurrences of SCC in LAS have been in boiling water reactor piping in which a thermal load or cyclical loading was present after reactor start-up or shut-down [78]. Reduced susceptibility to SCC is achieved when sulfur content and hardness levels are appropriately controlled. SCC was seen in LASs at intermediate temperatures of 288°C and at hardness values of >350 HV [78]. Weld residual stresses and microstructural grain orientations were found to be important for controlling the SCC propagation in shielded metal arc welds [79]. High-order grain misorientations contributed to higher stress levels at the grain boundary, exasperated by the concentration of S, P, Si, Mn, Nb, oxides, and slag inclusions that also segregated to the grain boundaries [79]. Additional fusion weld passes increased the amount of recrystallization, migration of grain boundaries, and diffusion of carbon from the LAS into the weld metal. SCC of RPV materials is of greater concern in areas of dissimilar metal combinations, particularly those containing nickel-based alloys. Testing conducted by EPRI and NAMRC have shown differences in hardness distribution, residual stress magnitude, and residual stress distribution between EB welds and traditional arc welding practices (see sections 2.8.1., and 2.8.2). Post weld heat treatment has been shown to reduce the hardness values and residual stress levels in the weld metal and HAZ of EB welds. Hardness was reduced significantly below 350 HV, and residual stress levels were reduced below 100 MPa [2, 44]. PWHT largely mitigates the concern of SCC through reduced hardness and residual stress. Because PWHT would be required by the ASME Code for RPV steels, hardness and residual stress should be sufficiently reduced to limit SCC susceptibility. If EBW were proposed to be used without PWHT, then this issue would require careful investigation to ensure that there would be no increase in SCC susceptibility from elevated hardness and residual stress as compared to arc welds.

2.4.19 Irradiation Embrittlement

One of the primary issues for welds in a nuclear environment is neutron degradation. Ideally, welds should be moved away from the beltline of the reactor vessel (i.e., the area directly surrounding the reactor core) because of its high flux [80]. EB welds benefit from the use of traditional materials with

known environmental effects. Copper has been shown to be deleterious to welds exposed to the neutron radiation in a reactor. EBW would not necessarily require a filler material, so this eliminates one source of copper contamination. A cleaner steel with less amounts of trace element impurities could be used to minimize radiation effects [80-82].

Odette and Lucas [80] have studied the mechanisms of embrittlement through the formation of copper-rich phases (CRPs), unstable matrix defects (UMDs), and stable matrix features (SMFs). These nanostructures are the result of impingement of high-energy neutrons on the cellular structure of the LASs. The combination of the irradiation-induced nanofeatures and fine-scale Mo_2C results in an increase in yield strength directly related to embrittlement of the LASs. The irradiation embrittlement increases the ductile-to-brittle transition temperature (DBTT) with shifts as large as 200°C [83]. The microstructure of the weld plays a significant role in the irradiation embrittlement of the weld. Tempered martensite was shown to be generally less sensitive to radiation than tempered upper bainite or ferrite structures [84].

Canonico [64] notes that A533 Grade B Class 1 steel was quenched from the austenitizing temperature. In Charpy V-notch tests taken at various positions through the thickness of the sample, a shift was seen after irradiation. The sample near the surface that cooled faster resulted in a microstructure of lower bainite with an upward shift of 27°C after exposure to a fluence of 5×10^{19} n/cm^2 [85]. The same material at quarter thickness and a fluence of 4×10^{19} n/cm^2 shifted by 57°C [85]. These differences are due only to the variation in microstructure. Because of its faster cooling rate after austenitizing, the top surface contains a lower transformation product (lower bainite structure) than that observed at the quarter-thickness location [64].

The microstructures reported in EB welds are martensite and bainite. Gandy and Baufeld have demonstrated full penetration welds with martensitic and bainitic structures comparable to that seen in the base metal after heat treatment. Based on the resultant microstructure, EB welds are expected to outperform conventional arc welding processes with respect to embrittlement, but this should be validated by testing.

No published material could be found on the irradiation of PM-HIP SA508 EB welds.

2.5 NONDESTRUCTIVE EVALUATION

In addition to radiographic examination, and either liquid penetrant or magnetic particle inspections, full penetration EBW is required to be ultrasonically examined per ASME Section III NB-5277 [86]. The following sections were compiled to provide EB-specific information for commonly used radiographic examination/testing (RT) and ultrasonic examination/testing (UT).

2.5.1 Radiographic Examination/Testing / Computed Tomography

Radiographic examination, also referred to as *radiographic testing* (RT) of welds, is commonly used to determine weld quality, particularly for volumetric indications of what may be porosity or voids. Radiography and computed tomography (CT) both rely on the use of x-ray exposure on a film or detector, with the suspect weld between the source and detector. RT will reveal Indications that cause a deviation in density of the material's through thickness. Less dense features such as porosity will be darker, whereas higher density indications will be revealed as bright spots. The resolution achievable through RT depends upon the density and cross-sectional area of material to be penetrated by the x-ray. Thicker weld joints will require higher powered x-ray sources, and the resulting images will have less resolution compared to those of thin sections. Line-to-line defects such as cracks and incomplete joint fusion are not easily identified by RT because there is little-to-no change in the defect's cross sectional density. Full penetration welds are less prone to root porosity and voids because the through thickness keyhole allows

for gasses to be expelled through the weld root and reinforcement. Partial penetration welds are more likely to generate root porosity and voids because of beam instabilities and the rapidly cooled root of the weld, as discussed in Section 2.4.16. Transition points formed during ramp up or ramp down of the weld are the areas most susceptible to formation of porosity and voids.

RT produces a single image cross section of the weld, revealing low- or high-density indications in the through thickness direction. The location of the indication may take multiple shots from different angles to determine the approximate location within the weld. CT uses a series of x-ray images at various angles to produce a 3D image of the component. CT systems are less flexible for accommodating large components and are primarily used for small components or sections that have been removed from larger components.

When performing a partial penetration weld, a witness feature is sometimes used to validate whether a minimum joint thickness has been achieved. As shown in Figure 32, a witness feature is machined into one of the components making up the joint, often a chamfer on the mating component. The size of the witness feature must be balanced between detectable limits of the radiography equipment and the size of the weld. A weld that achieves full penetration should obliterate the witness feature, providing verification that the entire weld joint was consumed. A common size for penetration depths up to 0.250 in. is a chamfer of 0.005 to 0.012 in. on each leg. An underpenetrated weld does not consume the witness feature (shown on the left), but a full joint penetration fully consumes the witness feature (shown on the right). Although the configuration shown below would not be used in a pressure-retaining weld in an NPP, it demonstrate how a witness feature could be used to permit detection of a lack of penetration in a partial penetration weld when using RT.

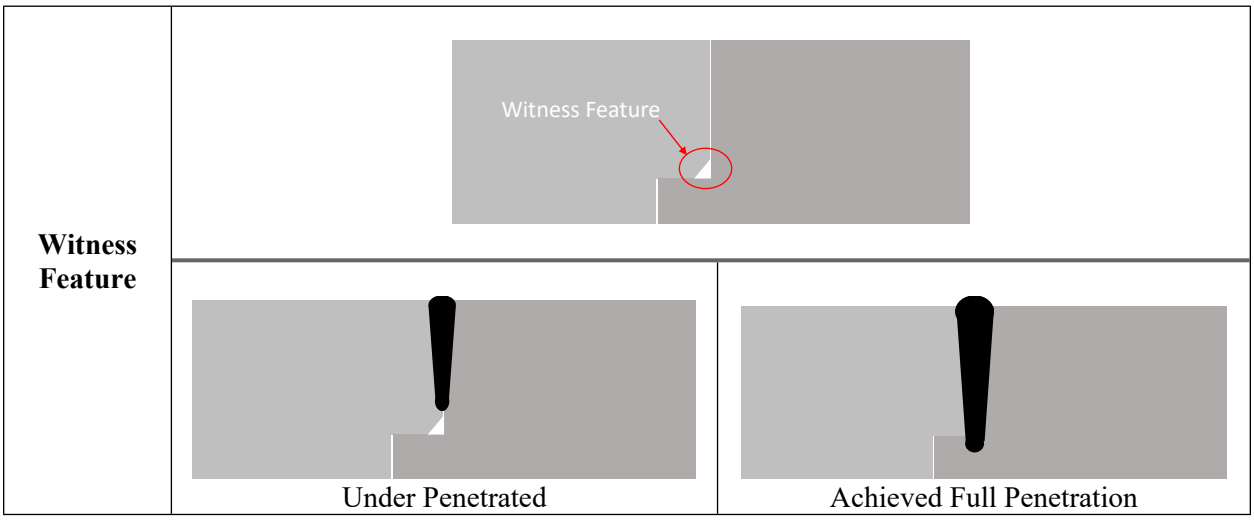

Figure 32. Witness feature added to partial penetration joints for NDE.

2.5.2 Ultrasonic Testing

Ultrasonic inspection of EB welds is commonly used and is required by ASME BPVC for full penetration EBW. For full penetration EBWs in Class 1 components, ASME Code Section III requires UT, in addition to RT to detect linear indications parallel to the weld. These indications could be missed by RT but can be detected by UT. An ultrasonic wave is transferred to the part through use of a piezoelectric transducer. Multiple transducers are often used to evaluate welds, including normal (0°) and angle beam transducers. The two primary sound waves used to evaluate welds are longitudinal and shear waves with velocities of 5,940 m/s and 3,240 m/s in carbon steel, respectively [87]. UT has many advantages, because the process can penetrate thick sections with high sensitivity [87]. Skilled, experienced

technicians are required for proper interpretation. The equipment used for UT varies from portable manual equipment to automated systems with advanced data processing capabilities.

In the analysis of NPP welds in development, including those developed by EPRI, phased array transducers and time-of-flight diffraction (TOFD) techniques have been used. The phased array transducers differ from the standard transducer by allowing multiple incident angles or positions to be scanned at each placement of the transducer. Figure 33 shows conventional transducers at the required positions to inspect the full thickness of the weld joint. In this case, the transducer must be moved from the inner position to the outer position at increments along the length of the weld. A phased array transducer such as that shown on the right can pulse at varying angles of incidence. This allows for an area to be scanned by the UT system with added sensitivity to aligned discontinuities. The use of PAUT allows for volumetric scanning of the weld area with real time imaging of the signal response allowing for easier interpretation of the data.

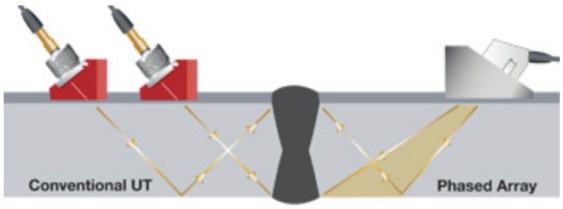

Figure 33. Conventional transducers (left), and phased array transducer (right) (Courtesy of Olympus [88]).

TOFD is commonly used for weld testing circumferential and axial weld seams [88]. The technique uses two transducers placed on opposite sides of the inspection area. One transducer is used as the source of the ultrasonic wave, and the other transducer is used to receive and record any diffracted signals. Unlike traditional UT inspection, TOFD detecting the large amplitude reflections. Instead, the diffracted signals caused by impinging upon a crack tip or other anomaly are sought. The time-of-flight (TOF) data and intensity of the diffracted signals provide precise information about the location and size of the anomaly. A small portable TOFD setup is shown in Figure 34. Mechanized systems can be fitted to tracks for automated inspection.

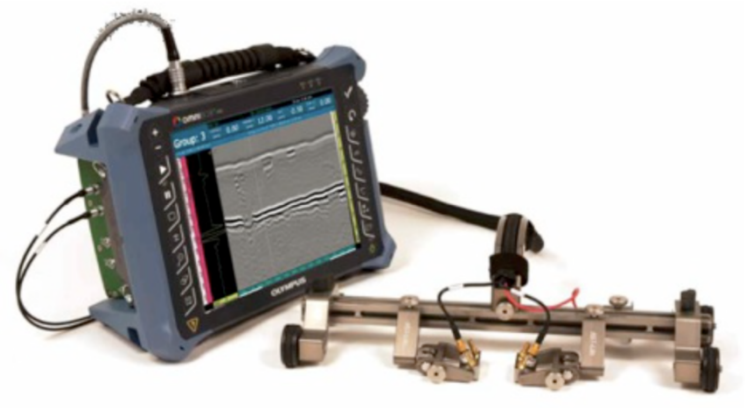

Figure 34. Portable TOFD system (Courtesy of Olympus [89]).

2.6 MICROSTRUCTURE AND WELDABILITY

EBW can be used on many different alloys. This section focuses on the aspects of welding stainless steels and carbon/LASs. Other alloy systems will be covered as an introduction to EBW for these alloys. To some extent, the energy input can be advantaged to minimize its effect on the material properties through

the thermal effects of welding. Two metallurgical zones will exist after welding: the fusion zone (FZ), which consists of material that was melted and subsequently resolidified, and the HAZ, a region immediately outside the FZ that was exposed to a high-temperature cycle without gross melting. Some alloys may have an extremely narrow HAZ, depending upon the solidification temperature range. AWS summarizes metallurgical effects that can take place in the HAZ and FZ shown below [15].

A. Heat-affected zone (HAZ)
    a. Annealing, solution annealing, recrystallization, and grain growth
    b. Phase transformations, tempering, and age hardening
    c. Liquation and hot cracking
    d. Sub-solidus cracking
B. Fusion zone (FZ)
    a. Grain structure and orientation
    b. Phase transformations
    c. Segregation, precipitation, and cracking
    d. Dissolution of gases and porosity formation

Two unique aspects of EBW that separate it from traditional arc welding processes are (1) fast welding speeds which produce fast solidification rates, and (2) welding under a vacuum. Fast solidification rates can influence the microstructural evolution of the weld metal. As mentioned by Carl Cross [66] in Section 2.4.14, grain growth will occur along the direction of the highest temperature gradient, often resulting in long columnar grains. Precipitation of solutes and strength gained through thermomechanical processing of the base material will be eliminated in the FZ. Bulk properties of the material will remain, and some elements will be lost from alloy depletion of lower vapor pressure elements. EBW in a vacuum will reduce the atmospheric absorption of detrimental hydrogen and oxygen, but a loss of low melting point elements in the base metal may affect final weld properties [15].

2.6.1 Solidification Cracking

Solidification cracking, also known as hot cracking, is often a result of three factors: a susceptible material (alloy composition), high restraint in the weld metal (weld fixturing), and/or a thermal cycle conducive to weld solidification cracking (welding parameters) [66]. This is well portrayed by Carl Cross in Figure 35. A cracking conference convenes regularly and has published the proceedings, [70-72, 90].

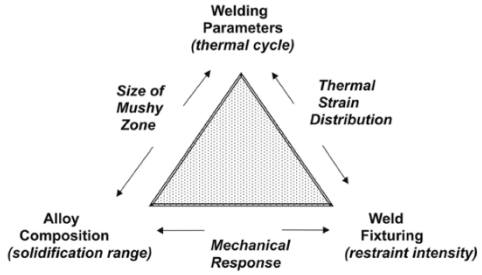

Figure 35. Solidification cracking (From Cross, [66] reprinted with permission from Springer Nature).

It is important to understand the current theory of solidification cracking. Zacharia observed that cracking did not always occur at the trailing edge of the weld as previously believed and proved that a compressive stress behind the weld pool delayed solidification cracking, as shown in Figure 36 [69]. The conclusion that a liquid film at grain boundaries failed as a result of the dynamic stresses is the current topic of study. Solidification cracking is currently understood as a rupture of liquid films that undergo a tensile stress

during solidification [66, 90]. EBW, with its high-energy density, results in high-temperature gradients and elevated stress levels that may enhance crack sensitivity in some materials [59, 66, 91]. Manufacturers have developed multibeam electron optics that raster the beam to multiple positions at extremely fast speeds. This technology has been used to slow cooling rates, modify weld pool shapes, and deliver post-weld heat treatments during completion of the welding pass. Further research is required to prove its capabilities.

Alloy composition is one factor of solidification cracking and is difficult to generalize for all alloy types. Many EB joints are designed without the need for additional filler materials. Unlike many materials, for which a general understanding of weldability is sufficient, EBW requires more attention to base metal selections. In wire-fed EBW, a favorable alloy added to improve the weld's alloy composition. This process can be difficult or impossible, depending upon the geometry of the part and access to the weld pool. Alloys with high thermal expansion coefficients, such as stainless steels, and high solidification shrinkage, such as some aluminum alloys, add to the cracking susceptibility [92].

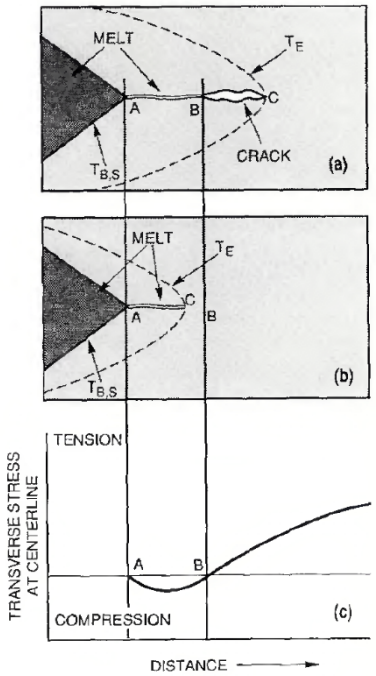

Figure 36. Compressive and tensile stresses (From Zacharia [69], reprinted with permission from American Welding Society).

2.6.2 Stainless Steels

Austenitic stainless steels are some of the more common alloys that are welded. These alloys are processed with a solution heat treatment in which the primary phase is austenitic. Welding of these alloys can produce a dual phase weld metal consisting of ferrite and austenite, the balance of which affects the ductility, strength, corrosion resistance, and crack susceptibility of the alloy. Many publications addressed changes in the solidification behavior of austenitic stainless steels in the 1980s. Many of these behaviors were evaluated using conventional arc welding methods (Suutala [93], Lippold [94-96]), and high-energy density welding was addressed by David [97], Lippold [98] and Elmer [99], among others.

Upon rapid solidification, the primary phase morphology can shift [99]. As shown in Figure 37, a shift in solidification mode from primary ferrite solidification to primary austenite solidification may occur at faster travel speeds: faster grain growth rates resulting in dendrite tip undercooling [97, 100].

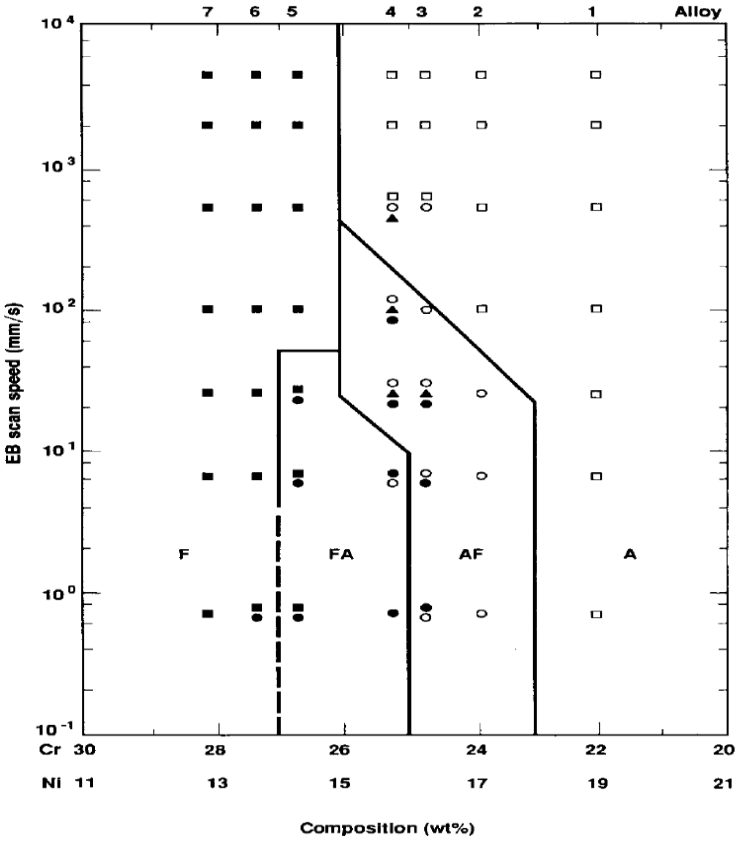

Figure 37. Predictive solidification mode depending upon welding speed (From Elmer et al. [99], reprinted with permission of Springer Nature)

The construction of a Cr/Ni equivalency was completed by Suutala [93]. This equivalency has been used extensively in austenitic stainless steels to determine the solidification mode and been established as a requirement for procurement of the raw material by some users. A table developed by Suutala is included as Figure 38 for arc welding processes. The solidification mode and the amount of impurity contents in the base metal important considerations for austenitic stainless steels. Impurities such as sulfur, phosphorous, and boron are known to cause solidification cracking in arc welds and EBW. Leinert performed a weldability study of various austenitic stainless-steel alloys of varying Cr/Ni equivalencies and impurity contents. Leinert was able to revise the Suutala diagram for rapid solidification mode welding. In Leinert's study, alloys initially solidifying as austenite would crack when below 1.59 Cr/Ni eq. and greater than 0.02 wt% impurity content (P+S)[101]. A Cr/Ni eq of 1.59 is recommended for alloys containing normal impurity levels (<0.02 wt% P+S), and a 1.69 Cr/Ni eq is recommended when impurity levels are higher than 0.02 wt% for rapid solidification processing [101].

When rewelding austenitic stainless steels, the change in chemistry resulting from multiple cycles of welding should be considered. Rodelas investigated the change in laser weld solidification mode during rewelding of 304L base material of nominally excellent chemistry: 1.8 Cr/Ni eq. After as few as three rewelds, the solidification mode could be seen changing from primary ferrite to primary austenite as a

result of selective alloying loss through vaporization during rewelding, with cracks forming at three rewelds [102]. This was completed using laser welding, but because of its similar high-energy density, those implementing EBW should be aware of this potential shift in solidification mode and solidification cracking susceptibility.

AF = Austenitic-ferritic (fraction > ¾)
FA = Ferritic-austenitic (fraction > ¾)
AF + FA = Both modes

Code	Cr_{eq}/Ni_{eq}	Welding Speed, cm/min					
		2.5	5	10	20	40	80
AF1	1.38	AF	AF	AF	AF	AF	AF
AF2	1.45	AF	AF	AF	AF	AF	AF
AF3	1.49	AF	AF	AF	AF	AF	AF
AF4	1.51	AF	AF	AF	AF	AF	AF
X1	1.54	AF + FA	AF + FA	AF + FA	AF	AF	AF
X2	1.54	FA	FA	AF + FA	AF + FA	AF	AF
X3	1.54	FA	FA	AF + FA	AF + FA	AF + FA	AF
X4	1.55	FA	FA	FA	FA	FA	AF + FA
FA1	1.57	FA	FA	FA	FA	FA	FA
FA2	1.61	FA	FA	FA	FA	FA	FA

Figure 38. Change in solidification mode due to welding speed (i.e. dendrite tip undercooling) (From Suutala [93], reprinted with permission from Springer).

Ferritic stainless steels will solidify as ferrite as a result of their high chromium and other stabilizing elements (i.e., Al, Nb, Mo, and Ti). Some austenite may form upon cooling in alloys with high interstitial contents. This austenite may then transform to martensite upon further cooling, which may affect the ductility of the weld metal. Note that the grain growth and carbide formation in the HAZ reduce toughness and corrosion resistance [15].

Martensitic grades of stainless steels are similar to carbon and LASs in which a subsequent tempering heat treatment of the martensitic structure is necessary to improve toughness and ductility [15].

Precipitation-hardened alloys are weldable, but cracking may occur as a result of the lack of toughness in the HAZ and the FZ. A preheat may be necessary as a result of the higher carbon content. EBW can be completed with suitable pre- and post-weld heat treatment to temper the martensite and to relieve residual stresses in the material. Application of these heat treatments may be more costly or difficult because the fixturing and equipment are required to work with the EB welder. During welding, the precipitates will be dissolved in the FZ, resulting in a loss of strength. Additional heat treatment is necessary to re-establish the precipitates to regain strength. Of the precipitation hardened alloys, the austenitic grades remain difficult to weld because of cracking in the HAZs and FZs [15].

2.6.3 Carbon and Low Alloy Steels

Carbon and LASs are generally used because of their higher strength properties which may correspond with a higher level of residual stress upon welding. Hydrogen sensitivity, commonly of great concern during arc welding, is mitigated through use of a vacuum environment during EBW. Carbon contents greater than 0.2 wt% may harden significantly, requiring additional attention to phosphorous and sulfur content to prevent hot cracking. The AWS recommended practices for EBW note that preheat and PWHTs of low carbon (<0.25 wt.%) may be needed, whereas with high carbon (>0.50 wt.%), they are required. ASME Code Section III requires PWHT of all carbon steel and LAS welds (Table NB-4622.1-1). Some exemptions to these requirements are provided in the Code based on material type, carbon

content, thickness, and the application of a specified preheat. However, none of these exemptions could be applied to heavy section welds (Table NB-4622.1-1). The effect of carbon content on toughness is shown in Figure 39. Heat treatments completed using the EB as the heat source are sometimes successful, depending upon the thickness of the joint and mass affecting the cooling of the joint [15]. However, this method of heat treatment would not be applicable to heavy section welds.

Carbon equivalence (CE) is often used to evaluate the need for preheat and PWHT. A higher CE value represents the material's higher hardenability and lower weldability. A value below 0.35 is generally regarded as very weldable, with reduced hydrogen cracking susceptibility. The ASME equation for carbon equivalence is shown in Equation 1 [3, 15].

$$CE = C + Mn6 + Cr + Mo + V5 + Cu + Ni15 \quad (1)$$

Carbon Equivalence – ASME BPVC SEC IX – QW-403.26 [50]

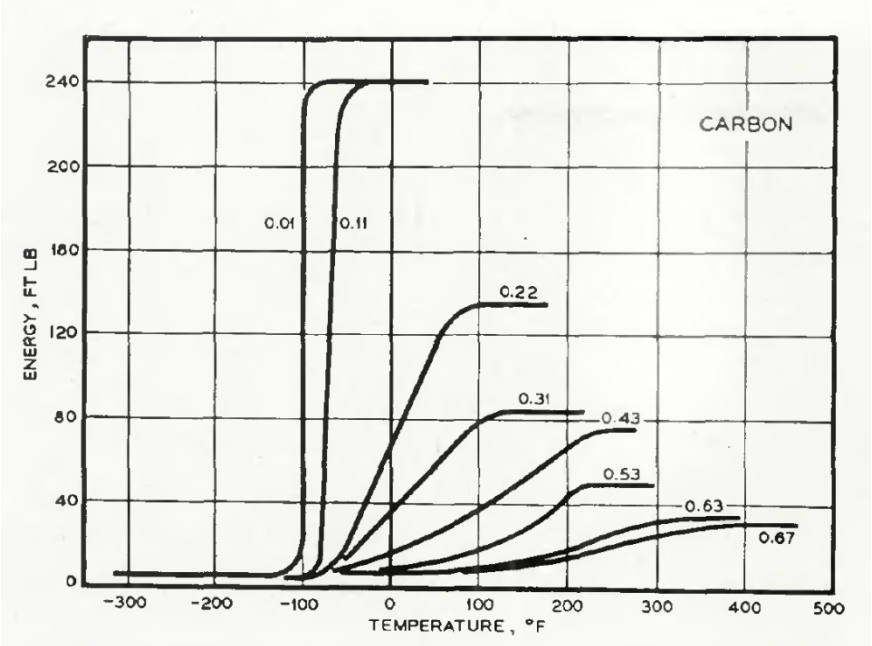

Figure 39. Charpy V-notch toughness as a function of wt% carbon content in steels (From Canonico [85]).

2.6.4 Reactor Pressure Vessel Steels – Base Material Properties

Typical RPV steels have a CE value of about 0.62 [103]. This relates to a higher amount of austenite stability in these steels, leading to a propensity to form martensite and bainite [103]. Therefore, a greater amount of hardenability is expected. Reported CE values for SA508 Grade 3 steels have been reported in the range of 0.54 to 0.67 for forged materials used by Suzuki [104] and between 0.55 and 0.69 for PM-HIP heats proved by Carpenter for research at EPRI [7]. Chemical requirements of SA508 steels taken from ASME BPVC Sec II are listed in Table 7. SA508 Grade 3 Class 1 and 2 steels have identical chemical composition requirements, but the tensile strength requirement for Class 2 is higher, with a

slight reduction in minimum ductility. As may be expected, Class 2 chemical compositions are often reported in literature with higher carbon contents than Class 1 alloys to meet the higher tensile requirements. SA508 Grade 4N alloys have been investigated for use as a pressure vessel steel with improved strength, toughness, and transition temperature [105, 106]. Sulphur and phosphorus are reduced in Grade 2, 3 and 4N alloys. Both elements are known for their deleterious effects on cracking susceptibility: phosphorus has been linked to reduced fracture toughness [65], whereas sulfur has been linked to faster crack growth rates in fatigue tests [107].

Table 7. RPV steel chemical composition (wt%, not all elements shown) [108]

Steel	C	Mn	Si	P*	S*	Cr	Mo	Ni
SA508 Grade 3	0.25	1.20–1.50	0.40	0.015	0.015	0.25	0.45–0.60	0.40–1.00
SA508 Grade 4N	0.23	0.20–0.40	0.40	0.015	0.015	1.50–2.00	0.40–0.60	2.80–3.90
*ASME BPVC Sec II also places restrictions on Grades 2, 3, and 4N Phosphorus: 0.012 heat and 0.015 product, or 0.015 heat and 0.018 product Sulfur: 0.015 heat and 0.018 product Copper: 0.010 heat and product or 0.015 heat and product								

The solid-state phase transformations of upper bainite, lower bainite, and martensite are the primary phases of interest, particularly for SA508 steels. Bainite forms at intermediate temperatures through solid-state transformations, nucleating ferrite at austenite grain boundaries [109]. Upper bainite forms at the higher temperature range of approximately 400 and 550°C, and lower bainite forms between 250 and 400°C. Because carbon is more soluble in austenite than ferrite, the accumulation of carbon allows for carbides to precipitate between the ferrite plates. The number of carbides is therefore related to the carbon content of the steel, with lower amounts of carbides in the low carbon steels. The two forms of bainite are very similar, with a distinction in lower bainite having additional precipitation of carbides within the ferrite grains. The carbides formed may be cementite or other carbides such as M_2C, M_3C, or $M_{23}C_6$ carbides [80, 106, 110] [109].

The continuous cooling transformation (CCT) diagram presented in Figure 40 shows cooling curves from the austenitizing temperature of 890°C. An extremely fast cooling rate (> 900°C/min) will result in a martensitic microstructure, whereas intermediate cooling rates will pass through the bainite phase region and result in a mixture of martensitic and bainitic phases. The amount of each phase present will be affected by the rate of cooling and the previous phases that were present before cooling. SA508 steel is typically used in the quench and tempered condition, consisting of martensite and lower bainite [107]. The austenite grain sizes prior to cooling are of particular interest for RPV steels. Austenite grain size can be restricted by the formation of oxides and carbides at grain boundaries. Because the transformations are in the solid state, diffusion of elements to the grain boundaries will be a function of the distance and time allowed upon cooling [72].

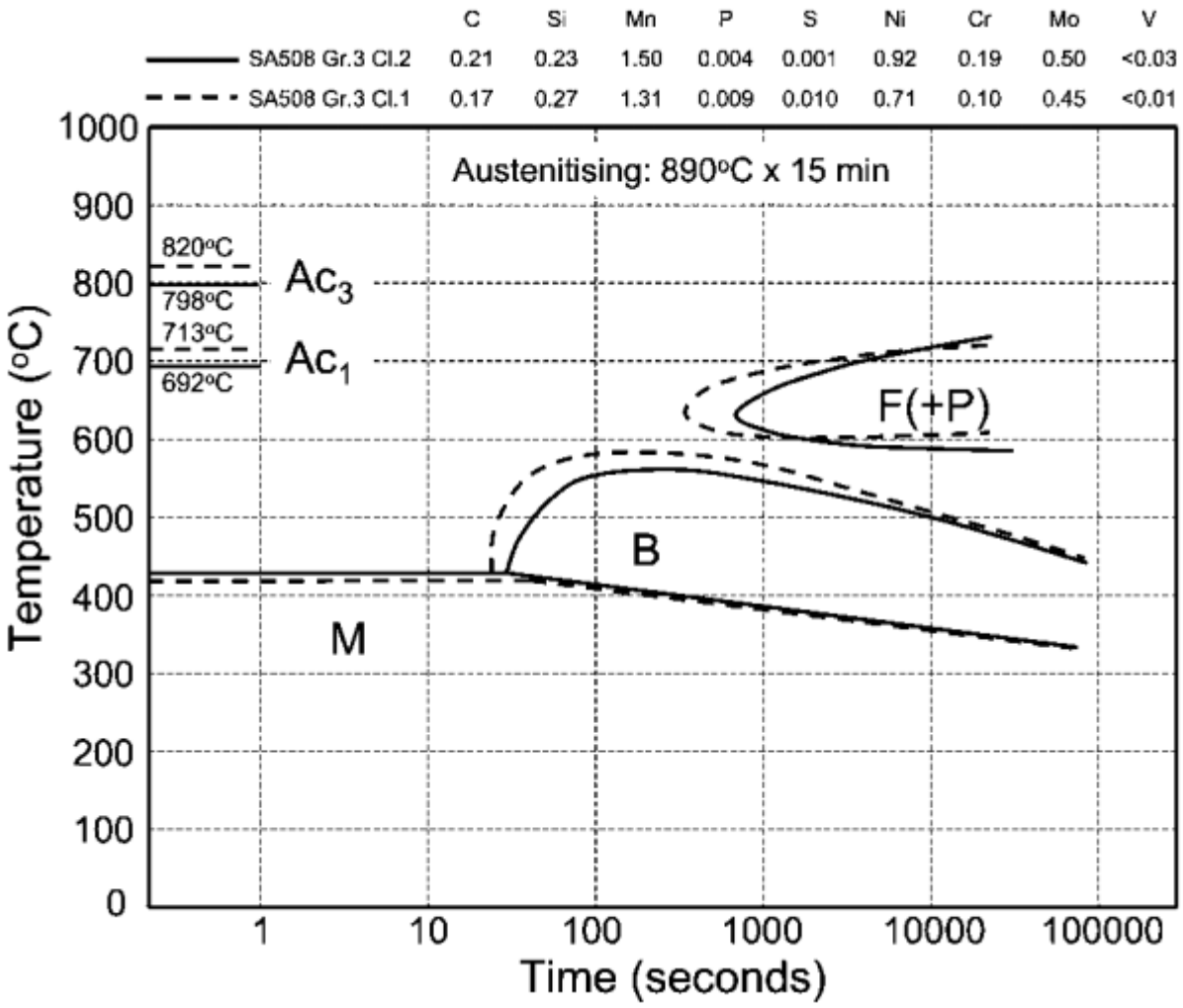

Figure 40. CCT diagram for RPV steel, SA508 Grade 3, Class 1 and 2 (From Suzuki et al. [104], reprinted with permission from Elsevier).

Figure 41 presents metallographs provided by Suzuki from a series of SA508 Grade 3 Class 2 samples subjected to varying cooling rates ranging from 10 to 300°C/min [104]. At the slowest cooling rate of 10°C/min, the material passes through the ferrite and pearlite regions. Black blocky regions are most likely ferrite, with pearlite or bainite shown in light gray, and with the remainder comprised of martensite. From 30 to 300°C/min, a martensitic and bainitic microstructure forms and can be seen in the remaining metallographs. Differences in grain size and bainite lath spacing would be expected, with smaller lath spacing at the faster cooling rates. Suzuki reported little difference in hardness between 15 to 200°C/min, as may be expected based on the similar microstructures [104]. Higher toughness values have been reported in samples containing lower bainite than in those containing upper bainite [65].

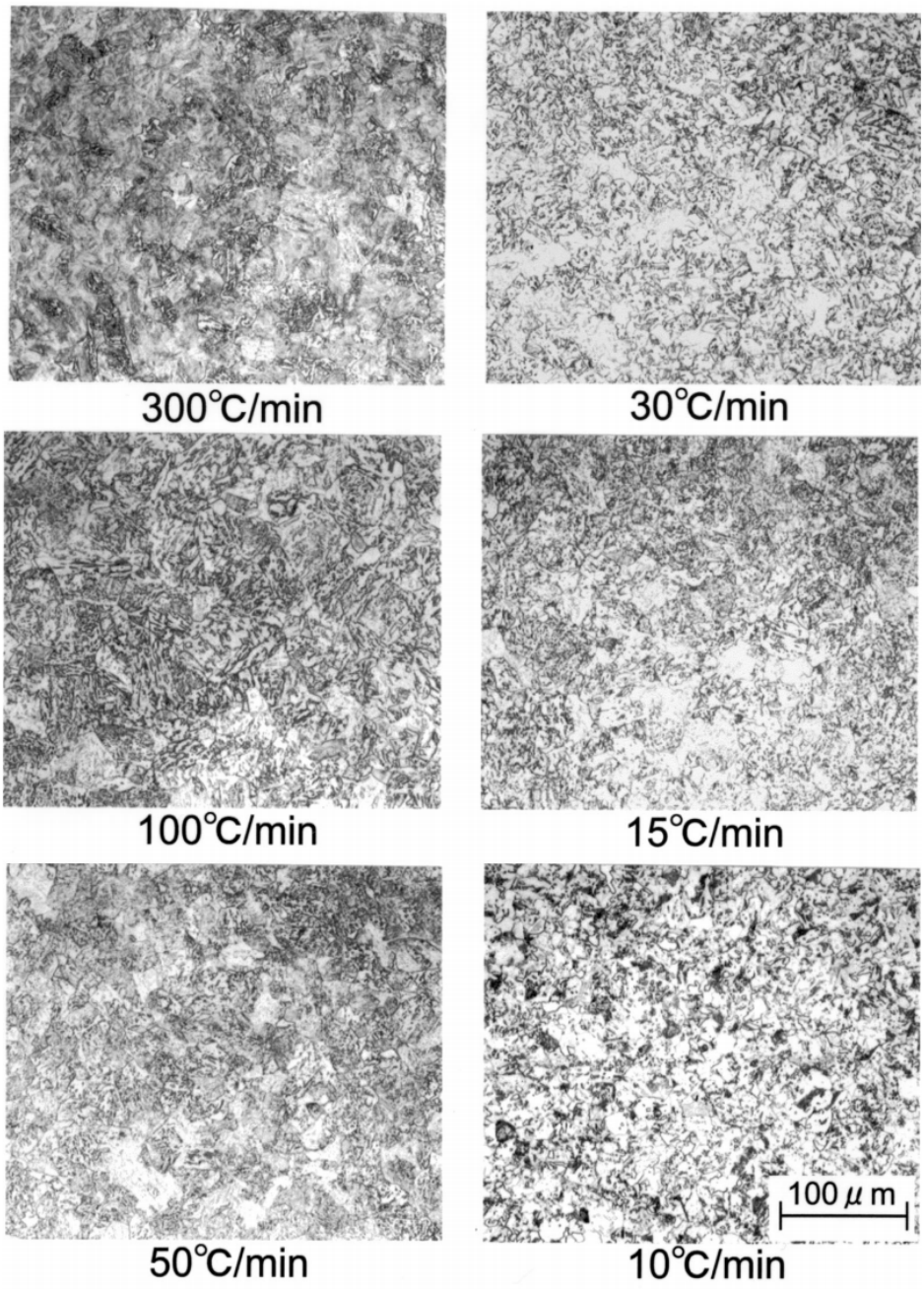

Figure 41. Microstructures produced by quenching at various cooling rates for SA508 Grade 3 Class 2 steel (From Suzuki et al. [104], reprinted with permission from Elsevier).

A base metal characterization performed by Kim [106] of SA508 Grade 3 Classes 1 and 2, as well as Grade 4N steels was completed to determine the microstructures and mechanical properties of the SA508 steels. Microstructure was evaluated using optical metallography and electron microscope techniques. Results of the optical and scanning electron microscopy (SEM) evaluation can be seen in Figure 42. A bainite structure was reported in the SA508 Grade 3 Class 1 and 2 (Figure 42a and b), whereas tempered martensite and bainite were seen in the Grade 4N steel (Figure 42c) [106]. Grain sizes of 13.5 μm, 11.0 μm, and 6.8 μm were reported for each alloy for the Class 1, 2, and 4N materials, respectively, as noted on Figure 43a, b, and c [106]. Precipitates seen in the Class 1 and 2 steel were similar, with long, rod-shaped cementite found along ferrite laths with spherical cementite and fine M_2C type carbides within the

ferrite grains (Figure 43d, and e). More carbides can be seen in the Class 2 material, likely due to the higher carbon content (0.24 vs. 0.21 wt%) reported for these materials. The greater quantity of small carbides may account for the reduced grain size in the Class 2 steel. Kim notes an even finer size of carbides in the grade 4N steel of M_7C, $M_{23}C_6$ morphologies as shown in Figure 43f [106]. Grade 4N steel has a higher nickel and chromium content, as shown in Table 7, thus increasing the amount of tempered martensite in the final microstructure [106].

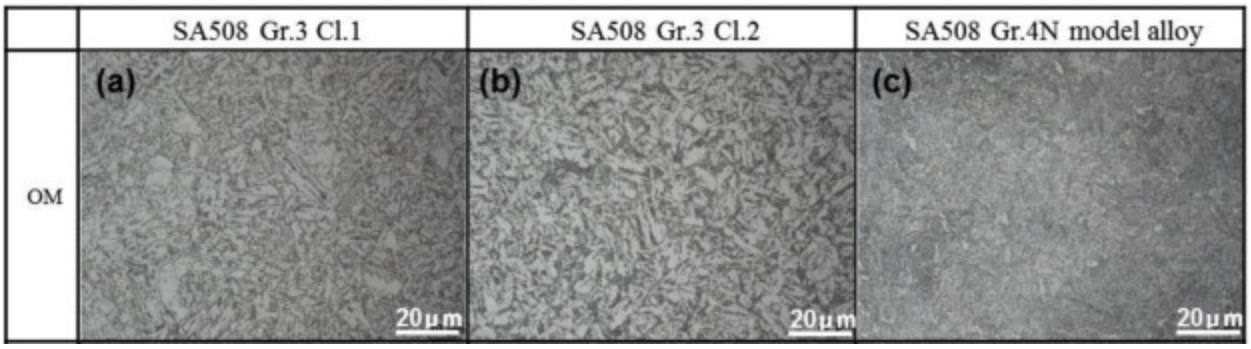

Figure 42. Base metal microstructures for SA508 alloys: Grade 3 Class 1 (a), Grade 2 Class 2 (b), and Grade 4N (c) (From Kim et al. [106], reprinted with permission from Elsevier).

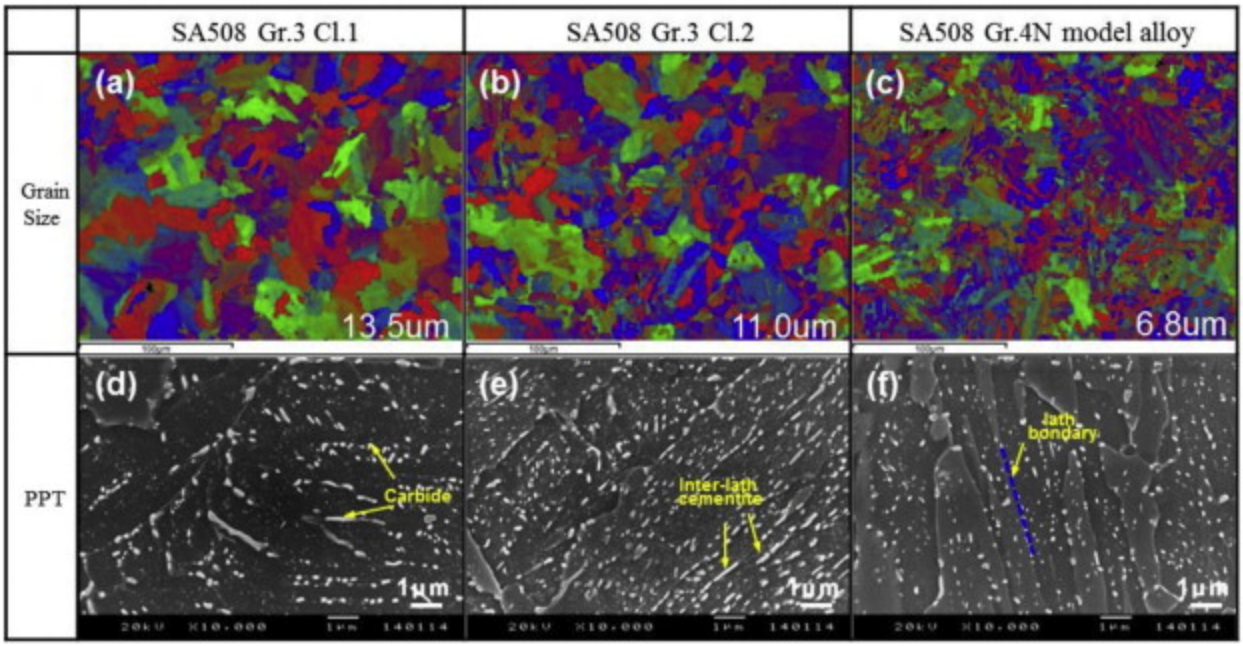

Figure 43. Electron optical images of SA508 alloys revealing grain size and precipitates (From Kim et al. [106], reprinted with permission from Elsevier).

2.6.5 Reactor Pressure Vessel Steels – Arc Welding

Arc welding methods are used to produce the through-penetration weld joints on existing nuclear RPVs. Arc welding is an involved process requiring strict control of filler materials with pre- and post-weld heat treatments. Some weldments were reported to require over 40 hours of PWHT [111]. The resulting weld and HAZ has a complicated thermal history resulting in equally complex microstructural properties of the material. Submerged arc (SA) and shielded metal arc (SMA) welding are typically used for girth weld operations. The filler materials are generally chosen to improve the strength, toughness, or crack susceptibility of the weld metal primarily by reducing carbon content with additions of nickel [65, 85,

112]. Therefore, the chemical composition of the resulting weld metal does not match the base material. The weld's metal chemical composition will depend on the amount of dilution of the filler and base metals that occurred, which may also be a function of the location in the weld procedure specification. The difference in weld metal dilution by categorizing it into regions of high dilution and low dilution, as shown in Figure 44. Each weld FZ undergoes cooling according to its chemical composition and cooling rate. Areas around the FZs and the HAZ will experience temperature profiles imparted upon the material by the many fusion passes used to fill the joint.

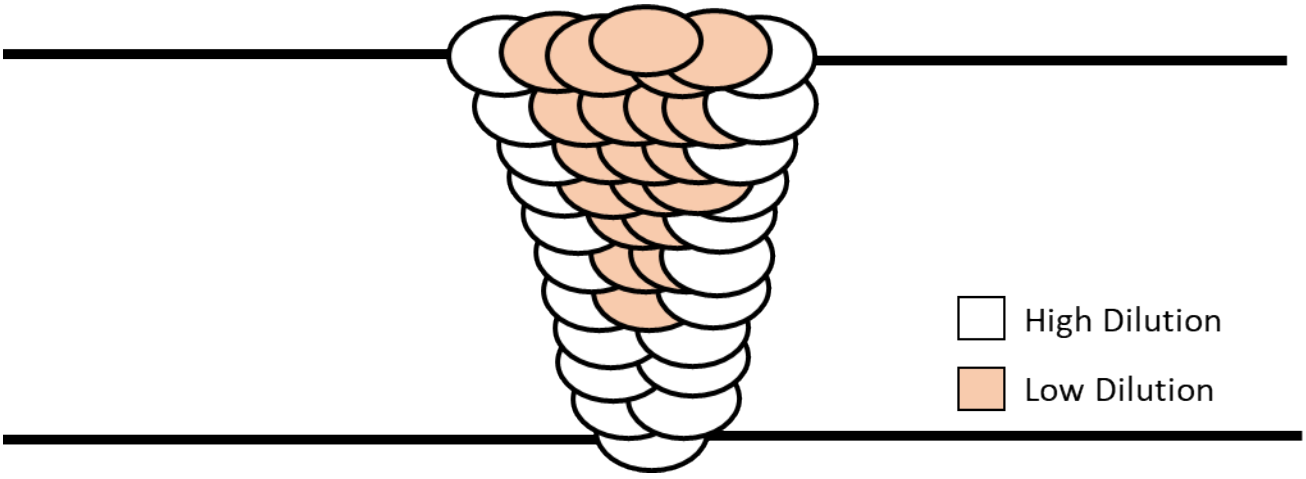

Figure 44. Multipass weld schematic of weld metal dilution.

The multipass welding processes can exhibit a complex microstructure, depending upon the number of passes and thermal cycles to which the material is subjected, as well as prior microstructure evolution. McCabe schematically illustrates potential HAZ microstructures in Figure 45, showing the complex microstructures that result after undergoing peak temperature cycles at various levels above and below the austenitizing temperature [103]. This diagram shows two heat cycles, depicting the additional passes that may be seen in a multipass weld. Figure 45D, which depicts the region of the coarse grain heat-affected zone (CGHAZ), shows large prior austenite grains that grew because of heating to near melting temperature. Upon cooling, the austenite may form martensite under rapid cooling, and it may form martensite with bainite (ferrite and cementite, Fe_3C) at intermediate cooling rates for RPV steels. The formation of martensite and lower bainite results in a lower toughness that can be recovered through PWHT. In Figure 45C, the fine grain heat-affected zone (FGHAZ) shows a region of the HAZ that reaches a temperature just above the austenite transformation temperature, Ac3, resulting in formation of fine austenite grains. This occurs as a result of the presence of precipitates that were not dissolved by the second peak temperature. This precipitates pin grain boundaries, preventing grain growth and resulting in a fine microstructure that transforms to a combination of martensite and bainite with densely spaced carbides, and perhaps retained austenite or granular bainite [112, 113]. Figure 45B shows the intercritically reheated coarse grain zone (ICCGHAZ also reported as ICGHAZ) which lies between the Ac1 and Ac3 temperatures. This results in a mixture of austenite and ferrite precipitated at prior austenite grain boundaries. A phenomenon called *local brittle zone* (LBZ) was seen in offshore welding and was investigated in RPV steels. This phenomenon was not seen in RPV steels as discussed by McCabe and English, a concern of temper embrittlement of the large prior-austenite grains is noted [103, 114]. Prior austenite grain size (PAGS) has been reported to have a significant effect on the sold-state phase transformations (SSPT) by limiting the available nucleation sites [115]. The subcritically reheated coarse grain zone (SCCGHAZ), also referred to as *over-tempered*, is a region of large austenite grains that is reheated below the Ac1 temperature with little change to the microstructure and properties [103, 114, 116].

Because of the many weld passes, tempering of the previously deposited weld beads does occur in multipass arc welds. This results in a lower hardness throughout the FZ, with peak hardness values typically found in the CGHAZ [115].

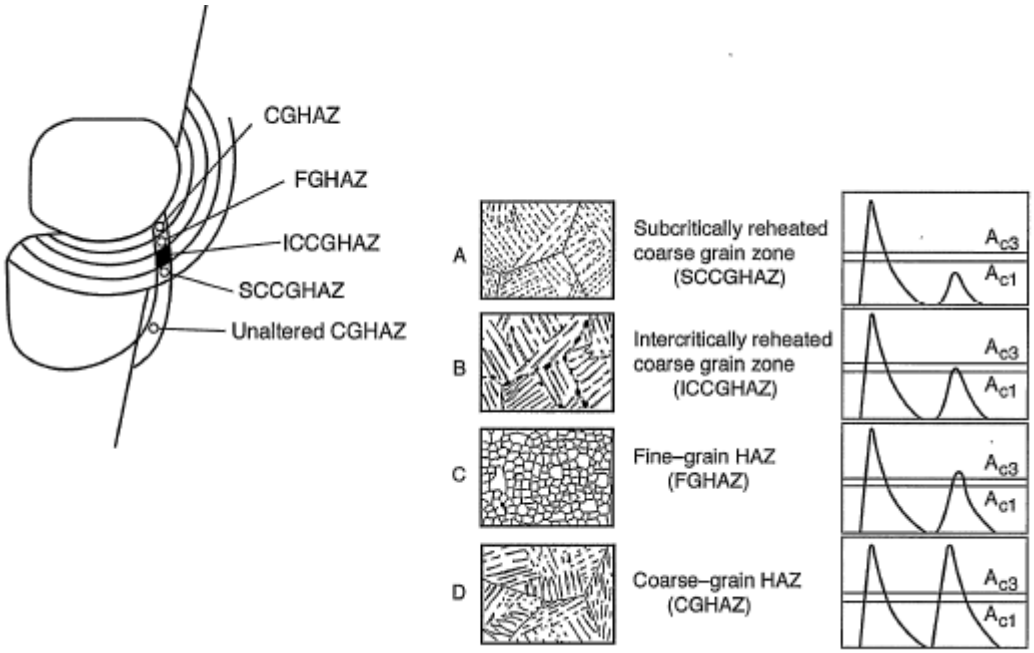

Figure 45. Complex microstructural evolution of RPV steel under various thermal profiles (From McCabe et al. [103]).

Lundin evaluated welding conditions on the microstructure and properties of arc-welded RPV steels. The many cycles of arc welding were found to be essential for optimizing the toughness of the HAZ [111]. The preferred microstructure during arc welding is primarily martensitic because of its superior toughness after PWHT [111]. Welding conditions in general use were said to match suggested cooling rates, resulting in martensite [111].

2.7 ELECTRON BEAM WELDING OF STEELS

Few publications are available for EBW of RPV steels. This section provides a generalized discussion of EB-welded steel mechanical properties. In 1984, Elliot published a paper on welding of carbon manganese steels to investigate the effect of the weld parameters on the microstructure and mechanical properties of EB-welded 75 mm thick BS4360-50D plates. The thick section welds were completed at TWI using an accelerating voltage of 150kV. Elliot notes that the travel speeds that could be used to weld of the thick steel were limited because of the increased restraint in the thick plates, resulting in solidification cracking at higher speeds. Speeds of 100 and 150 mm/min were evaluated. Figure 46A and B show the fracture toughness results for the 75 mm plate trials. Figure 46A shows that for a constant weld width of 3 mm, the curves were not significantly different from those with similar weld microstructures. Considerable improvement was achieved after PWHT. Figure 46B compares the toughness of narrow 3.0 mm and wide 5.5 mm weld width specimens. The wide weld with higher heat input produced a coarser microstructure than the narrow weld, resulting in a decrease in toughness [117].

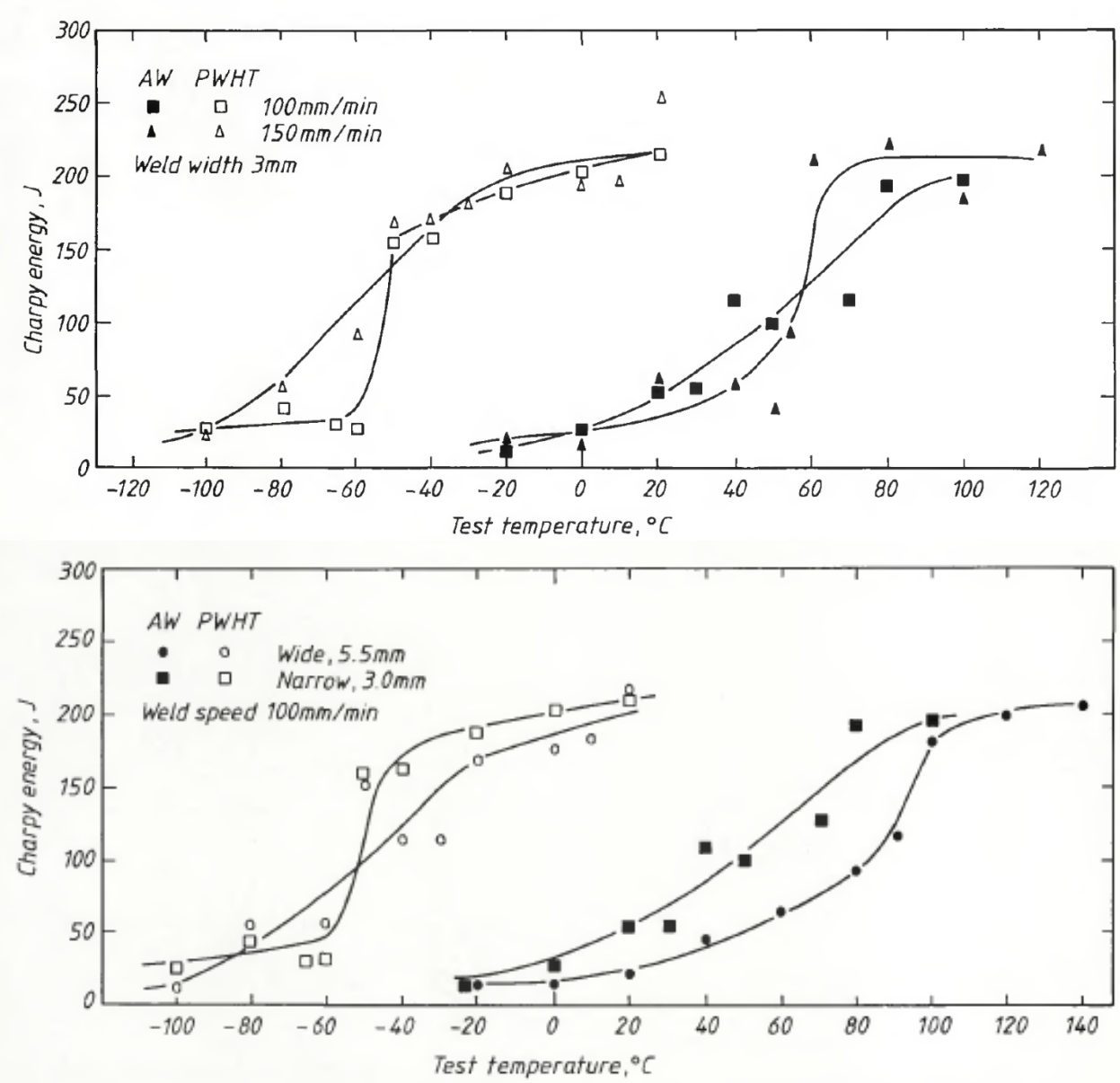

Figure 46. 75 mm thick C/Mn steel, EBW toughness BS4360-50D steel: same weld width (top), and varying weld width (bottom) (From Elliot [117], reprinted with permission from American Welding Society).

Fatigue information on the RPV steel EB weld metal properties is not common. Elliot provided a comparison of fatigue properties of C/Mn steel weld metal produced by EB, submerged arc welding (SAW), and shielded metal arc welding (SMAW), as shown in Figure 47. EB welds were found to be equal to SMAW, and they their fatigue performance was better than that of SAW. As with other welding processes, the surface condition of the weld can have a drastic effect on the weld's fatigue life. Undercutting, a common problem for EBW, can have a significant effect on fatigue life. In Figure 47, Elliot plots the S-N curve—number of cycles to failure, or N(S)—for welds with undercut alongside welds without undercut. A distinct loss in fatigue life can be seen in the samples with undercut, resulting in a loss of 40% at 10^6 cycles [117]. However, it should be noted that ASME Code requirements limit

undercut to 1/32-inch, and surfacing of welds to facilitate preservice inspection would ensure that significant undercut does not exist in EBW RPV welds [86].

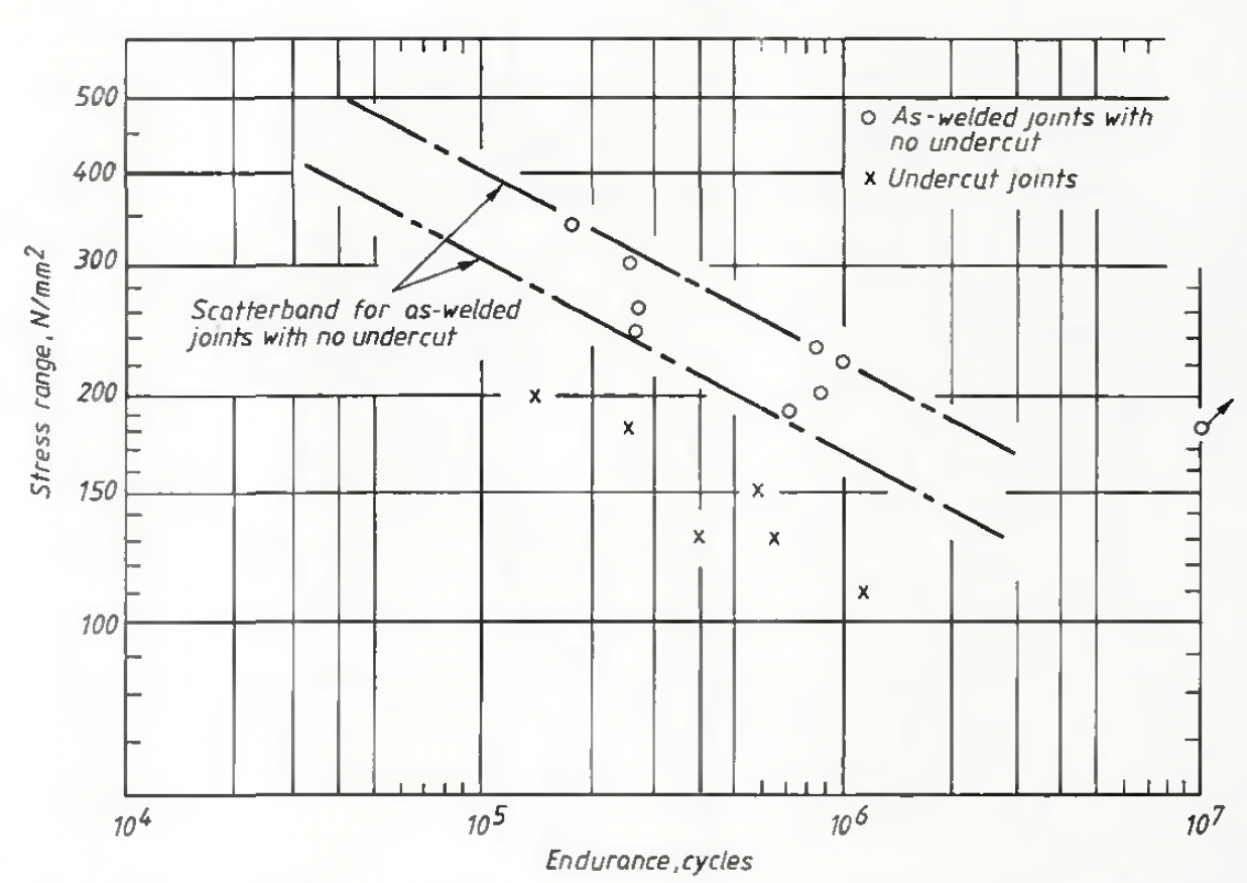

Figure 47. Fatigue test of EB-welded C-Mn steel (From Elliot [117], reprinted with permission from American Welding Society).

2.8 EBW OF RPV STEEL (SA533)

An article published by Nippon Steel Corporation in 1996 describes an investigation of EBW of SA533 Grade B Class 2 steel. Tomita sought to preferentially form lower bainite over upper bainite in the resulting EB welds. Significant quantities of martensite are not expected in this alloy. EBW was investigated to reduce the number of weld passes for thick-section PWRs without increasing overall heat input. The chemical composition of the SA533 steel was varied within the specification limits to produce heats of varying hardenability. The samples were then EB welded and Charpy impact tested. The results can be seen in Figure 48. Segregation of phosphorus, manganese, nickel, and molybdenum was reduced in the low phosphorus steel (0.002 wt%) vs. the medium phosphorus (0.006 wt%) steel [65]. Initial tests led the investigator to seek faster cooling rates to achieve lower bainite in the solidified weld metal, to reduce carbon content to lessen upper bainite formation, and to lower the nitrogen content to 50 ppm. The reduction of phosphorus was also sought to reduce the intergranular segregation of the low melting point constituents to improve toughness of the EB welds [65].These changes were sought to improve impact toughness while staying within the material specification.

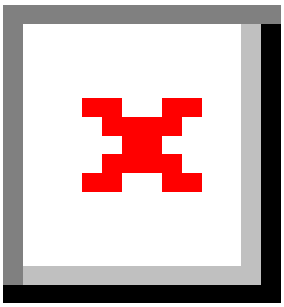

Figure 48. Effects of EB bead width and chemical composition of SA533 Grade B Class 2 steel on toughness (From Tomita [65], reprinted with permission from Taylor and Francis).

Based on the previous results, an improved composition of SA533 Grade B Class 2 steel was produced. The chemical composition of the steel can be seen in Table 8. Nitrogen content was reduced to 50 wppm from the normally observed 80 wppm in SA533 Grade B Class 2 steel plates [65]. All elements were within the compositional allowances of the SA533 steel. Steel plates were destructively tested to ensure compliance with the mechanical property requirements in the material specification. Results of the tensile tests and impact testing can also be seen in Table 8. Impact tests were conducted using v-notch samples at -23°C. A target bead width of 4 mm was chosen using parameters of 150 kV accelerating voltage, 200 mA, and 9 cm/min travel speed. A PWHT of 615°C for 10 hr was performed after welding. Samples were made using a single pass, as well as 4 passes to simulate repair welding using EBW. Plate thicknesses up to 120 mm were welded successfully.

Table 8. SA533 Grade B Class 2 steel composition and mechanical properties (From Tomita et al. [65])

	C	Si	Mn	P	S	Ni	Cr	Mo	Al
Mass %	0.18	0.26	1.43	0.002	0.002	0.67	0.15	0.57	0.027
Specification limit	≤ 0.25	0.15 0.40	1.15 1.50			0.40 0.70		0.45 0.60	

	Tensile test			Charpy impact test
Heat treatment	YS (N/mm2)	UTS (N/mm2)	El (%)	-23 °C (J) (avg/min)
Before PWHT	534	671	27	259/254
After PWHT	525	663	27	244/223

After PWHT, weld metal hardness values reached a peak of approximately 260 HV, whereas base metal hardness is near 200 HV. Peaks can be seen (Figure 49, left) at the interface between the weld metal and HAZ, but the microstructure of the weld and HAZ was not reported. All samples were subjected to PWHT of 615°C for 10 hours. Charpy impact tests were conducted at -23, -40, and -50°C for the single-pass and four-pass welds. Results are shown in Figure 49 (right). Impact energy values for the single pass

weld exceeded the values obtained in the parent material. A drop in impact energy was seen at the fusion line, likely due to the HAZ microstructure, although no discussion is provided.

Figure 49. Hardness values for EB of SA533 Grade B Class 2 (left); toughness of EB welds (right) (From Tomita et al [65], reprinted with permission from Taylor and Francis).

EBW properties were compared to the properties of conventional arc welding as shown in Table 9. EB weld metal impact energy exceeds that of the other processes, including SAW, narrow gap submerged arc welding (NG-SAW), and narrow gap gas metal arc welding (NG-GMAW). This was accomplished by specifying lower carbon and nitrogen, with modest increases of chromium and nickel. Promoting the formation of lower bainite over upper bainite and reducing the segregation of elements through reduced phosphorous content were identified to improve weld toughness [65].

Table 9. Toughness comparison for EBW, SAW, NGSAW, and NGGMAW in SA533 Grade B Class 2 steel (From Tomita et al. [65])

Welding method	Toughness at weld metal vE-23 (J) (avg./min)
EBW	270 / 261
SAW	151 / 123
Narrow Gap SAW	230 / 173
Narrow Gap GMAW	153 / 142

2.8.1 Reduced-Pressure Electron Beam Welding of RPV Steel

A limiting factor of EBW is the chamber normally required for deep penetrating EB welds. TWI is developing an RPEB system to achieve deep penetrating welds in thick members without the need of a chamber. This process was recently chosen for two wind power monopile programs at Dogger Bank [118] and for modular reactors as part of the EBManPower program [41]. The first publicly available document on RPEB welding was published in 2000, and it discusses the potential welding of nuclear waste canisters and offshore pipe welds [119]. TWI produced an RPEB electron gun for Swedish Nuclear Fuel and Waste Management Company (SKB) in 1996 that could operate at 200 kV and 100 kW of power output [23]. The EB sealing of thick section copper canisters (60 mm thickness) was preferred because of its relative immunity to pressure fluctuations that may have occurred if EBW-HV were used; however, friction stir welding was ultimately chosen to be used at SKB [120]. The vacuum level needed for RPEB is as little as 0.075 Torr (0.1 mbar) to achieve a focused EB over long work distances [23, 119]. Additional publications were made to investigate the use of RPEB on RPV steels. A focus on residual stress can be

seen across publications by TWI to support the inclusion of EBW in the R6 (UK) and API 579-1/ASME FFS-1 fitness for service procedures [1, 24, 27, 43, 44, 82, 121-124]. A reduced pressure level between 75 × 10^{-2} Torr and 75 × 10^{-3} Torr (0.1 to 1 mbar) were used by Ayres, with later work performed at 2.2 × 10^{-2} Torr (3 × 10^{-2} mbar) by Balakrishnan and Rathod to evaluate the use of RPEB on thick section RPV steels [1, 22, 24]. The approximate range of RPEB use is highlighted in **Error! Reference source not found.**. Because of the interest in RPEB, TWI installed an in-chamber reduced pressure gun column in their large 150 m^3 chamber in 2006, with helium gas supplied to the beam path to replicate the mobile vacuum seal for further weld development [22, 23]. The mobile vacuum seal used in the RPEB system has localized pumping of the immediate welding area, with known losses caused by the imperfect seal. If a helium gas shroud is used on the exterior of the RPEB system, then helium is introduced into the chamber to simulate this environment.

The electron gun used for RPEB is an RF-excited diode gun. Two windings—one in the gun column and one in the gun cartridge—allow the primary filament to be heated. The primary filament (tungsten ribbon) is heated to the emission temperature indirectly in lieu of resistance heating using a filament current. One benefit of this system is that the beam power is controlled by the cathode temperature rather than by adjusting the voltage level on the gridded system used in a triode gun. Benefits include reductions in the axial focal position variation and excursions in beam power that may occur as a result of arc outs or beam spikes from vapor or gasses in the gun column. Using a simplified high-voltage cable consisting of a single core reduces the diameter of the cable and allows for easier manipulation of the gun. The beam power is also simplified by using a single cathode temperature parameter [23, 119]. Residual stresses in steels are known to be a factor in crack propagation, crack susceptibility, distortion, SCC, and irradiation behavior of steel [24, 125]. There are multiple methods to measure residual stress. Deep-hole drilling (DHD) is commonly used, but it only provides data in a single plane. Neutron diffraction is a much more capable method, but it is limited to specimens of 50 mm max in steels [125]. In measurement of the peak residual stresses in SA508 steels, the values reach the yield strength of the steel in both A533B and A508 Grade 3 Class 1, regardless of whether EB or arc welding is used [24, 125]. In thick section welds, the multipass process of arc welding allows for in-process tempering of the previous passes, thus reducing the residual stress as the joint is filled. In the case of a single pass EBW joint, no further tempering occurs, so the peak residual stresses remain equidistant from the weld centerline outside the weld and HAZ. Smith studied the residual stress in S508 Grade 3 steel and stainless steel of 98 mm thickness that was EB welded from both sides to achieve full penetration [125]. Components 1 and 2 were SA508 Grade 3 steel, and component 3 was made of 316 stainless steel. As shown in Figure 50, the SA508 steels in the as-welded condition exhibit an M-shaped profile of highest stress outside the weld and HAZ. Residual stress measurements were nearly identical in the ferritic steels, although they were welded with drastically different speeds of 0.2 mm/min for component 1 and 100 mm/min for component 2 [125]. The residual stress profile for the ferritic steels encompasses a width of about 40% of the joint thickness, symmetric about the weld centerline [125]. The stainless-steel weld, component 3, had a much wider stress distribution across the weld which was greater than the joint thickness. 316 SS has a higher coefficient of thermal expansion, resulting in the wider width of residual stress across the weld centerline. 316SS also does not strengthen through precipitation or through the formation of martensite, so it does not experience the peak stresses seen in the ferritic steel. After post-weld heat treatment of the ferritic alloy in component 2, the peaks near 600 MPa were reduced to less than 100 MPa [125].

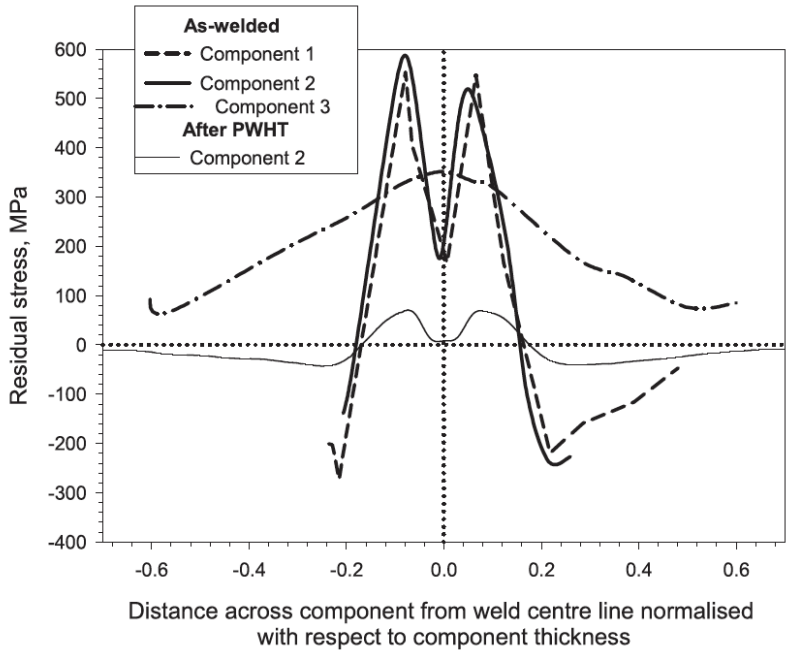

Figure 50. Components 1 and 2 are ferritic steels; component 3 is stainless steel (From Smith et al. [125], reprinted with permission from Elsevier).

Rolls-Royce and TWI evaluated the use of RPEB for RPV steels through welding sections of prolongation ring forgings ranging from 100 to 160 mm long [22]. An integral step was machined into the samples to provide the preferred joint thickness and to serve as a shelf to support the molten weld metal from drop out. A drawing section can be seen in Figure 51 (left). The forgings were of SA508 Grade 3 Class 1 material. The in-chamber RPEB system at TWI was used for the welds. The system consisted of a 100 kW electron gun mounted in the 150 m^3 chamber with an intentional helium gas leak at the beam location to simulate the reduced pressure environment and to reduce beam scattering [23]. Welds were completed at 0.1 to 1 mbar (0.075 to 0.75 Torr) of pressure in the 2G horizontal position, with beam parameters of 150 kV, 350 mA, and 100 mm/min travel speed [22]. Weld parameters are given in a dissertation by Duffy for performing additional analysis. A temperature profile of the 160 mm deep weld can be seen in Figure 51 (right) [22]. The cooling rate between the austenitizing temperature to the martensite start temperature can be used to help predict the resulting microstructure. As noted by Ayres [22], a martensitic microstructure was seen in the central HAZ region, with high hardness and low toughness in the as-welded condition.

Figure 51. SA508 Grade 3 Class 1 steel forging weld joint design (left); 160 mm thick weld temperature profile (right) (From Ayres et al. [22], reprinted with permission from ASME).

Samples were subsequently provided a PWHT at 607°C for 3.5 hours in compliance with the ASME Code Sec. III requirements. Hardness measurements taken after PWHT are shown in Figure 52. Very little difference can be seen in the traces along the cap, middle, and root of the weld. Values of around 260 HV were reached in the weld metal with a hardness of 200 HV in the base material [22]. A microstructure evaluation was not reported on these samples in this report. The reference temperature (T_0) was used which corresponds to a 1-inch thick size-corrected fracture toughness of 100 MPa$\sqrt{m}$ [22]. Fracture toughness of the as-welded sample was described as poor, with a T_0 value of +40°C [22]. The PWHT improved toughness to be comparable to the base metal, with T_0 values of 100°C to -88°C (see Figure 53 [22]).

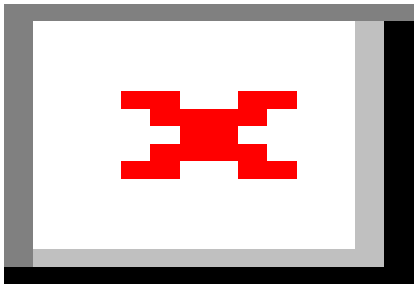

Figure 52. In-chamber RPEB hardness profile of 160 mm weld in SA508 Grade 3 Class 1 steel after PWHT (From Ayres et al. [22], reprinted with permission from ASME).

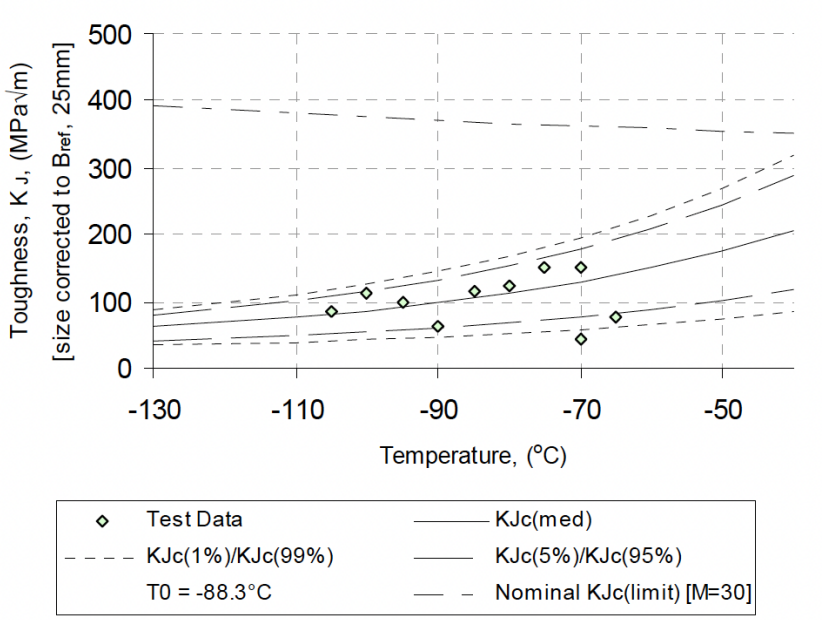

Figure 53. Fracture toughness of 160 mm RPEB welds in SA508 Grade 3 Class 1 steel forgings (From Ayres et al. [22], reprinted with permission from ASME).

A University of Cambridge report written by Duffy includes an analysis of welds created by Rolls Royce and TWI using RPEB [126]. This work is a continuation of work performed by Rolls Royce and is within the range of penetrations completed in the previous work (100 to 160 mm). A 140 mm through-thickness sample was provided by Rolls Royce and was evaluated by Duffy in the same as-welded condition that was used in the Ayers study [126]. The parameters used for the 140 mm thick sample were 150 kV, 318 mA, and 100 mm/min [126]. The hardness trace extended into the base metal of the sample on both sides. The weld FZ was approximately 10 mm in width with a 2.4 mm HAZ on each side of the weld. A base metal hardness of 195 HV can be seen with increasing hardness through the HAZ, reaching a peak near the fusion boundary at 340 HV in one location. Weld metal hardness was lower, with an average hardness of approximately 290 HV. This result can be compared to a previous hardness trace of the 160 mm thick weld by described by Ayres. Hardness values were reduced in the weld metal and HAZ after PWHT.

SA508 Grade 4N forgings were also procured and manufactured into coupons to match the Grade 3 sections at a joint thickness of 147 mm [126]. SA508 Grade 4, with its higher nickel and chromium contents, is viewed as a potential improvement for use in RPVs [105]. Welds were made using the in-chamber RPEB system at TWI with an intentional helium gas leak into the beam. Welds were made using 150 kV, 318 mA, and 100 mm/min travel speed [126]. A PWHT was also applied to the Grade 4N weldments at a lower temperature for longer duration: 565°C for 30 hr [126]. Grade 4N material has lower manganese, but it has higher nickel and chromium contents than Grade 3 steels. An important microstructural difference resulting from the chemistry changes is the lower bainitic start temperature. Theoretical bainite start temperatures calculated by Duffy using Bhadeshia's mucg65 model are 531°C and 440°C for Grades 3 and 4N, respectively [126]. This PWHT accomplishes two things: bainite forms at a lower temperature, and additional martensite can form upon cooling, leading to higher hardness in Grade 4N material.

In Lee's base material evaluation of SA508 Grade 4N material, the blocks of material were austenitized at 800ºC, tempered at either 660°C, or 630°C, for 10 hours, and then they underwent PWHT at four different conditions [105]. A uniform microstructure of tempered martensite and bainite with fine precipitates results from the 660°C temper not seen at 630°C [105]. A PWHT at 610°C resulted in

coarsening of the carbides, with greater changes seen in the largest carbides [105]. Tempering at 660° followed by a 610°C PWHT resulted in the unwelded material's greatest drop in hardness. This resulted in improved hardness, impact toughness, strength, and transition properties [105].

After PWHT, the hardness values of EB welded SA508 Grade 4N are approximately 240 HV in the base material, rising to 320 HV in the weld metal. These values exceed those in the Grade 3 material (200 base metal, 260 weld metal), as expected. Prior to the PWHT, the Grade 4N material hardness was high, reaching 500 HV through the FZ, with a base metal hardness of around 260 HV prior to PWHT [126]. A large drop in hardness was seen after PWHT, as may be expected from the tempered martensite, with somewhat higher hardness in the Grade 4N steel, possibly because of increased carbide formation as a result of its higher chromium content.

The New Nuclear Manufacturing (NNUMAN) program, a UK research program for GENIV fast reactors, included research on EBW of RPV steels, and the program also continued the efforts to develop thick section EB welds. The five-year research and development effort was spurred by new reactor designs going through the assessment process [127]. Design and fabrication of the 30 and 130 mm samples are discussed by Francis [82]. A comparison of NG-SAW, narrow gap gas tungsten arc welding (NG-GTAW), narrow gap laser welding (NG-LW), and reduced-pressure EBW was completed for 30 mm joint thickness by Balakrishnan [24], followed by a comparison of the same processes without laser at 130 mm joint thickness by Rathod [1] and Vasileiou [44]. Smith performed a NNUMAN program review [127], and additional work, including a collaboration with EPRI, is summarized by Vasileiou [115]. Welds completed by Balakarishnan on 30 mm thick SA508 Grade 3 Class 1 steel are shown in Figure 54, which clearly shows the number of weld passes required for traditional arc welding and the narrow gap laser process. The EB weld was completed using the RPEB process at TWI at 3×10^{-2} mbar (2.2×10^{-2} Torr) pressure with a preheat of 104°C achieved through a low-power EB raster over the weldment [115]. Plate distortion was measured with the least amount of butterfly distortion in the RPEB weld at 0.27 degrees. Butterfly distortion in the NG-SAW and NG-GTAW were 1.86 and 2.6, degrees respectively, indicating the RPEB welding and in-chamber EBW, which results in less weld distortion than arc welding processes.

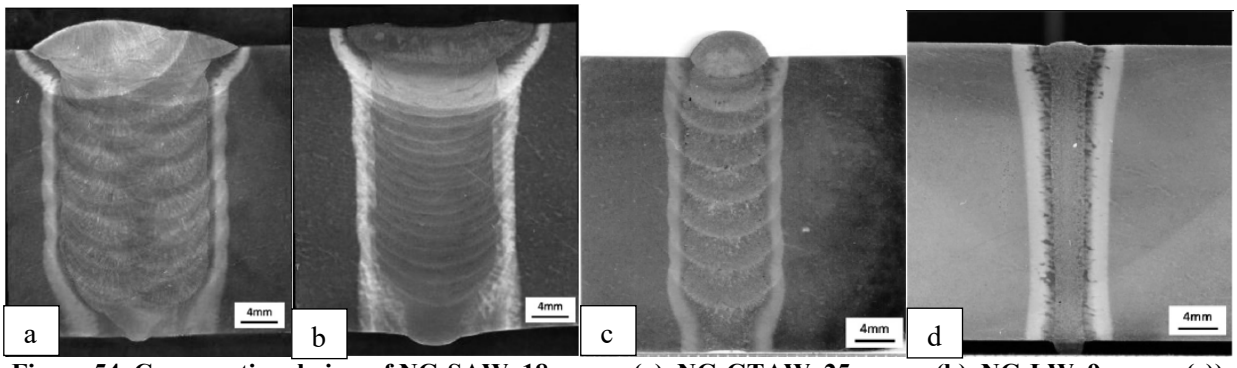

Figure 54. Cross sectional view of NG-SAW, 18 passes (a), NG-GTAW, 25 passes (b), NG-LW, 9 passes (c)), and RPEB, 1 pass (d) in 30 mm thick SA508 Grade 3 Class 1 steel (From Balakrishnan et al. [24], reprinted with permission from Elsevier).

Welds at 130 mm joint thickness were made using NG-SAW, NG-GTAW, and RPEB. Details of the manufacture of the samples are documented by Rathod [1], and measurements for residual stresses are recorded by Vasileiou [44]. EB welds were made using a 150 kV gun at 300 mA and 100 mm/sec, resulting in a heat input of 27 kJ/mm. Butterfly distortion was reported for each process, resulting in 1.87°, 3.65°, and 0.08° for NG-SAW, NG-GTAW, and RPEB, respectively [1].

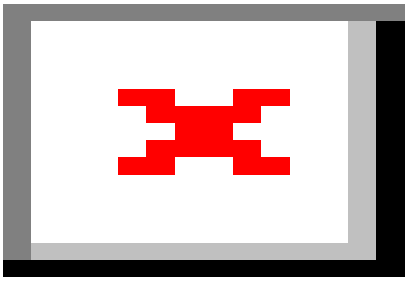

Figure 55. Cross sectional views of NG-SAW, 104 passes (left), NG-GTAW, 73 passes (middle), and RPEB, 1 pass (right) (From Vasileiou et al. [44], reprinted with permission from Elsevier).

Figure 56 shows hardness traces of each cross section before and after PWHT for the 30 mm sections. Increased hardness in what are likely the CGHAZs of the last pass can be seen in all welds. In the arc-welded specimens, the highest hardness can be seen near the toes of the weld near the weld reinforcement, and a slightly increased hardness can be seen in the HAZ through thickness. FZ hardness of the arc-welded samples is not significantly different than that of the base metal. Some tempering of the previously deposited welds can be seen in the laser-welded sample: a small portion of the previously deposited weld metal revealed rings of lower hardness. As with the arc-welded samples, the CGHAZ contained the highest hardness near the toes of the weld reinforcement. The single-pass RPEB weld does not benefit from additional thermal cycle tempering from its single pass, so a through-thickness region of the CGHAZ is present with high hardness. Peak hardness values were approximately equal in the weldments, nearing 450 HV except for the NG-GTAW process, which was lower with a peak near 400 HV. A review of the welding parameters in Figure 56 shows that the NG-GTAW process was completed at much slower travel speeds, resulting in significantly greater heat input, whereas NG-SAW was mentioned as having a lower heat input than that typically used as a result of the joint thickness. After PWHT, all welds were reported to have less than 300 HV.

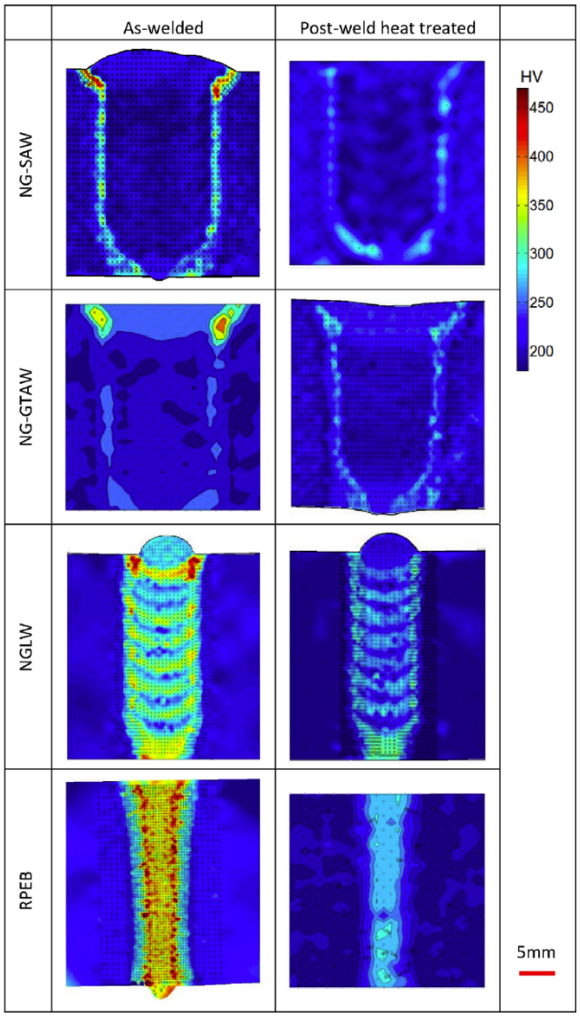

	NG-SAW	NG-GTAW	NGLW	RPEB
Voltage (V)	27	11	7 kW	150000
Current (A)	225/350	275/325		0.09
Welding Speed (mm/min)	450/325	75	240	200
Pulsing Frequency (Hz)	N/A	1	N/A	N/A
Beam diameter (mm)	N/A	N/A	6	2
Wire diameter (mm)	2.4	1.2	1.2	N/A
Wire Feed Speed (m/min)	–	0.8–1.0	5	N/A
Welding position	1G	1G	1G	2G
Heat Input (kJ/mm)	0.8–1.7	2.4–2.9	1.8	4.1

Figure 56. Hardness maps of 30 mm joint thickness by process, NG-SAW, NG-GTAW, NG-LW, and RPEB (left), welding parameters for each process (right) [24]

A similar comparison of the NG-SAW, NG-GTAW, and RPEB processes was completed at a joint thickness of 130 mm. Weld parameters, individual pass heat input, and the number of passes are included in

Table 10. Although total heat input was not reported, it was calculated to be 287 kJ/mm, 176 kJ/mm, and 27 kJ/mm for NG-GTAW, NG-SAW, and EBW, respectively, assuming that a single root pass and hot pass were used. As mentioned in Section 2.6.5, the multiple pass tempers the previously deposited weld passes below, resulting in reduced hardness throughout the FZ. The single-pass RPEB weld does not benefit from the tempering of multiple passes, so higher as-welded hardness can be seen throughout the FZ in Figure 57. A wider HAZ was also seen in the RPEB weld because of its higher individual pass heat input and cooling rate of 2°C/sec between 750°C and 400°C [1].

Table 10. 130 mm joint thickness parameters by process (From Rathod et al. [1] reprinted with permission from Elsevier)

Process	Current (Amps)	Voltage (Volts)	Type of Pass	Bead Type	Welding Speed, *v* (mm/min)	Wire Feed Speed (mm/min)	No. of passes	Heat Input (kJ/mm)
NG-GTAW	175	10–12	root	weaving	75	500	73	1.4
	190–220		hot		75	500–600		1.6–1.8
	325–450		fill		55–65	800–2100		2.7–5.3
NG-SAW	300	27–29	root	stringer	340	Auto	104	1.4
	300		hot		375	Auto		1.3
	350–370		fill		375	Auto		1.5–1.9
EB	0.3	150,000	full T		100	N/A	1	27

Although Rathod does not provide a discussion of the peak hardness values, hardness maps are provided as shown in Figure 57. A high hardness region is seen within the NG-SAW FZ of approximately 450 HV. This is likely a slag inclusion, but it cannot be verified through the optical images provided. No significant difference can be seen in the NG-GTAW and NG-SAW sample hardness values as compared to the 30 mm results given in Figure 56 and the 130 mm results in Figure 57. Using many passes to fill the joint and a 3D cooling profile allows for similar results, independent of joint thickness. A difference in hardness can be seen in the RPEB welds of Figure 56 and Figure 57. The cooling rate was reported to be 10°C/sec at 30 mm joint thickness and 2°C/sec at 130 mm joint thickness [1, 115]. The faster cooling rate of the 30 mm sample produced more martensite, so it was harder prior to PWHT. A PWHT of 607°C for 6 hours as specified in ASME Section III was performed, thus reducing the hardness values of the RPEB weld below 300 HV [1, 115].

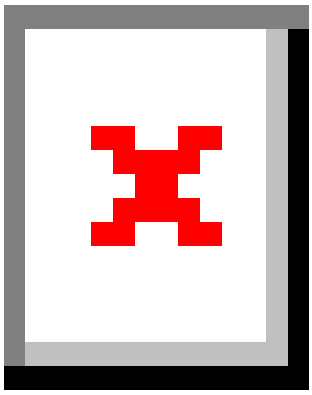

Figure 57. 130 mm SA508 Grade 3 Class 1 welded joint hardness maps of NG-SAW (left), NG-GTAW middle), and RPEB (right). Vickers hardness used for as-welded (top row) and after PWHT (bottom row) (From Rathod et al. [1] reprinted with permission from Elsevier).

Residual stress levels were measured in the 30 and 130 mm welded assemblies. Neutron diffraction and a contour method were used in the 30 mm samples. Balakrishnan [24] provides 30 mm sample results and an explanation of the contour methodology. The contour method using out-of-plane measurements of displacement after EDM slicing provided a profile that could be processed with a finite element analysis model. The 130 mm samples were measured using the contour method and the deep-hole drilling method, as reported by Vasileiou [44]. Contour maps of the arc-welded samples show the highest stress concentration to be at the weld centerline just below the weld reinforcement. Some anomalies in the contour maps near the edges of the arc-welded samples can be seen because of the pilot holes being used to restrain the samples during welding, as well as a vertical line to the left of the NG-GTAW weld that was caused by EDM cutting [44]. The RPEB contour map shows a different distribution, with peak stresses parallel to the weld centerline along the joint thickness. The region of highest stress is outside the HAZ. Peak stresses of >550 MPa exist in the base material, with a FZ stress level of approximately 350 MPa.

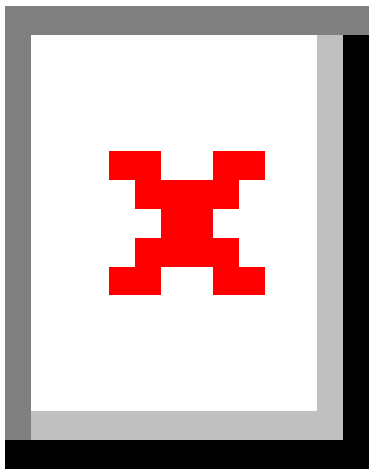

Figure 58. Residual stress contour maps in the as-welded condition for 130 mm thick welds using NG-SAW (top), NG-GTAW (middle), and RPEB (bottom) (From Vasileiou et al. [44], reprinted with permission from Elsevier).

These results agree with the results obtained using the deep hole drilling (DHD) method performed on the specimens. The DHD method allows for the capture of two stress tensors: normal and longitudinal. The

third stress, which occurs in the direction of the drilled hole, is disturbed as a result of material being moved in that orientation. To measure the stress levels from the base metal through the FZ, a mid-plate-length plane was chosen, as seen in Figure 59. Holes were drilled to a mid-thickness depth, and stress tensors for normal and longitudinal orientations were analyzed. This was repeated across the width of the plate from the base metal through the weld zone. The three different welding processes are overlaid on the same plot for comparison. In the hardness traces and contour methods, a peak stress level is seen at the edges of the weld, likely in the CGHAZ. The M-shaped distribution is evident in the transverse line at mid-thickness in the normal and longitudinal stress planes for the RPEB weld. This is a result of the single-pass and solid-state phase transformations common to ferritic alloys. Murakawa discusses the evolution of stresses caused by phase transformations at high and low transformation temperatures. Phase transformations—particularly austenite to bainite/martensite through a displacive transformation—have been shown to relieve stresses in the weld [128]. Depressing the transformation start temperature (Ts) causes an increase in the compressive stresses formed by the SSPT [128], as shown in Figure 60a and b. The RPEB weld clearly shows the M-shaped profile expected of the single pass weld. Faster cooling rates like those within the FZ depress the Ts, increasing the magnitude of the compressive stress upon cooling, thereby reducing the overall stress at room temperature [128]. The arc welding processes do not show the M-shaped stress profile because of the many lower heat input passes which anneal each previous pass as the joint is filled. Peak stresses of approximately 400 MPa and 150 MPa are seen in the longitudinal and normal directions in the FZ of all three weld processes.

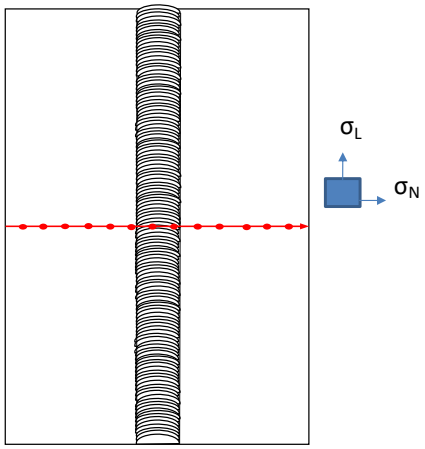

Figure 59. Normal and longitudinal stress tensors measured using DHD method along transverse line across weld. Holes were drilled down to mid-thickness from weld top surface, progressing across the specimen.

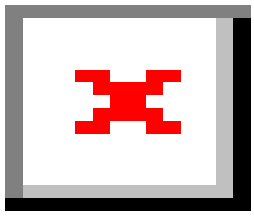

a)

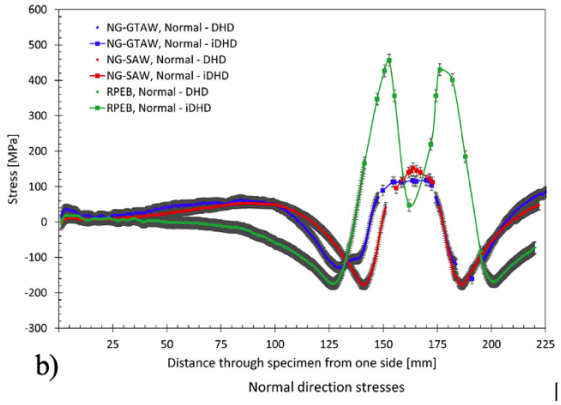

b)

Figure 60. Residual stresses at mid-thickness using DHD method in as-welded condition using method described for transverse line DHD (From Vasileiou et al. [44], reprinted with permission from Elsevier).

An incremental deep hole drilling (iDHD) method was used for evaluating high-stress locations in the FZ. In iDHD, a single hole is drilled from the top surface of the weld along the weld centerline. Normal and longitudinal stress tensors are analyzed at that depth. The hole is then drilled incrementally further through the joint thickness, stopping to analyze the stress tensors at desired intervals. This is represented schematically in Figure 61. Results of the iDHD method are shown in Figure 62. Through-thickness stresses peak near the surfaces of the reinforcement and root of the arc-welded samples, whereas peak stress is at the mid-thickness of the single-pass RPEB weld. The RPEB weld appears to show lower residual stress throughout the weld centerline than the results using the arc welding processes, but after reviewing the distribution of stress in Figure 58, it becomes clear. The RPEB weld centerline is flanked by two regions of higher stress outside the FZ. The distribution of stresses in the through-thickness plane differs between RPEB and NG-GTAW or NG-SAW.

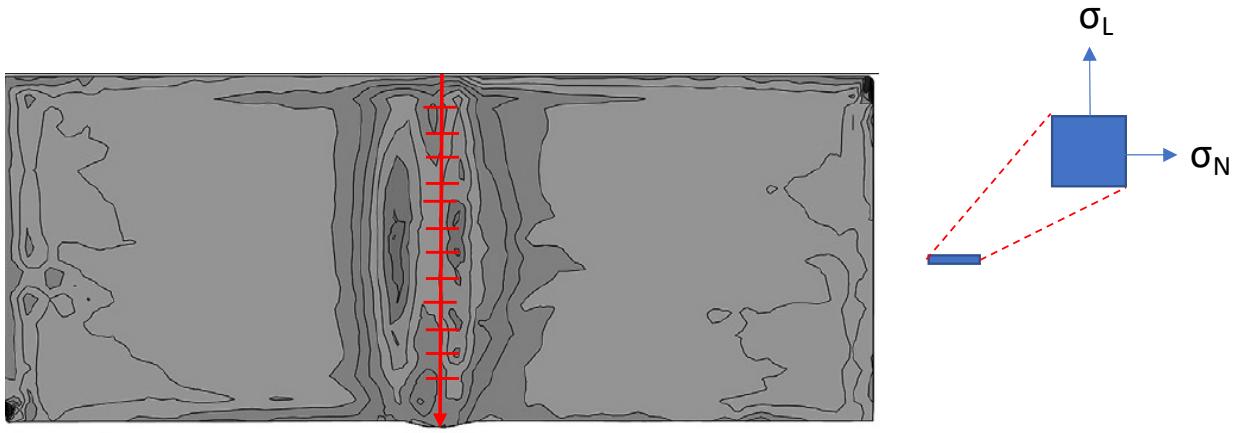

Figure 61. Normal and longitudinal stress tensor orientation for vertical line at weld center using iDHD method (Adapted from Vasileiou et al. [44]).

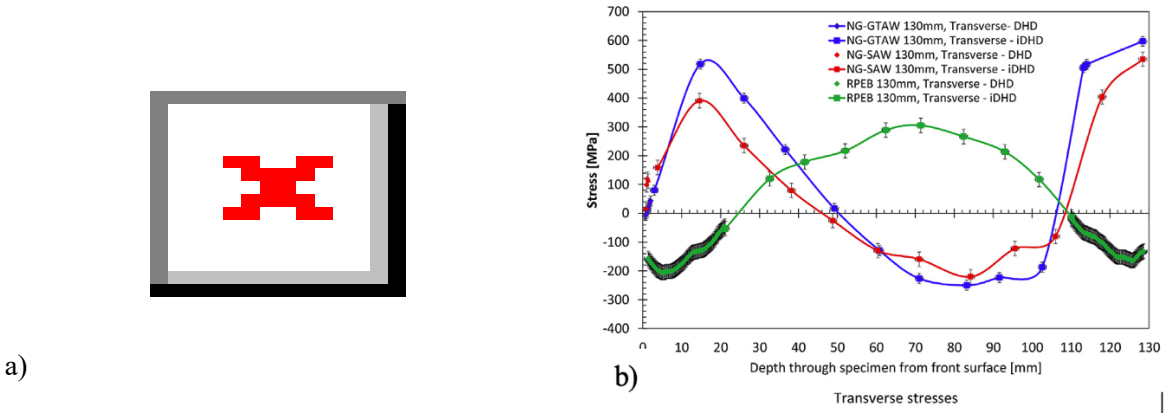

Figure 62. Results from iDHD method along weld centerline through-thickness for each weld process (From Vasileiou [44], reprinted with permission from Elsevier).

After PWHT, the residual stress levels of all welds are reduced. Residual stress levels measured using the DHD method after PWHT are shown in Figure 63. Residual stress levels of the NG-SAW and NG-GTAW were reduced from the peaks near 400 MPa to less than 50 MPa. Residual stress levels in the

RPEB weld were reduced to approximately 100 Mpa, with a less distinct M-shaped profile. This stress level after PWHT was noted as being higher than seen in historical structural integrity assessments [44]. Comparing the residual stress levels in RPEB welds by Balakrishnan at 30 mm and Vasileiou at 130 mm using the same heat of material shows a greater drop in residual stress in the FZ of the 30 mm welds. Residual stress levels before PWHT were compressive in the FZ, returning to slightly tensile after PWHT, without the distinctive M shape seen in the 130 mm samples.

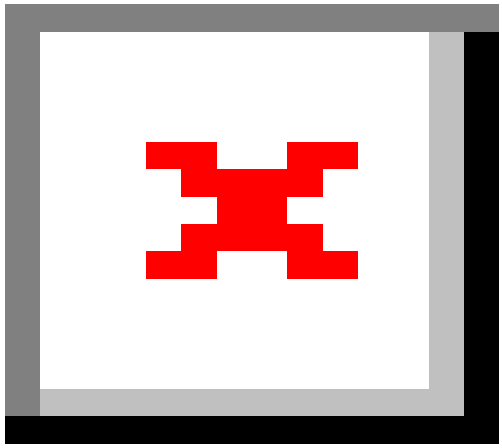

Figure 63. Residual stresses at mid-thickness using DHD method before and after PWHT: NG-SAW (a), NG-GTAW (b), RPEB (c), and combined processes (d) (From Vasileiou et al. [44], reprinted with permission from Elsevier).

Residual stress measurements completed at mid-thickness for NG-GTAW and NG-SAW do not include the areas of high residual stress according to the maps provided in Figure 58. A through-thickness measurement evaluation of the NG-GTAW was completed by Vasileiou and is shown in Figure 64. The maximum residual stress was recorded to be near 600 Mpa, as mentioned above for the RPEB weld. After PWHT, the residual stress of the NG-GTAW weld can be seen nearing 100 MPa near the weld reinforcement and root of the weld [44]. Residual stresses in the RPEB weld also reach 100 MPa, but they are distributed to the left and right of the transverse cross section and are reported to be outside the weld region [44].

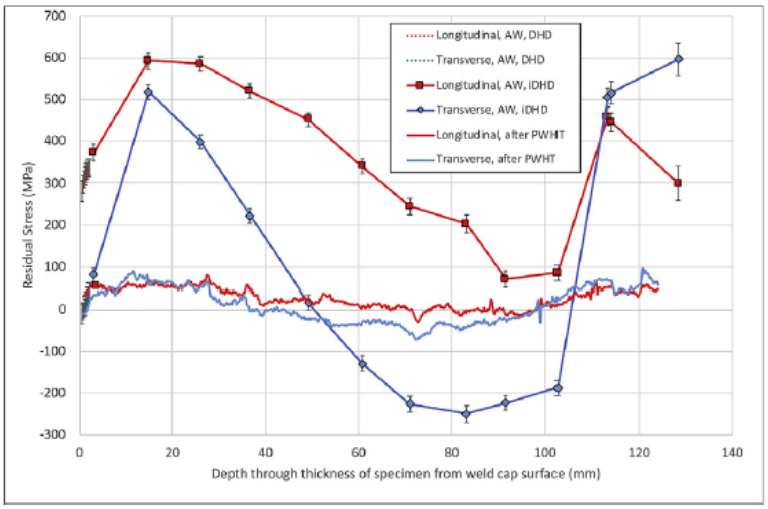

Figure 64. Residual stresses before and after PWHT of NG-GTAW weld along the weld centerline through-thickness (From Vasileiou et al. [44], reprinted with permission from Elsevier).

A follow-on study was performed using the SA508 Grade 3 Class 1 material from the NNUMAN program discussed previously, with collaboration from EPRI providing specimens from a quench and tempered SA508 Grade 2 steel. Carbon equivalency values between the two steels were calculated using the International Institute of Welding (IIW) formula of 0.60 and 0.53 for the Grade 3 and Grade 2 steels, respectively [115]. Different weld metal microstructures could therefore be expected in the FZ and HAZ of the deep-penetrating EB welds [115]. Welds were completed at TWI using a reduced pressure of 3×10^{-2} mbar (2.2×10^{-2} Torr) at identical welding parameters of 150 kV, 300 mA, and 100 mm/min in both alloys [115]. A helium background gas and preheat of 104°C was used for weldments of 30 and 130 mm joint thickness. Only the 130 mm welds are discussed in this report. A 6-hour PWHT of 607°C was performed in accordance with ASME Section III except, with slower heating and cooling rates [115]. Base metal microstructure was reported as “ferritic with heavily tempered bainite/ferrite-carbide aggregates” [115]. Transverse cross section metallographs can be seen in Figure 65. The SA508 Grade 3 Class 1 weld is shown on the left. The FZ shows the prior austenite grain boundaries with a combination of martensite and bainite, as shown in Figure 65 b, c, and d [115]. Also shown in Figure 65 b and c are large ferrite grains with the presence of carbides primarily at grain boundaries. The FGHAZ and intercritical HAZ (ICHAZ) consist of a mix of ferrite and carbides as reported by Vasileiou [115]. The SA508 Grade 2 material seen in Figure 65 on the right shows a microstructure of bainite with areas of auto tempered martensite as reported by Vasileiou [115].

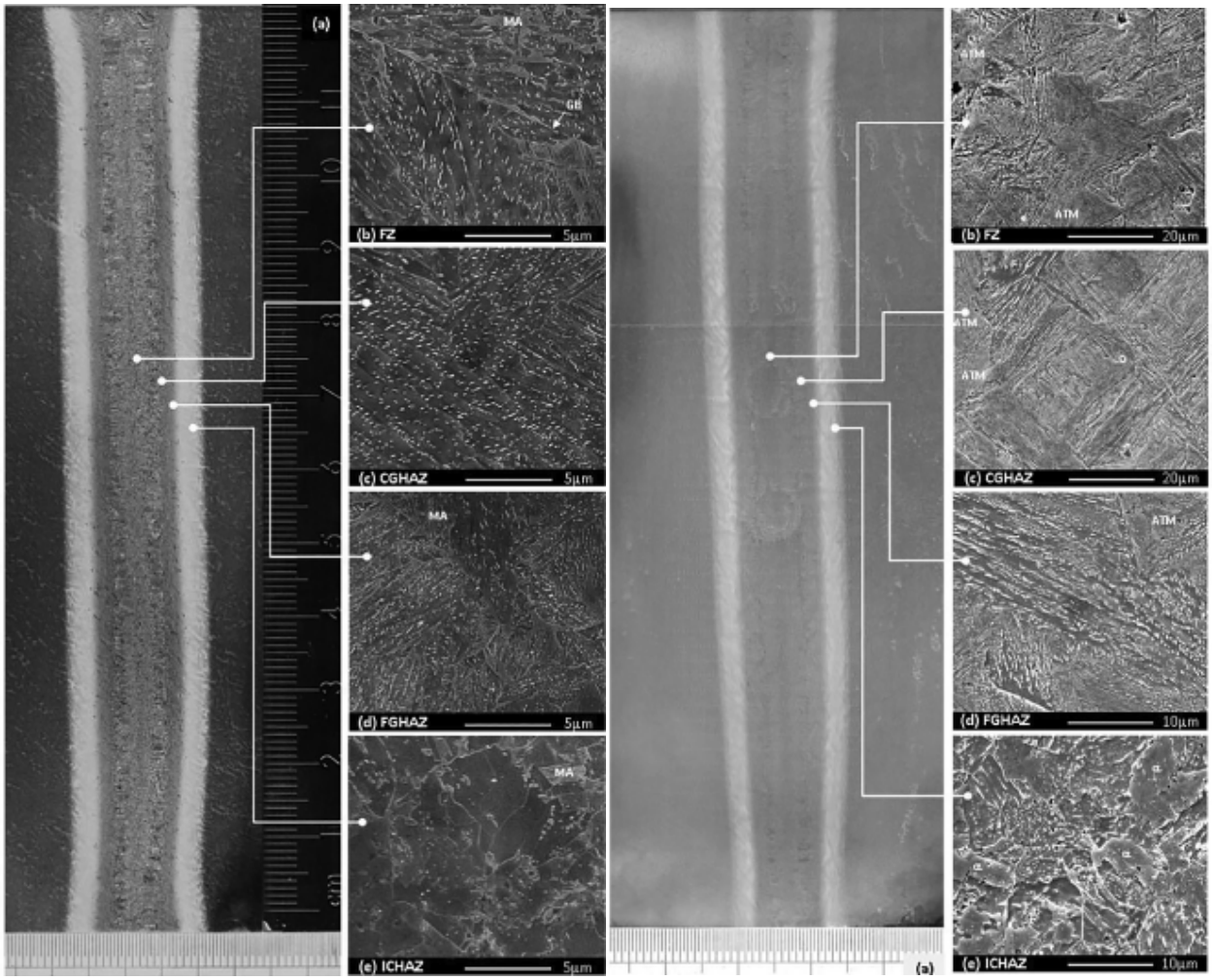

Figure 65. Thick section 130 mm RPEB welds in SA508 Grade 3 Class 1 (left), SA508 Grade 2 (right): for both figures, full transverse cross section (a), FZ (b), CGHAZ, (c) FGHAZ (d), and ICHAZ (e) (From Vasileiou et al. [115], reprinted with permission from Elsevier).

At a 130 mm joint thickness, hardness values between the two steels were comparable with higher hardness values seen in the Grade 3 Class 1 steel after EBW. Peak hardness values in the CGHAZ were measured near 450 HV, likely due to the formation of martensite. Hardness maps of the 130 mm EB welds before and after PWHT are shown in Figure 66. The difference in hardness is as expected after review of the as-welded microstructure shown previously in which higher hardness would be expected in the Grade 3 Class 1 steel EB weld. Higher hardness can be seen throughout the FZ, with higher hardness along the edges reported as being in the CGHAZ [115]. PWHT had a greater effect on the Grade 3 Class 1 material than on the Grade 2 material. The primarily bainitic weld microstructure seen in the Grade 2 material was not greatly affected by the PWHT. Hardness in the Grade 3 Class 1 material was greatly reduced after PWHT. A metallograph showing the microstructure after PWHT was not included, but a bainitic microstructure with tempered martensite is expected which would result in the drop in hardness seen with values near those of the Grade 2 steel.

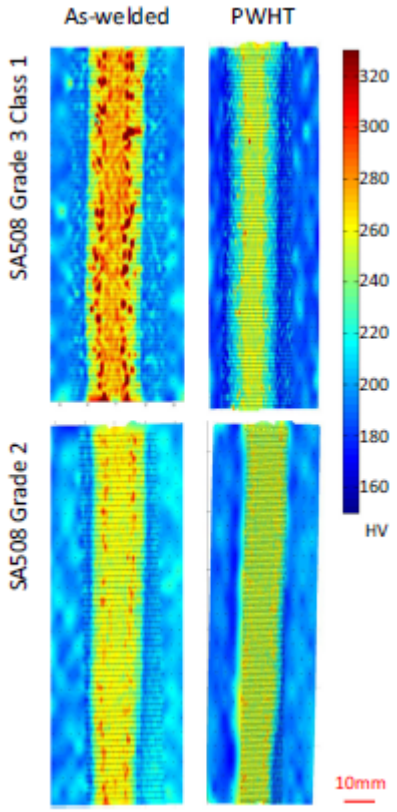

Figure 66. Hardness maps of EB welds in 130 mm SA508 steels using RPEB (From Vasileiou et al. [115], reprinted with permission from Elsevier).

Residual stress measurements through neutron diffraction and DHD were performed on the Grade 2 and Grade 3 steels. In agreement with the previous results shown in Figure 58, the SA508 Grade 3 Class 1 material shows two distinct bands to the left and right of the weld with the highest level of residual stress. Levels near 700 MPa are seen in these narrow bands, which are reported to be outside the HAZ in the parent material of the SA508 Grade 3 Class 1 weld in Figure 67 [115]. The SA508 Grade 2 material does not show the distinct bands; instead it shows a more traditional distribution of stress across the weld. The difference in hardness and residual stress measurements between the two materials was reported to be caused by the SSPTs that occurred in the Grade 3 Class 1 material. The grade 2 material consisting of bainite throughout the FZ does not undergo the SSPTs that affect the stress levels through that zone.

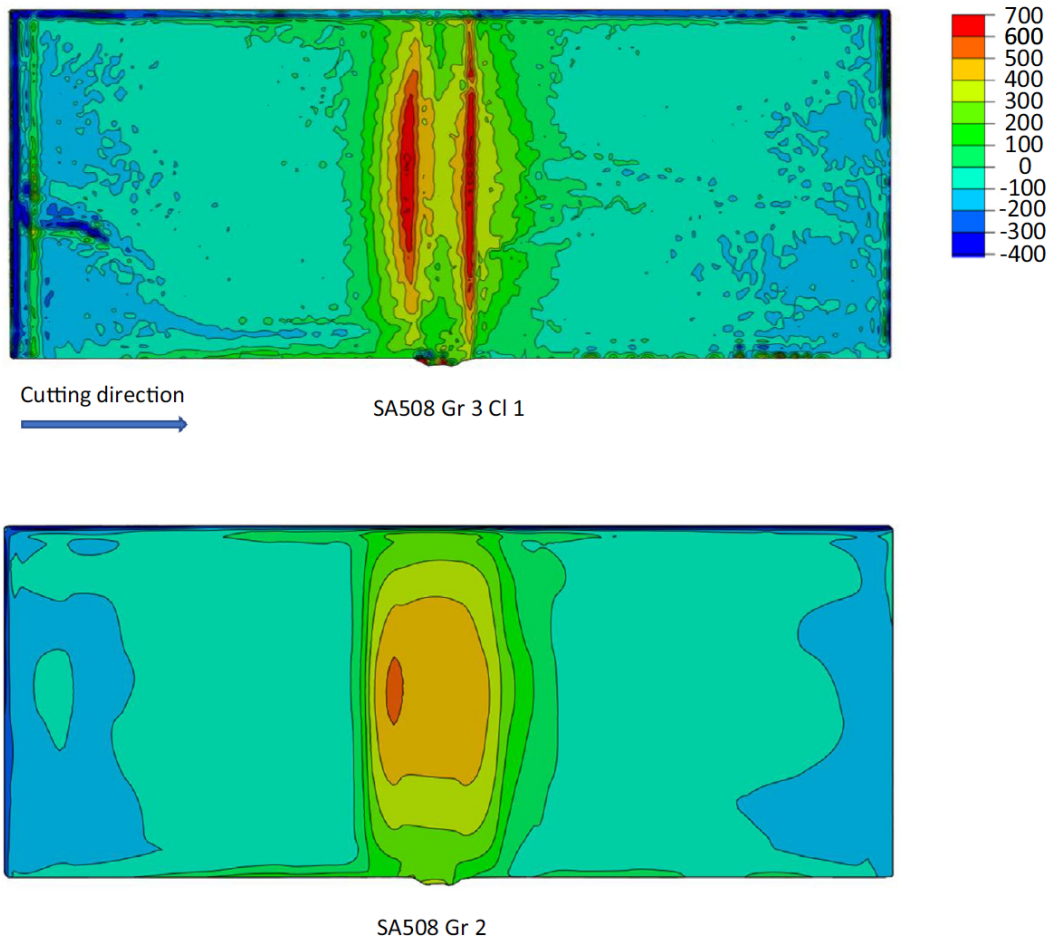

Figure 67. Residual stress measurements in 130 mm thick SA508 Grade 3 Class 1 (top) and SA508 Grade 2 (bottom) steel (From Vasileiou et al. [115], reprinted with permission from Elsevier).

Mechanical properties of the two weld materials were not reported. A separate report released in 2019 evaluating the use of vacuum laser in welding of 130 mm SA508 Grade 3 Class 1 did report Charpy impact data with comparisons to SAW, GTAW, EB, and vacuum laser. ASTM A370 Charpy specimens were extracted from the welds. Welds were completed in the same heat of material using the different weld processes. This project was a continuation of work completed by Rathod [1], with the vacuum laser welds added for further evaluation. The vacuum laser weld was completed from both sides of the plate to achieve full penetration, and the results are shown in Figure 68. The evaluations were performed after PWHT at 607 + / - 13°C for 4 hr. The results of the EB welds show a lower upper shelf energy level near 200 J and a higher ductile-to-brittle transition temperature than that of the base material.

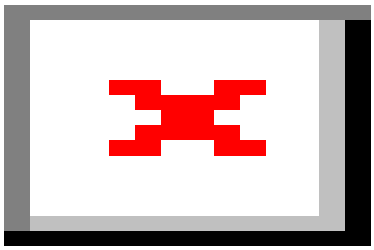

Figure 68. Charpy impact test result of laser and EB (2.2 × 10-2 Torr pressure with helium) welds in 130 mm thick SA508 steel (From Francis [27] reprinted with permission from Elsevier).

Work completed using reduced pressure EBW has shown promise when used in the welding of components for RPVs. The work highlights the role of SSPTs and residual stress levels present in deep-penetrating EB welds in SA508 Grade 3 Class 1 steels. Residual stress levels recorded in NG-SAW, NG-GTAW, and RPEB welds were found to be similar in magnitude, nearing 100 MPa after PWHT, yet varied in distribution. Peak stresses were found in the weld reinforcement and root of traditional arc welds, whereas RPEB welds had peak stresses outside the weld region on both sides of the weld with maximums near mid-thickness. The different distribution of stresses and its impact on the structural integrity procedures were not discussed.

2.8.2 Modular In-Chamber Electron Beam Welding (MIC-EBW) of RPV steel

This section summarizes part of the work completed by EPRI in collaboration with Nuclear AMRC, NuScale Power, and other industrial members to develop assemblies that are part of the ⅔-scale SMR pressure vessel. This work is being conducted to demonstrate the use of advanced manufacturing processes to reduce the cost of SMRs and advanced reactors (GEN IV) [2]. The project aims to demonstrate the production of vessel sections in less than 12 months (reduced by 18 months), a reduction in welding time of 90%, with a cost reduction of over 40% [10]. Time and cost estimates are based on the combination of PM+HIP, EB, and diode laser cladding (DLC) [10]. The thick section EBW plans are to evaluate welding of SA508 Grade 3 Class 1 and 2 RPV steel in (1) forging to forging, (2) forging to PM-HIP, and (3) PM-HIP to PM-HIP material combinations. EBW development is summarized in three yearly reports produced by EPRI with an equipment-specific report on the MIC-EBW development.

2.8.2.1 Small modular reactor vessel manufacture and fabrication - Year 1

This section summarizes work reported by EPRI in the report entitled *Small Modular Reactor Vessel Manufacture and Fabrication Phase 1 – Progress* (3002015814) [10]. Initial work on the project was conducted at Nuclear AMRC, located in the United Kingdom, using their large ProBeam K2000 EBW machine. S355J2+N steel, which is similar to ASTM A572 grade 50, was used for the initial evaluation because of its availability and low cost and its mechanical properties that are similar to SA508 [10]. Plate coupons of S355J2+N carbon (S355) steel at thicknesses of 78, 90, and 100 mm were used to develop the initial weld parameters. The K2000 EBW system uses a mobile internal gun with a power supply capable of 80 kV and 40 kW [122]. Test welds were made at various travel speeds and beam current levels to achieve a good weld. Upon evaluation of the plot in Figure 69, it is apparent that slower speeds were

required for the deeper penetrating thicknesses. No difference in hardness was measured in the S355 steel at the various heat inputs used.

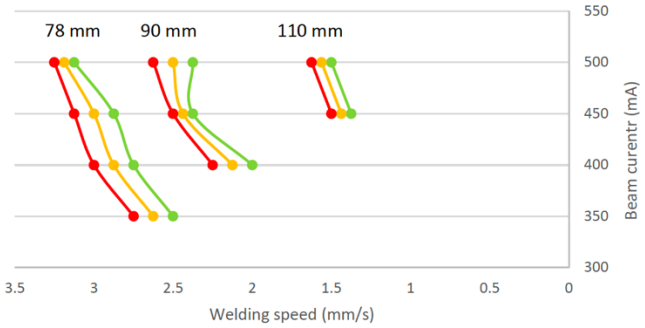

Figure 69. Initial weld development on low kV (60 kV) system at Nuclear AMRC on S355J2+N plate coupons: color indicates quality of weld, red = failed, yellow = poor, green = good (From Gandy [10], reprinted with permission from Electric Power Research Institute).

The results were used to transfer the parameters to an SA508 Grade 3 Class 2 joint at 90 mm thickness. The middle parameter set of 60 kV, 450 mA, and 2.00 mm/sec was used, resulting in a power output of 27 kW and a heat input of 13.5 kJ/mm. The authors note the difference in weld metal fluidity between the two materials. The SA508 Grade 3 Class 2 steel had greater fluidity than seen in the S355 steel [10]. In Figure 70, a cross section of the weld can be seen with a slight undercut of the material near the weld crown on the left side of the image. The EB welds were completed in the 2G horizontal position, mimicking the expected orientation of the reactor girth welds. Fluidity of weld metal is a concern if the volume of molten material is large and if the orientation is unfavorable (i.e., overhead). In the horizontal position, the crown and root are susceptible to droop and weld metal fallout, which occurred along the joint.

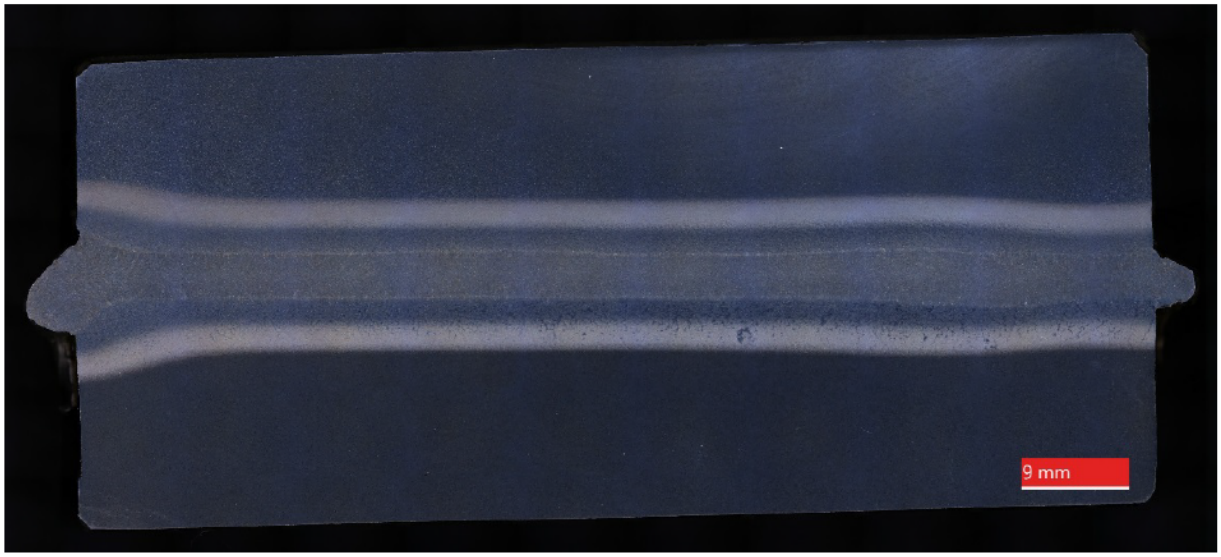

Figure 70. SA508 Grade 3 Class 2 steel weld at 90 mm joint thickness welded in the 2G horizontal position (From Gandy [10], reprinted with permission from Electric Power Research Institute).

Hardness measurements of the as-welded specimen were completed at depths of 30 and 60 mm. The hardness profiles presented in Figure 71 show the M-shaped profile consistent with other work performed on the SA508 grade steels. It is likely that this region is just outside the FZ at a point where the material was heated just below the melting point, fully austenitizing the material. Upon cooling, carbide formation

and large prior austenite grains contribute to an increased amount of hardening when compared to neighboring areas of the weld [85, 129]. Tensile tests were then conducted on the weld in the as-welded and PWHT conditions. Tensile properties for the as-welded specimens averaged 728 and 720 MPA after PWHT, thus meeting the ASME II requirements [10].

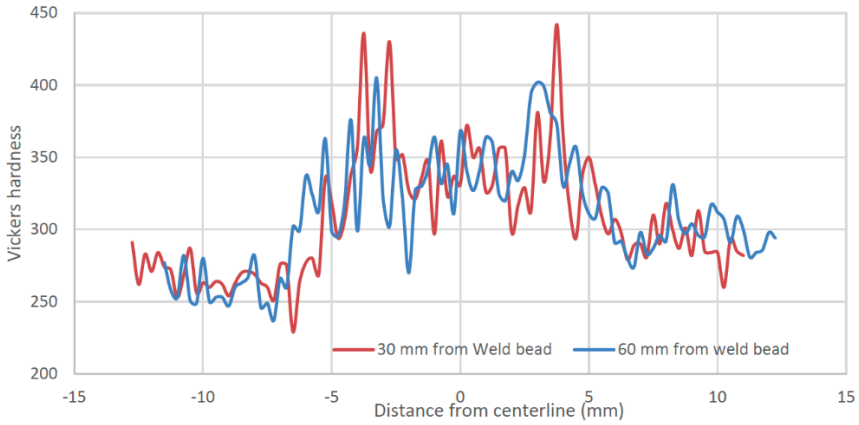

Figure 71. Hardness trace on 90 mm thick SA508 Grade 3 Class 2 steel plates, as welded (From Gandy [10], reprinted with permission from Electric Power Research Institute).

The 60 kV EB welder was sufficient to penetrate the 110 mm thick material, but it was done at a slow travel speed of approximately 1 mm/sec. To increase the operating window and production efficiency, additional welds were completed at 80 kV at beam powers of 32 to 40 kW [2]. Again 78, 90, and 110 mm plates of S355 were used for development, and results were compared to those obtained at 60 kV. Results of the beam power studies are shown in Figure 72. The increase in accelerating voltage to 80 kV allows for deeper penetration and faster travel speeds. A 150 mm weld was made in S355 material with parameters of 450 mA, 80 kV, and 1.5 mm/sec, also noted in Figure 72.

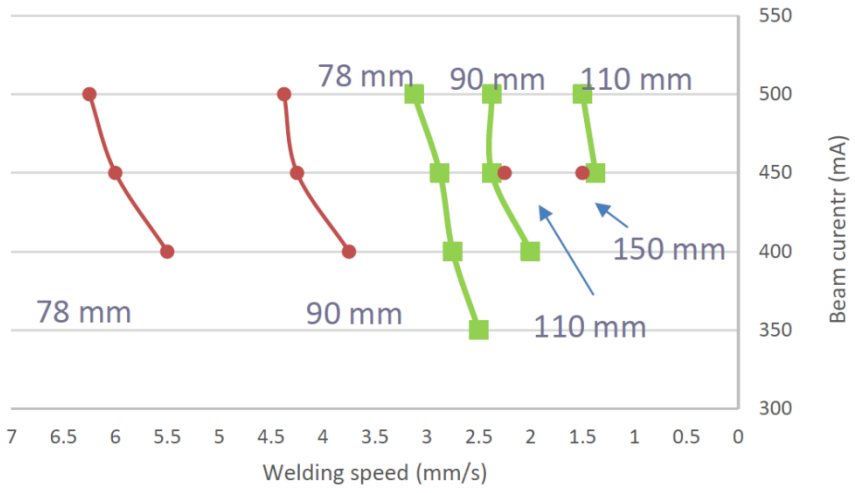

Figure 72. 80 kV system improves capability to achieve deeper penetration (60 kV = green, 80 kV = red) (From Gandy [10], reprinted with permission from Electric Power Research Institute).

Parameters developed on the S355 steel plates were transferred to be used on the SA508 Grade 3 Class 2 material. Unexpectedly, the fluidity of the SA508 Grade 3 Class 2 material was accentuated, causing additional weld fallout at the crown of the weld. The reason for the differing material response between

SA508 Grade 3, Class 2 and S355 steel is not fully understood. A drip tray or integral groove (discussed in Section 2.4.11) could be used to support the weld crown and/or root. SA508 Grade 3 Class 1 material was then used for analysis of Charpy impact toughness. Two samples were produced, one at 60 kV (S/N BJ09), and one at 80 kV (S/N BJ06). At 60 kV, a beam current of 450 mA and travel speed of 2.0 mm/sec resulted in a heat input of 13.5 kJ/mm [10]. At 80 kV, a beam current of 450 mA and travel speed of 3.5 mm/sec was used with a heat input of 10 kJ/mm [10]. Two different methods were used for the support bar: an integral backing bar on BJ06, and support bars on BJ09, as shown in Figure 73. The welded plates were cut in half so that one could be analyzed in the as-welded condition and one could be subjected to PWHT at 607°C ± 13°C for 150 minutes.

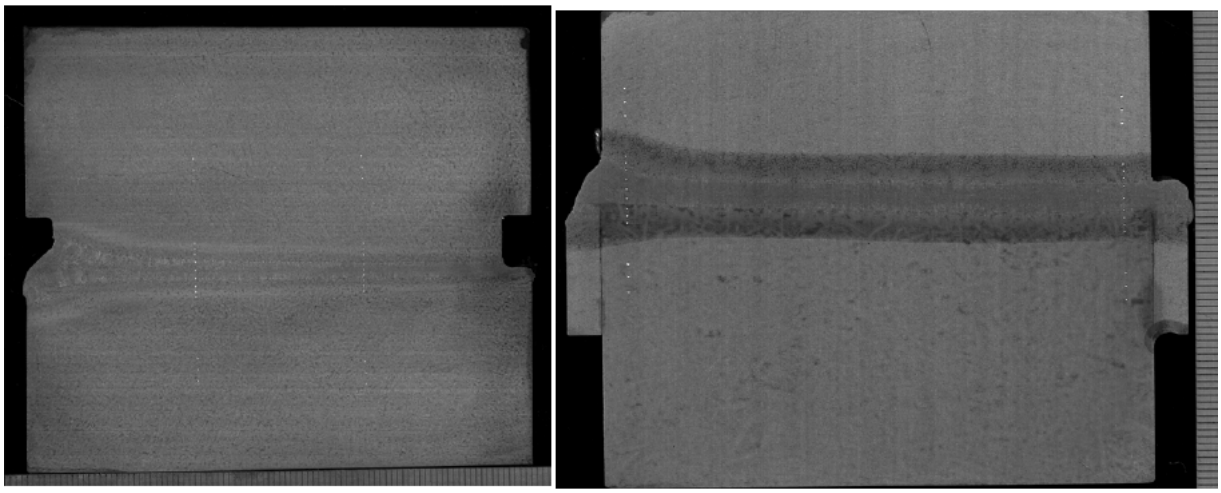

Figure 73. SA508 Grade 3 Class 1 weldments. BJ06 using integral backing (left), and BJ09 using support bars (right) (From Gandy [10], reprinted with permission from Electric Power Research Institute).

Charpy specimens were then removed from the weldments with V-notches located on the weld centerline, HAZ, and base material. Results from the toughness tests can be seen in Figure 74. Toughness was greatly improved in the FZ (weld center line) and HAZ after PWHT. A higher weld metal toughness was achieved in the weld metal of the lower heat input 80 kV sample. Further analysis of the weld microstructure is needed to characterize this difference in toughness between weld metal and HAZ toughness values before and after heat treatment.

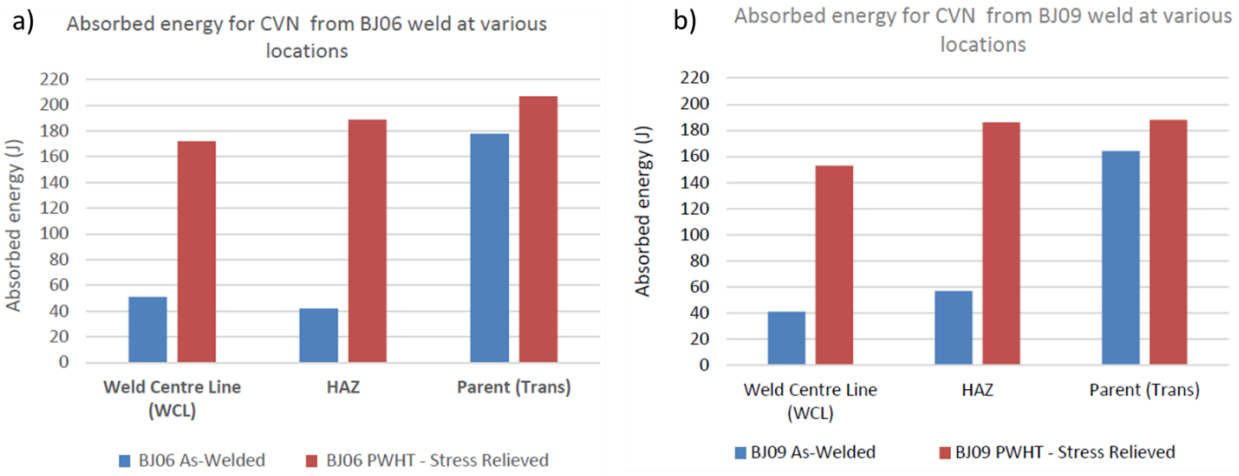

Figure 74. Charpy impact values from SA508 Grade 3 Class 2 EB welds: BJ06, 10 kJ/mm, 80 kV (a), and BJ09, 13.5 kJ/mm, 60 kV (b) (From Gandy [10], reprinted with permission from Electric Power Research Institute).

A mockup weld was completed at the end of the year 1 study to weld an 1,805 mm diameter flange-to-cylinder mockup. The joint consisted of a 76 mm wall thickness and was welded using the BJ09 parameters developed on the plate material. The cylinder was tack welded in 16 locations around the cylinder before being welded with a continuous beam. This weld successfully demonstrated the ability of the EB weld to reduce the cycle time of a full penetration thick section weld. It took a total of 1 hour, including 47 minutes of full penetration welding time, to complete the assembly weld.

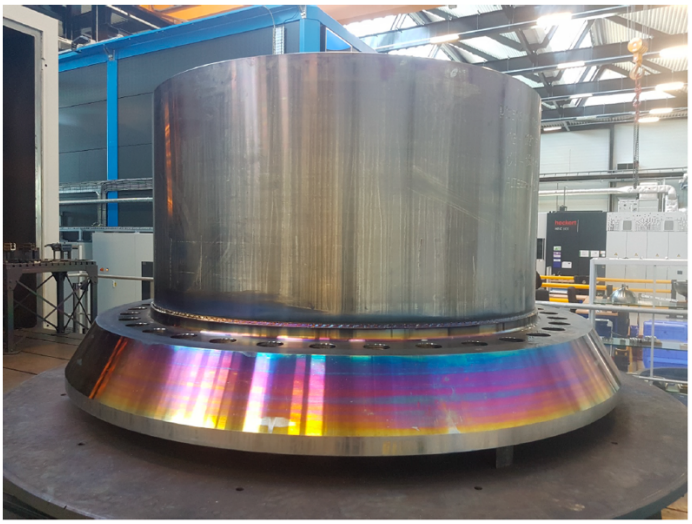

Figure 75. Flange-to-cylinder mockup weld completed in 47 minutes (From Gandy [10], reprinted with permission from Electric Power Research Institute).

2.8.2.2 Small modular reactor vessel manufacture and fabrication – Year 2

Year 2 development focused on the slope-in and slope-out segments of the EB weld and the joining of two half sections of the lower head assembly. The slope-in of the weld involves the ramping of weld parameters to the steady-state full penetration weld parameters quickly over a short distance. Travel speed and beam current are often sloped from zero to the full penetration parameters while high voltage and focus are maintained. Once the weld is completed, a slope-out is programmed to lower the beam intensity to transition from full penetration to zero. Beam current, travel speed, and focus are often adjusted at the

end of the weld during slope-out. Sloping out of the weld is considered more important, because the slope-in is often fully consumed by the full penetration weld upon completion of a circular weld, with the slope-out remaining as part of the final product. The transitory nature of sloping out of the full penetration parameters to no penetration is more difficult with higher energy, deep penetrating welds. As discussed in Section 2.4.8 and as illustrated in Figure 20, the weld parameters must transition from keyhole mode welding to conduction mode and finally to no melting. The transition between each mode can be abrupt because of the energy densities and material vaporization. The length of the slope-out is generally over several millimeters, but longer slope-out lengths are needed for high-power deep-penetrating welds. A slope-out test conducted by EPRI is shown in Figure 76. The weld was made from the bottom outer circumference of the sample and can be seen progressing from full penetration on the left side of the image and approaching the outer surface on the right side of the image.

Figure 76. Longitudinal section from slope-out region of EB test weld (From Gandy [7], reprinted with permission from Electric Power Research Institute).

To develop the slope-in and slope-out segments, a 1.9 m diameter × 80 mm thick ring of S355 steel was used. The BJ09 welding parameters were used with added oscillation defined at a 2 mm sweep normal to the weld direction, 1 mm in the weld direction, and at 501 Hz frequency [7]. Welds were made sloping out over 400 mm in length, with an initial focus value of -490 mA, noted as being 20 mm below the top surface of the joint [7]. The initial trials for the slope-out were conducted by varying the focal position by changing the lens current and the beam current. Over the 400 mm, the beam current was reduced to 0 mA and the lens current was changed from -490 mA at +160 mA intervals, with a final value of +640 mA (i.e., +1,130 mA greater than the true focus lens current) [7]. This is shown graphically in Figure 77. The slope-out is from right to left in the figure, with the beam current of 450 mA and the lens current (defocus) of -490 mA, thus representing the full penetration parameter set.

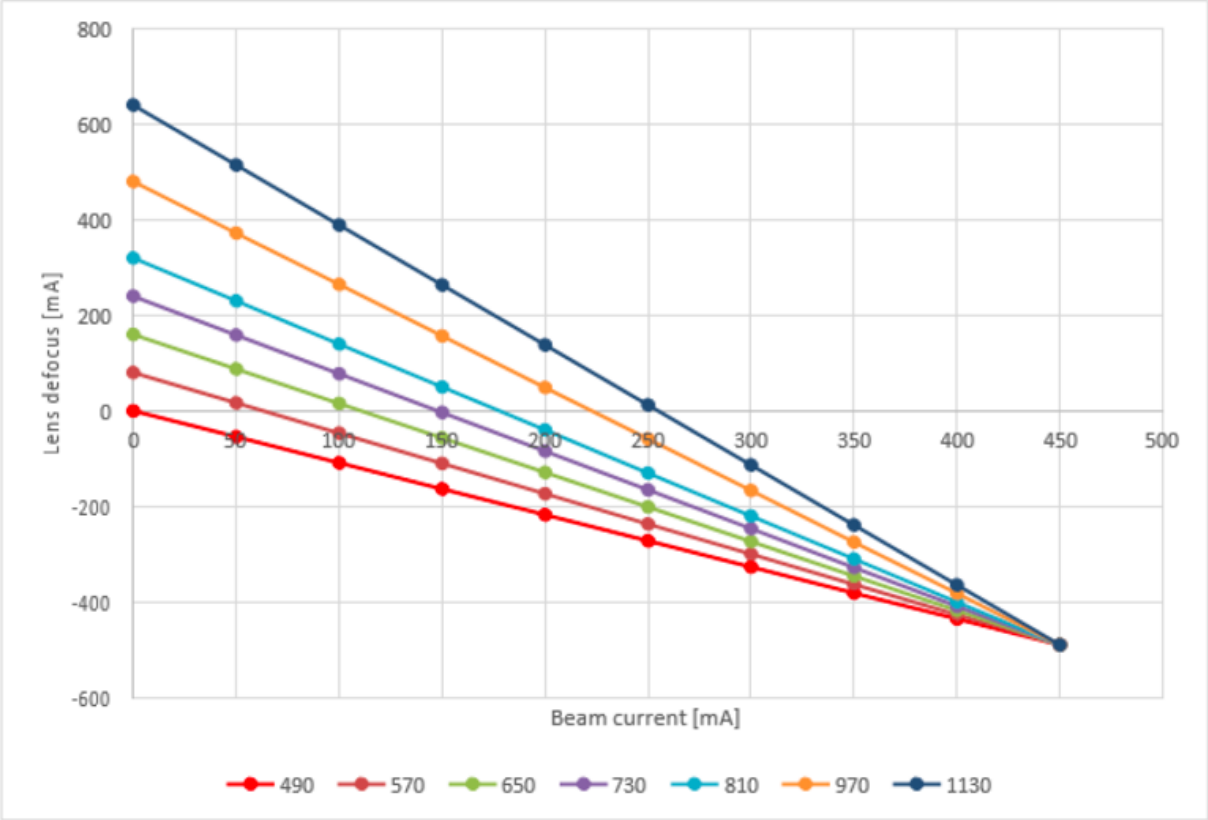

Figure 77. Slope-out conditions from right to left: beam current reduced to 0 while adding 160 mA to lens current to adjust focal position (From Gandy [7], reprinted with permission from Electric Power Research Institute).

Results of the test conditions can be seen in Figure 78. Red arrows indicate the positions at which focus was at the original joint surface. Positions to the left of the red arrow in the direction of the weld are over-focused, being above the surface of the original joint. Upon visual examination of the slope-out parameters, the bead profile can be seen changing along with the parameters. It is not specified whether the beam oscillation is terminated at the start of the slope-out or if it is continued throughout. If the beam oscillation was turned off, that may be the reason for the change in visual appearance at the onset of the slope-out. At +490, the crown of the weld shows obvious defects, including pores and loss of material. Because the focal position is increasingly varied, the slope-outs improve until at +1,130, the crown can be seen sagging in the over-focused segment. Manual and phased array ultrasonic testing (PAUT) were conducted on the slope-out regions to assess weld quality. Through manual UT, the +970 mA setting provided for the condition with the least defect [7].

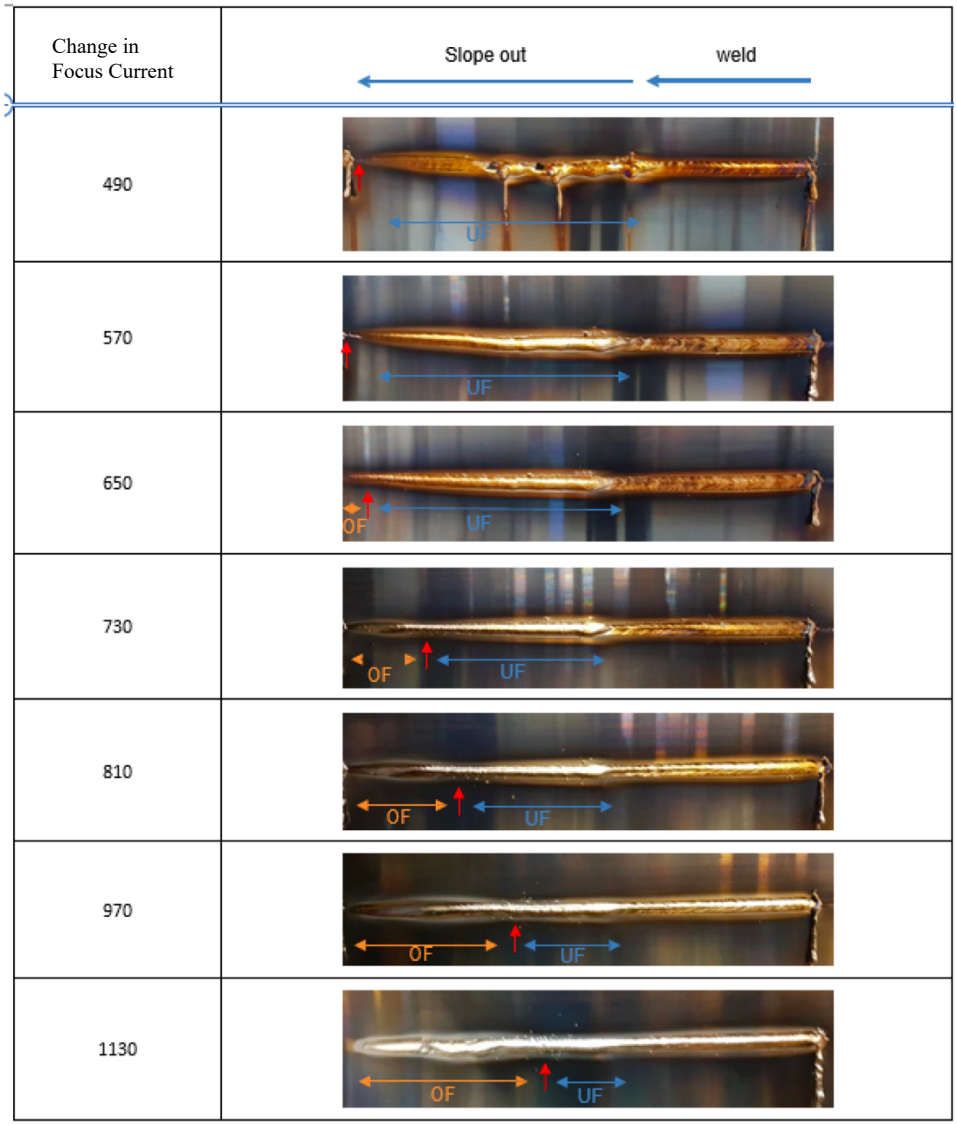

Figure 78. Slope-out trials on 1.9 m diameter × 80 mm thick S355 ring, changing focal position from under focus to over focus (From Gandy [7], reprinted with permission from Electric Power Research Institute).

PAUT was used to further evaluate the quality of the slope-out regions. Traces generated during testing are shown in Figure 79. Pores and spiking defects were seen during UT. Pores at the onset of the slope-out and spiking defects defined as a sudden increase in penetration beyond the average penetration line were noted in the report [7]. Review of the PAUT results shown in Figure 79 indicates that pores appear to be primarily near the top surface of the weld in all conditions. Spiking defects as referenced in the report are not seen in the weld slope-out that changes the focal point +1,130 mA, and spiking defects decreased as the length of weld in the over-focused position increased. The report states that the over-focused condition does not suffer as much in terms of spiking defects as the under-focused condition.

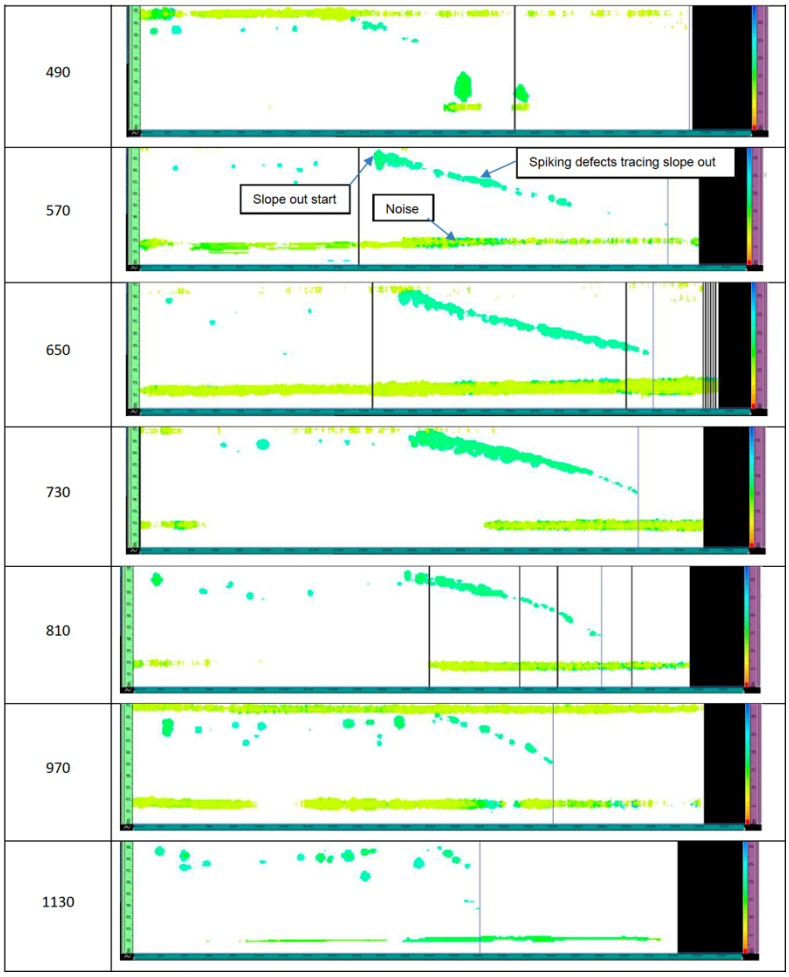

Figure 79. PAUT traces of slope out regions; welds from left to right, with root of weld at top of scan image (From Gandy [7], reprinted with permission from Electric Power Research Institute).

Tabulated results of the PAUT traces can be seen in

Table 11. All welds were characterized as having pores and spiking defects. The position of the last defect was the smallest, with a focal position parameter of +1,130. However, under visual inspection, the weld cavity was beginning to sag. A best parameter set was not explicitly stated, but the +970 focal position parameter was chosen as the best effort for the next round of tests.

Table 11. PAUT of slope-out regions (From Gandy [7]).

Parameters	Weld Length (Steady State)	Slope Length	Welding Defocus	Welding End Focus	Defect Types	Position Last Defect
[]	mm	mm	mA	mA	Open cavity	mm
490	100	400	-490	-490+490=0	Pores/spiking	320
570	100	400	-490	-490+570=80	Pores/spiking	435
650	100	400	-490	-490+650=160	Pores/spiking	420
730	100	400	-490	-490+730=240	Pores/spiking	410
810	100	400	-490	-490+810=320	Pores/spiking	382
970	100	400	-490	-490+970=480	Pores/spiking	342
1130	100	400	-490	-490+1130=640	Pores/spiking	285

Based on the previous results, a second set of experiments was completed. The +970 mA focal position parameter set was chosen as the baseline for further development of oscillation parameters. Initial welds made with reduced travel speed were not successful and were not evaluated further. An increase in the slope-out length (800 mm) was incorporated into the next round of tests to include alternate oscillation patterns. The increase in slope-out length and oscillation size allowed for additional time for weld degassing, which was sought in this trial [7]. These parameters are tabulated in Table 12. Welding parameters of voltage and beam current were maintained, along with the increase in focal position of +970 mA over the length of the slope-out, resulting in an over focus position at weld termination. The oscillation parameters are reported as *vertical*, *horizontal*, and *frequency*. For Weld 1, the welding oscillation was 2 mm vertically, 1 mm horizontally, and at 501 Hz frequency. All welds were completed horizontally in the 2G position. Through the slope-out, the parameters are programmed to linearly ramp between the welding oscillation to the slope oscillation over the slope length, at which time the weld is terminated.

Table 12. Slope-out experiment 2 with adjusted oscillation parameters (From Gandy [7])

Parameters	V	I	Welding Defocus	Welding End Focus	Oscillation Welding	Oscillation Slope	Slope Length
[]	kV	mA	mA	mA	mm/mm/Hz	mm/mm/Hz	mm
Weld 1	60	450	-490	480	2/1/501	2/1/501	800
Weld 2	60	450	-490	480	2/1/501	3/1/501	800
Weld 3	60	450	-490	480	2/1/501	4/1/501	800
Weld 4	60	450	-490	480	2/1/501	4/2/501	800

The parameters were incrementally adjusted after visual inspection of each weld. The increase to 3 mm of vertical beam oscillation (normal-to-weld direction) was deemed too slow after weld 2 and was increased to 4 mm [7]. An increase to the horizontal direction (weld direction) was completed for weld 4. Photos of the four weld conditions are included in Figure 80. PAUT was used to ascertain the quality of the slope-out region of the four welds.

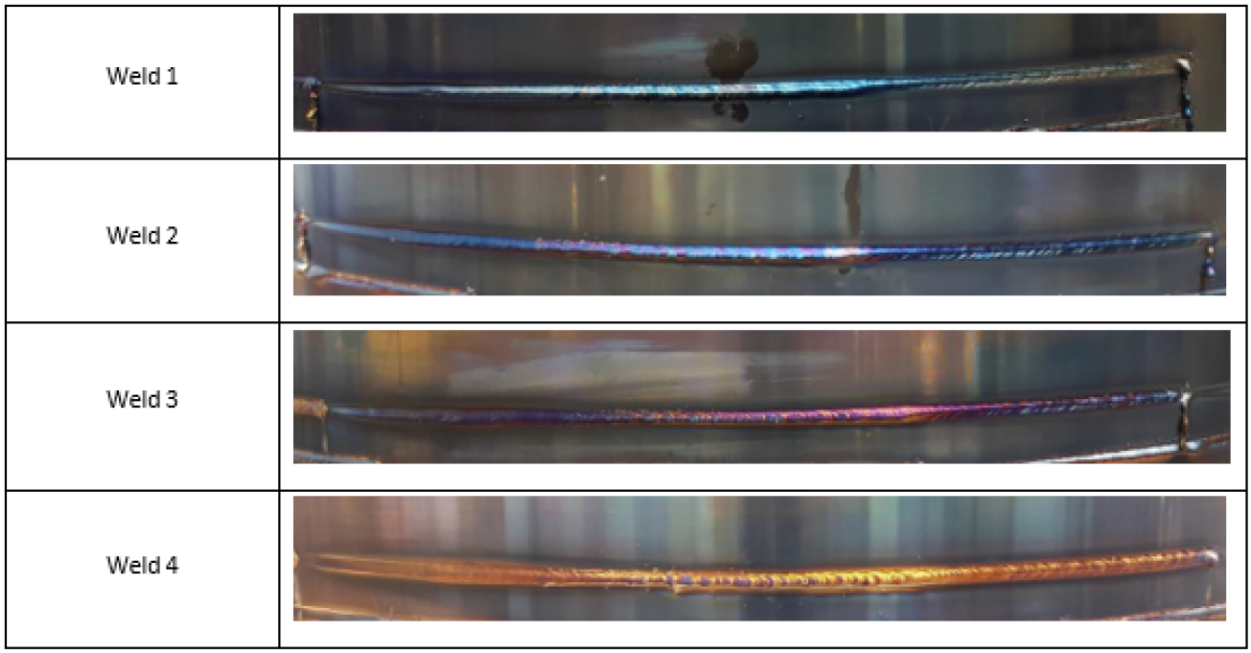

Figure 80. Visual weld appearance of slope-out experiment 2; weld direction is right to left (From Gandy [7], reprinted with permission from Electric Power Research Institute).

PAUT traces of the four welds are shown in Figure 81. The welds progressed from left to right in the PAUT traces with the backwall and the root of the weld at the top of the image. During the slope-out, the penetration decreases sloping to the bottom weld reinforcement. The exact location of the slope-out start position cannot be ascertained from the photos provided, but the back wall echo indications can be seen in all welds leading up to the slope-out location. In welds 1 and 2, the backwall indications can be seen linearly sloping towards the weld reinforcement. These indications may be caused by root spiking or porosity. In weld 3, no indications are seen as the backwall echo disappears without additional indications in the slope-out region. Weld 4 was noted as having similar results. Small indications in weld 4 may be PAUT artifacts, or they may be outside of the slope-out area of interest. Without additional information, interpretation is deferred to the NDE technician performing the evaluation.

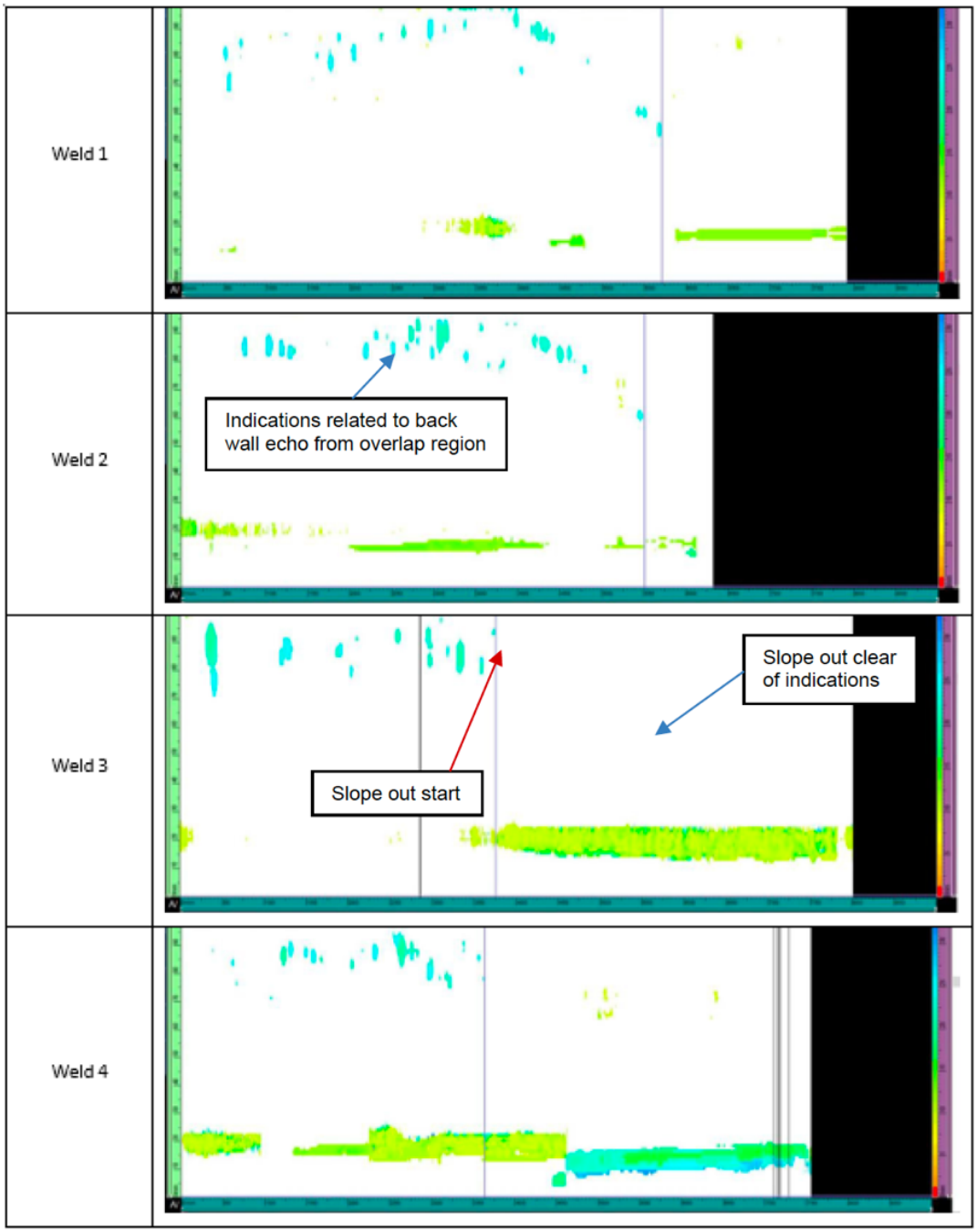

Figure 81. PAUT traces of slope-out experiment 2 (From Gandy [7], reprinted with permission from Electric Power Research Institute).

A complete weld was tested on a ring of S355 steel 1.9 m diameter and 80 mm wall thickness to include the new slope-out settings. The parameters developed for the SA508 steel were used: BJ09 (60 kV, 450 mA, 2.00 mm/sec) with weld 3 slope-out [7]. With the different weld behavior, less fluidity of the S355 steel resulted in a flatter crown and a more pronounced root. Undercutting was evident on the top surface of the weld, which was more pronounced at the start of the overlap [7]. A PAUT trace of the weld slope-out region was reported to be clean and free of defects [7].

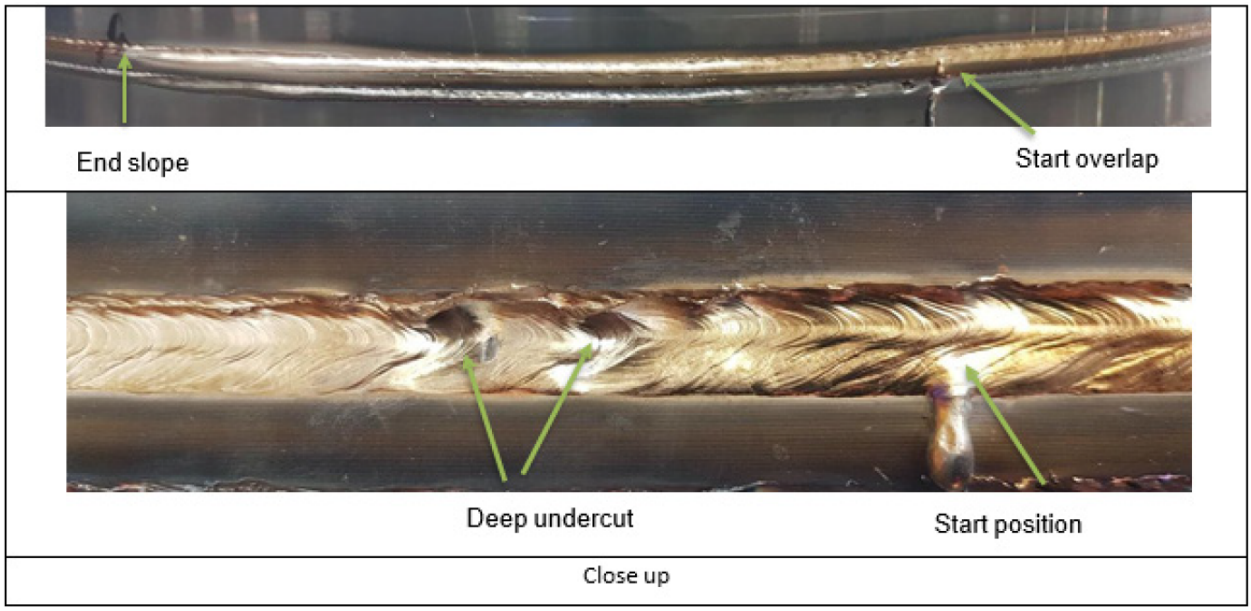

Figure 82. S355 circumferential weld with improved slope-out (From Gandy [7], reprinted with permission from Electric Power Research Institute).

Welding of a lower head section was completed as part of the Year 2 effort. Two S355 steel head halves were welded together to form a mockup lower head assembly. The assembly process is shown in Figure 83. The parts were prepared to be welded in the 2G position with backing bars, impingement blocks installed on the inside of the fixture, and an integral step on the internal and external sides of the bottom component to provide support of the molten puddle during welding. For welding of the lower head assembly, a maximum magnetism of 2 G was required to prevent beam deflection [7]. The method for determining the level of magnetism is not described. The tooling path was manually programed using electron optics seam tracking, along with automated seam tracking to correct for deviations from the joint line. Welding parameters were again BJ09 (60 kV, 450 mA, 2.0 mm/sec), and welding was completed using the K2000 EB system at Nuclear AMRC. Tacking of the assembly was conducted at reduced beam current, 100 mA, and faster travel speed of 10 mm/sec [7].

Figure 83. Lower head section halves assembly and fixturing (From Gandy [7], reprinted with permission from Electric Power Research Institute).

The welded lower head assembly is shown in Figure 84. The entire welding operation was said to be completed in 25 minutes, with minor fluctuations in high voltage recorded by the data acquisition system [7]. Nondestructive testing of the welding assembly was conducted according to ASME code requirements. Time-of-flight UT and manual UT techniques were used to evaluate and characterize the weld. Small indications were documented and deemed acceptable according to code requirements.

Results of the Year 2 study show that the weld is capable of sloping out under stable conditions without causing defects. Parameters were developed to increase the slope-out region to 800 mm and to extend the oscillation parameters to further stabilize and slow the collapse of the keyhole. This work led to the successful demonstration of a full assembly weld on the lower head assembly. Seam tracking and data logging of the beam parameters were noted as being helpful for decreasing the time to setup and evaluate the stability of the weld in process [7].

Welded dome

Close up

Root

Figure 84. Complete welded lower head assembly (top left), welded dome (top right), root of weld (bottom) (From Gandy [7], reprinted with permission from Electric Power Research Institute).

2.8.2.3 Small modular reactor vessel manufacture and fabrication - Year 3

Year 3 results are reported in the EPRI report entitled *Program on Technology Innovation: Small Modular Reactor Vessel Manufacture and Fabrication Phase 1 – Progress* (Year 3), 3002021037 [2]. The first welding trails for Year 3 focused on the replication of the slope out characterization on SA508 Grade 3 LAS instead of the S355 material used in Year 2. Welding parameters for the SA508 Grade 3 alloy welds are shown in Table 13. The EPRI Year 3 report discusses a bead-on-plate (BOP) trial #1 consisting of 5 welds evaluating the change in focal position during the slope out. The report then refers to additional tests as BOP trials #1 through #4, with trial #1 repeating the best condition from the BOP trial #1 welds. The present report refers to the first tests as the *focal position slope-out tests*, and the following tests are referred to as the *BOP trials* to help clarify the testing conditions.

To set up the focal position slope out tests, the lens current that would be needed to focus on the top of the plate was determined. This was referred to as the *electron optics* (ELO) focus and was set at a lens current of 2,520 mA for this machine. The weld defocus, as discussed previously in the section on Year 2, was -490 mA from the top surface, equating to 2,030 mA of lens current. Subsequent slope-out tests increased the amount of defocusing over the same slope-out length of 400 mm. The primary focus of BOP trial #1 was to evaluate the change of focal position which was tabulated as welding end defocus. Test conditions at +490 and +1,290 mA were noted as losing the positive reinforcement of the weld. At +730 and +970 mA, the weld met visual appearance criteria to be very stable. PAUT results of the trial #1 welds found indications in the +490, +1,130, and +1290 mA defocus parameter sets. Spiking flaws were present in both the +730 and +970 mA PAUT scans, with fewer flaws noted in the +970 mA test weld. Matching the results of the previous year, the +970 mA slope procedure produced the fewest defects, was noted as being very stable, and contained a small region of spiking indications.

Table 13. Focal position slope-out tests on SA508 Grade 3 low alloy plates (From Gandy [2] reprinted with permission from Electric Power Research Institute)

Parameters	V	I	Speed	ELO focus	Welding defocus	Oscillation
	kV	mA	mm/s	mA	mA	mm/mm/Hz
Steady state welding	60	450	2.00	2520	-490	1/3/501
Slope out welding	60	450	2.00	2520	Variable	2/1/501

Slope Defocussing	Steady State Weld length	Slope length	Welding defocus	Welding end defocus	Indications	Position of last defect
	mm	mm	mA	mA	N/A	mm
490	100	400	-490	+490	Pores	350
730	100	400	-490	+730	Spiking	360
970	100	400	-490	+970	Spiking (reduced)	270
1130	100	400	-490	+1130	Pores/spiking	300
1290	100	400	-490	+1290	Pores/loss of crown	350

The second set of tests further evaluated the slope-out through use of a longer slope-out length followed by an oscillation change. The results of the second set of BOP trials #1 through #4 is shown in Figure 85. BOP #1 is the best weld from the focal position slope-out tests at +970 mA defocus and 400 mm slope-out length. BOP #2 increased the slope-out length to 800 mm, which was double the BOP #1 slope-out length with all other parameters equal. BOP #3 repeated BOP #2 with an oscillation change from a horizontal to vertical pattern. The horizontal pattern was termed a *full penetration oscillation pattern* whereas the vertical pattern was termed a *partial penetration oscillation pattern*. This naming convention is correct when welding in the 2G position, in which the horizontal pattern maintains the beam along the axis of the weld for a greater amount of time. The beam spends more time near the highest heat area of the weld aiding in penetration. A vertical oscillation in the case of a horizontal weld would distribute the heat normal to the weld direction, thus minimizing the time at the central region of the weld. During steady-state conditions, this would have the effect of widening the weld. During the slope-out, the vertical oscillation was tested to soften the intensity of the beam as it partially penetrates the material. BOP #4

maintained the vertical, less penetrating oscillation used in BOP #3 and extended the slope-out length to 1,600 mm. PAUT was used to determine weld quality.

Table 14. BOP #2 slope-out length trial welds (Adapted from Gandy [2])

BOP #	Slope length (mm)	Oscillation	Welding defocus (mA)	Welding end focus (mA)	Indication	Position of last flaws (mm)
1	400	Horizontal	-490	+970	spiking	250
2	800	Horizontal	-490	+970	spiking	470
3	800	Vertical	-490	+970	spiking	470
4	1600	Vertical	-490	+970	Defect free	N/A

PAUT results shown in Figure 85 contain images from all four welds and scan results. BOP #1 was a repeat from the focal position tests and had some indications that were determined to be root spiking. BOP #2 had some indications following the slope-out indicative of root spiking or porosity. These indications were found to be well below the reportable indication size in accordance with ASME Section V, as stated in the EPRI report [2]. BOP #3, which added the change in oscillation direction, was shown to further reduce PAUT indications, with small indications seen at approximately ⅓ of the joint thickness. These indications were also below the reportable indication size in accordance with ASME Section V criteria [2]. The last weld, BOP #4, included another increase in slope-out length to 1,600 mm. No indications can be seen in the PAUT results of the slope-down region.

+970 mA 400mm long Repeat		
+970 mA 800mm long		
+970 mA 800mm long Oscillation change	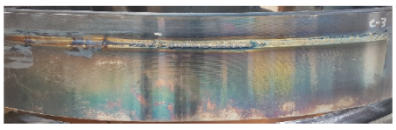	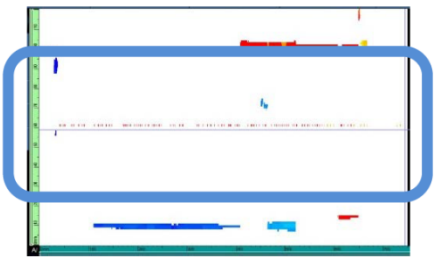
+970 mA 1600mm long Oscillation change		

Figure 85. SA508 slope-out PAUT results of BOP #2, trials #1 through #4, top to bottom (From Gandy [2], reprinted with permission from Electric Power Research Institute).

Gandy does not specify the reason for choosing the 800 mm slope-out length instead of 1,600 mm, but other factors such as heat input, visual inspection criteria, and overall length may have been factors. The final slope-out parameters developed for SA508 Grade 3 material are shown in Table 15. The table includes slope steps 1 and 2. Beam power and welding defocus ramp linearly throughout the two steps. A closer look at the beam oscillation shows that the vertical oscillation also linearly ramps throughout, progressing from 1 to 3 to 5 mm. However, horizontal oscillation required the additional slope step as a result of the change from 3 to 1 mm over the first 266 mm, and then it stayed at 1 mm over the remaining 533 mm. Without this step, the change from horizontal to vertical would occur at a slower rate. The

details on this change and a description of how it was developed are not discussed in detail in the Year 3 report.

Table 15. SA508 Grade 3 welding and slope-out parameters (From Gandy [2])

Parameters	Section length	Beam power	Welding defocus	Beam oscillation
[]	mm	mA	mA	mm/mm/Hz
Welding	As required	450	-490	1/3/501
Slope step 1	266.66	Down to 300	-490+323	3/1/501
Slope step 2	533.33	Down to 0	-490+970	5/1/501

The successful development of a slope-out procedure on SA508 Grade 3 plate material was then tested on a test ring mockup of the production weld. A test ring was welded using two forged rings of SA508 Grade 3 Class 1 material. This sample was named *test ring weld 1*, with both pieces from the same forging. The parameters shown in Table 15 were used to complete the weld. A photo of the slope-out region can be seen in Figure 86. The weld can be seen progressing from right to left in the image, with the slope-out near the far left of the image. Using TOF diffraction (TOFD) ultrasonic scans and PAUT, there were indications that followed the expected slope-out profile of the weld.

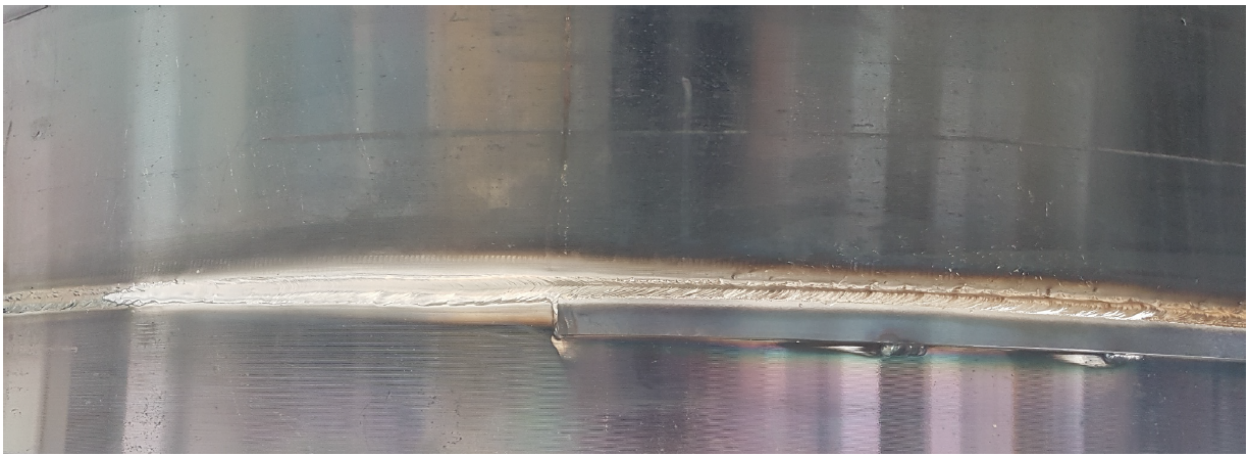

Figure 86. SA508 Grade 3 Class 1, test ring weld 1 (From Gandy [2], reprinted with permission from Electric Power Research Institute).

In Figure 87a, the indications can be seen in the PAUT scan following the expected slope-out profile. In this case, the weld progressed from right to left in the PAUT scan images. The indications were filtered using ASME Section V criteria for reportable indications, and results are shown in Figure 87b. No indications exceed the ASME Section V criteria [2]. Test ring weld 2 was completed as a repeat of test ring weld 1 using the same SA508 Grade 3 Class 1 forging for both pieces to see if the slope out was repeatable [2]. The PAUT and TOFD data were reported to be nearly identical [2]. A cosmetic weld pass was applied to the test ring weld 2 assembly, which reduced the underfill areas on the weld face. The as-welded photo of the test ring weld 2 is shown in Figure 88, and it is also shown after the cosmetic pass in Figure 89.

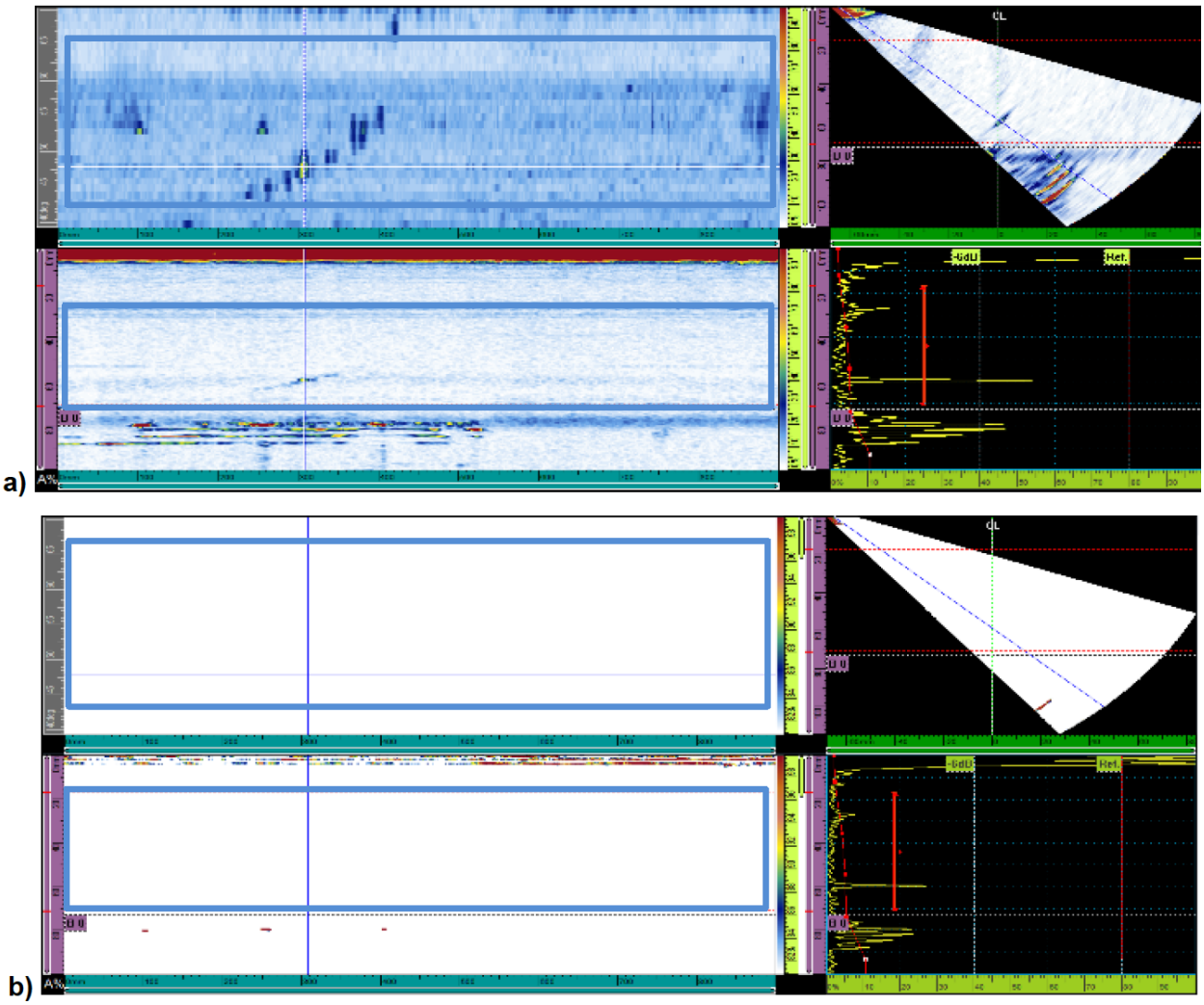

Figure 87. PAUT scans of test ring weld 1: scan with all data showing indications at slope-out region (a), and data filtered to ASME detection requirements (b) (From Gandy [2], reprinted with permission from Electric Power Research Institute).

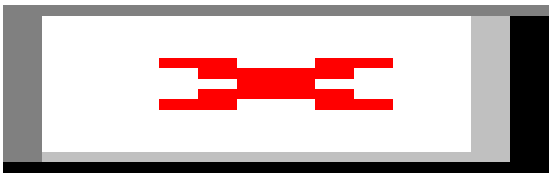

Figure 88. Test ring weld 2, as welded at slope-out location (From Gandy [2], reprinted with permission from Electric Power Research Institute).

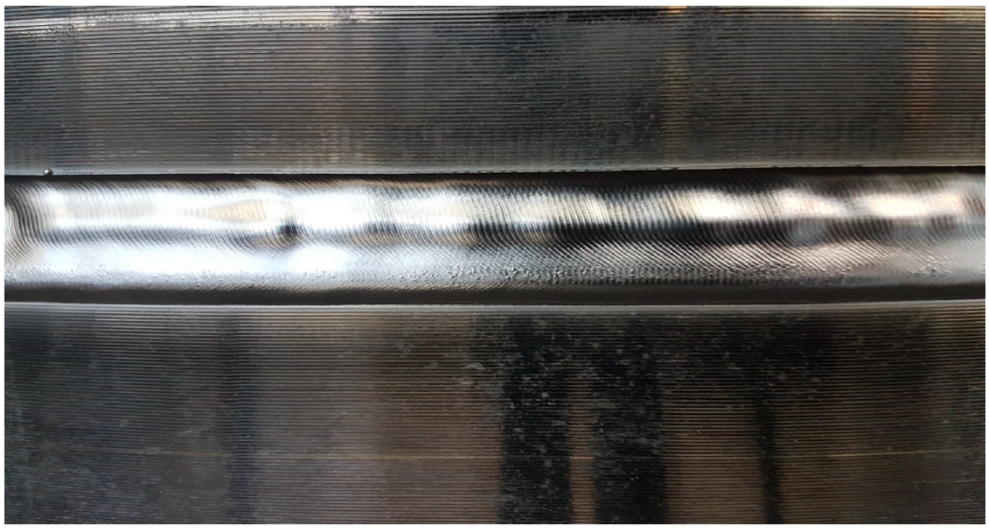

Figure 89. Test ring weld 2 after cosmetic welding pass (From Gandy [2], reprinted with permission from Electric Power Research Institute).

A mockup assembly was completed after developing the welds on rings. The mockup consists of a forged flange, shell cylinder, and lower dished head made of SA508 forgings. This assembly made up the third and fourth full diameter welds that were completed as part of the milestones of this project. An outer diameter of 1,780 mm and a joint thickness of 80 mm for the shell-to-flange was used for the mockup of the NuScale RPV [2]. Welding support bars were integrated into 5 mm steps on the inside and outside of the flange section. The semi-automated setup included seam tracking and tacking. The final weld was completed in 50 minutes of beam time and 2 hours overall using the weld parameters developed previously at 60 kV and 450 mA [2].

Figure 90. Shell-to-flange mockup weld 1, assembly (left); completed weld (top right); overlap (lower right) (From Gandy [2], reprinted with permission from Electric Power Research Institute).

Nondestructive testing of the shell-to-flange mockup included TOFD, PAUT, and dye penetrant inspection (DPI). To complete the DPI, the weld crown and root were machined smooth. DPI indications on the outside diameter were caused by underfill [2]. Photos from the DPI can be seen in Figure 91. Four regions were hand dressed to a depth of 4 mm. The slope-out region was the only section of the weld with

TOFD indications. These were reported to be identical to the test ring weld 1 and 2 results, with no recordable indications found using PAUT [2].

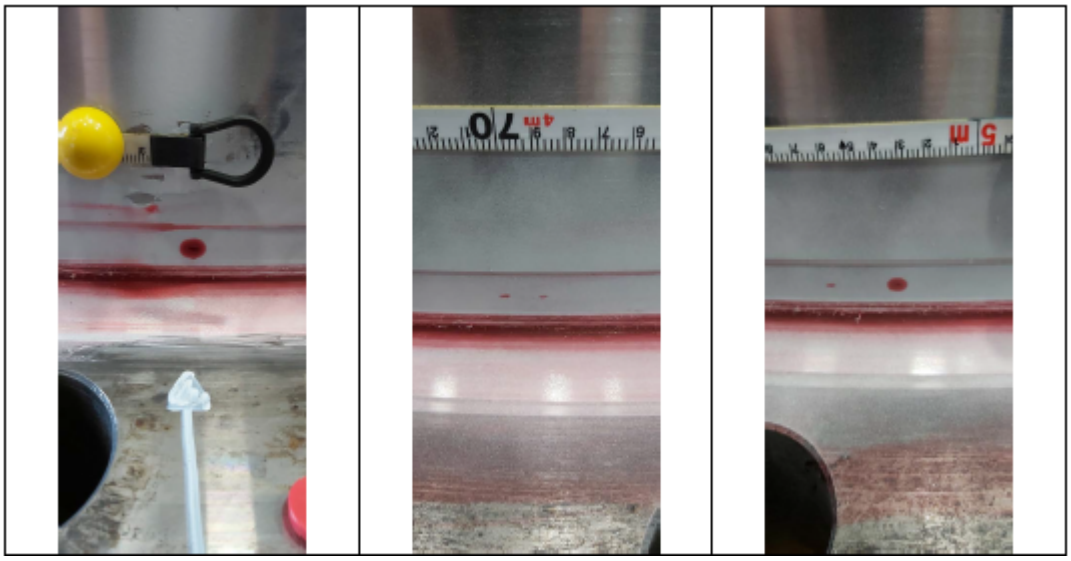

Figure 91. DPI of the shell-to-flange weld (From Gandy [2], reprinted with permission from Electric Power Research Institute).

After successful completion of the shell-to-flange weld, the assembly was prepared for welding of the shell to the dome, making up the fourth full diameter weld. This component was measured for magnetism prior to welding, with readings between 3 and 4 on the entire joint face [2]. The assembly exceeded the maximum level of 2 G that was set as part of this project [2]. No magnetic lifts or tooling was used on the mockup to avoid magnetizing the components. The assembly was demagnetized through the use of an AC power supply and through wrapping a coil around the unit as shown in Figure 92.

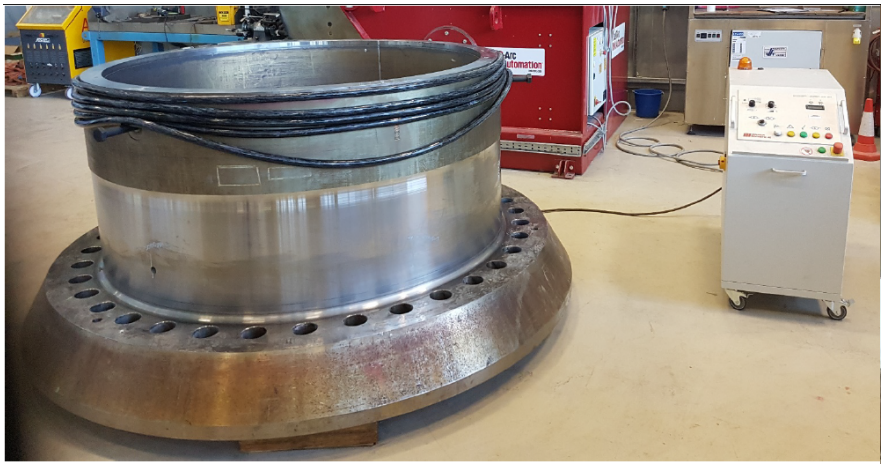

Figure 92. Demagnetizing the shell-to-dome joint on the mockup (From Gandy [2], reprinted with permission from Electric Power Research Institute).

Setup of the shell-to-dome weld included placement of an impingement device within the mockup to absorb excess beam energy after it fully penetrates the joint, as shown in Figure 93. The lower dome assembly was then lowered on top of the shell-to-flange mockup to complete the assembly.

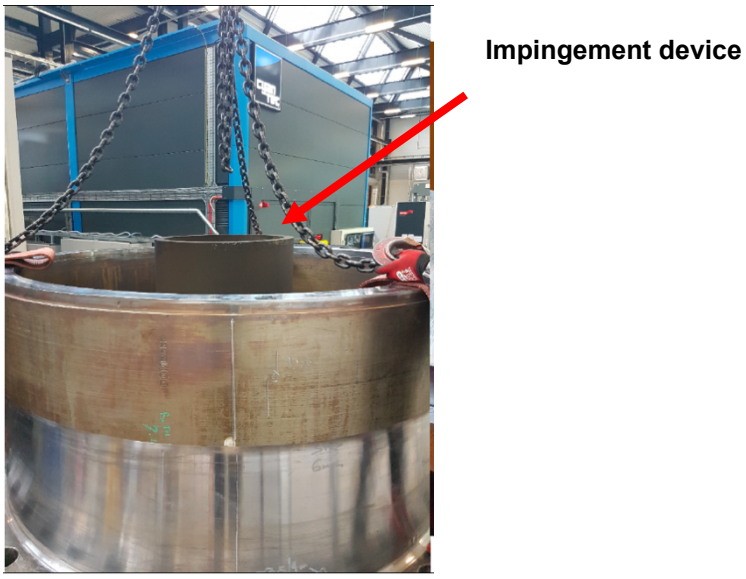

Figure 93. Installation of impingement device within mockup (modified to identify device) (From Gandy [2], reprinted with permission from Electric Power Research Institute).

The shell-to-dome mockup was welded using the SA508 Grade 3 weld parameters previously used on the other mockup weld joints. These parameters consist of the welding parameters in Table 13 and the slope-out parameters in Table 15. Visual and NDE was completed with no indications reported. The slope-out region again showed a similar response when using TOFD, as may be expected when using the same parameters. The final welded assembly is shown in Figure 94. A lower head (dome) weld was also completed, joining two PM-HIP halves together to make a single lower head unit. The welding of the lower head is addressed in Section 2.8.2.4 of this report. EPRI reported that all welds were free of major flaws or indications within the weld, including the slope-out regions [2]. Future work efforts will be performed to complete the lower assembly, including a highly magnetized transition shell (up to 30 G), as well as machining of the lower dome to allow for inspection of the weld joint. A ⅔-scale demonstrator RPV flange and shell are currently being machined for welding [2].

Figure 94. Shell-to-dome mockup assembly after welding (From Gandy [2], reprinted with permission from Electric Power Research Institute).

2.8.2.4 Welding of PM-HIP SA508 steel

Components manufactured by PM-HIP are being investigated for use in RPV fabrication in conjunction with EB-welded joints. The lower and upper heads, transition shell, steam plenum, and steam plenum access ports using PM-HIP are being fabricated as part of the project [10]. Joints to be evaluated will consist of (1) forged material to PM-HIP and (2) PM-HIP to PM-HIP. The ⅔ (66%) scale components will be fabricated in sections and joined using EBW to form the final components. Thick plates were fabricated using the PM-HIP processes developed by Synertech-PM for welding samples. These plates were welded to forged SA508 Grade 3 Class 1 plates in the 2G position, thus simulating the final assembly welds of the SMR.

The forged material was placed as the upper block in the welding trials with an offset of 5 mm to allow for integral support [10]. The welding of PM+HIP materials vs. traditional plate or forging material can exhibit different welding characteristics. The weld schedule used for BJ09 (60 kV, 450 mA, 2.0 mm/sec) was used for the PM-HIP evaluation. Weld characteristics were noted as being “notably different” in the EPRI report [10]. In Figure 95, the forging material–to–PM-HIP material on the left compared to the PM-

HIP–to–PM-HIP material on the right has a noticeably different visual appearance. A weld with more spatter on the top surface can be seen in the PM-HIP–to–PM-HIP weld.

Figure 95. Top surface of forged–to–PM-HIP (left) and PM-HIP–to–PM-HIP (right) (From Gandy [10], reprinted with permission from Electric Power Research Institute).

Cross sections of the welds can be seen in Figure 96. The wrought-to-wrought and PM-HIP–to-wrought welds were similar in weld dimensions, but the PM-HIP–to–PM-HIP resulted in a much narrower weld width. The spatter and the narrow weld profile may be caused by the evolution of entrapped oxygen or nitrogen from the PM-HIP process [2, 10].

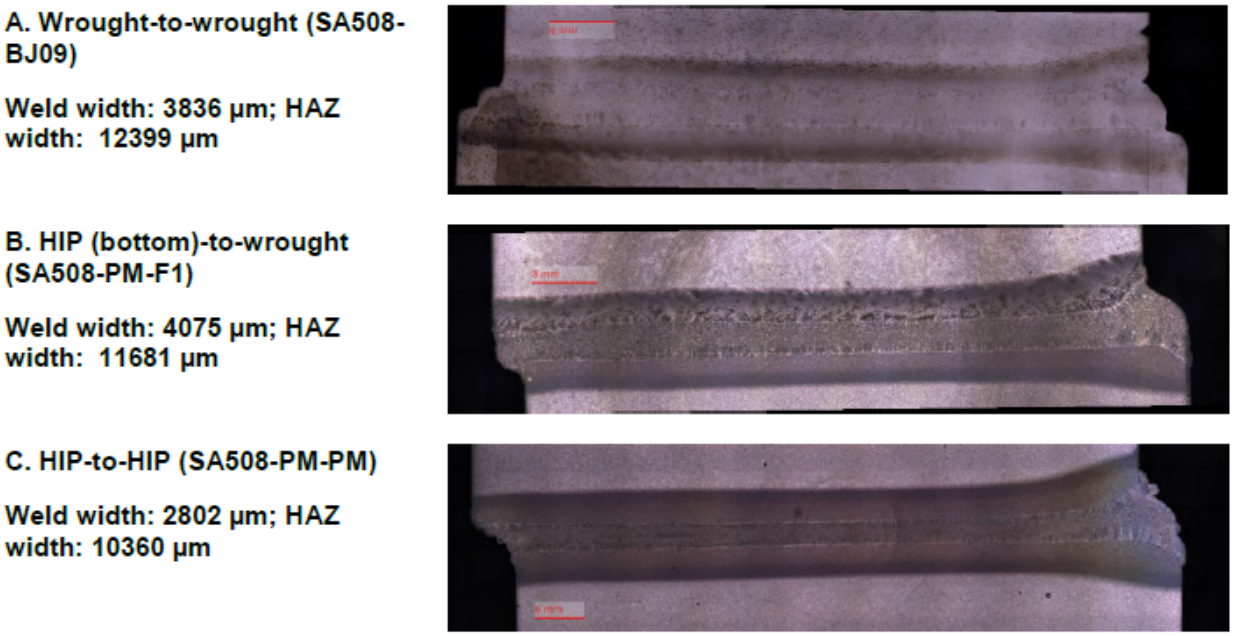

Figure 96. Welding of wrought-to-wrought, wrought–to–PM+HIP, and PM+HIP–to–PM+HIP (From Gandy [10], reprinted with permission from Electric Power Research Institute)..

Next, three lower head halves were completed as part of the PM-HIP development. The first head-half, article 1, was initially made to develop the PM-HIP process only, but it was also used for weldability testing using EBW and GTAW. Articles 2 and 3 were used exclusively to evaluate EBW. Gas content analysis of these three articles showed that they included nitrogen, oxygen, and argon, as reported in

Table 16. Results of the weldability scans can be seen in Figure 97. Because the argon content of article 1 was exceedingly high, it does not represent future welding of PM-HIP materials, but it provides insight into the evolution of gas during welding. The weld surface of article 1 shows a much rougher surface than that of articles 2 and 3 in Figure 97. Article 3 was noted as having "markedly better" results than article 2, although the argon and oxygen content were similar, but with higher nitrogen content (330 ppm vs. 260 ppm) [2]. However, the cause of improved weldability of article 3 is not known [2]. SEM/EDS analysis of article 2 and 3 was completed, showing silicates and manganese sulfides seen at grain boundaries [2]. Material toughness met ASME specification requirements for SA508 material, but the toughness was much lower than that typically found in SA508 type wrought materials for both articles [2]. EPRI and Nuclear AMRC decided to produce another half lower head assembly, article 4, for further development and EBW studies. Articles 2 and 3 were welded to produce the lower head assembly for the final demonstration assembly.

Table 16. Lower head assembly gas content, articles 2 and 3 used in EB assembly (From Gandy [2])

Part	Part ID	Sample ID	N (%)	O (ppm)	Ar (ppb)
Lower head—1st article	17019-001	1	0.0389	172	exceeded detection limit (>14,000)
		2	0.0399	106	
		3	0.0277	169	
		4	0.0242	239	
		5	0.0251	204	
Lower head—2nd article	18004-002	AH	0.027	100	8
		PWHT	0.024	160	-
		QHT	0.028	90	-
Lower head—3rd article	18004-003	AH	0.032	130	7
		PWHT	0.034	80	-
		QHT	0.033	120	-
Test cylinder	168-C3	n/a	0.030	90	-

Figure 97. EBW trials on article 1 (left), article 2 (middle), and article 3 (right) (From Gandy [2], reprinted with permission from Electric Power Research Institute).

The two halves of the assembly were machined at the joint line, leaving the remaining PM-HIP surfaces as processed. The rough state of the two halves required the use of hydraulic jacks and shims to ensure

that the weld joint was kept in the horizontal position [2]. A joint thickness of 90 mm was welded. Welding parameters were not listed in the Year 3 EPRI report. Images of the setup in Figure 98 show the run-on / run-off blocks and beam impingement plates internal to the assembly. The weld was completed in the horizontal position and lasted for 20 minutes of beam-on time [2]. The weld characteristics, as previously discussed, are different than those created when using forged material. The images of the outer weld profile show a more turbulent visual appearance. EPRI notes that the high amount of inherent dissolved gas in the components may cause fluctuations in the weld pool, thus resulting in increased spatter [2]. Prior to welding, the gas contents of articles 2 and 3 were 370 and 450 ppm, respectively [2]. Also mentioned are the voltage spikes that may be caused by ionized gas emitted from the weld pool, disrupting the electron gun [2]. The final assembly remained to be machined at the writing of the Year 3 report. The inspections of the weld joint were not complete, and a final acceptance of weld quality was not available at time of publication [2].

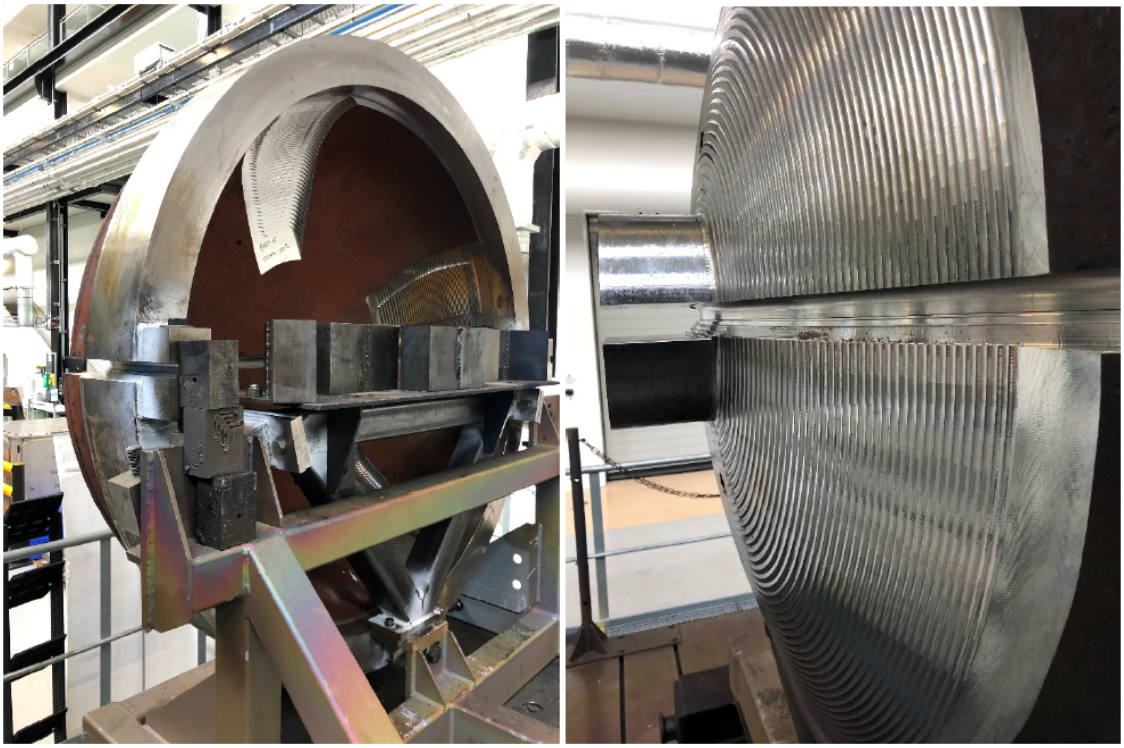

Figure 98. Two-piece lower head produced using SA508 PM-HIP EB weld setup using run on / off blocks (left) and machined weld joint (right) (From Gandy [2], reprinted with permission from Electric Power Research Institute).

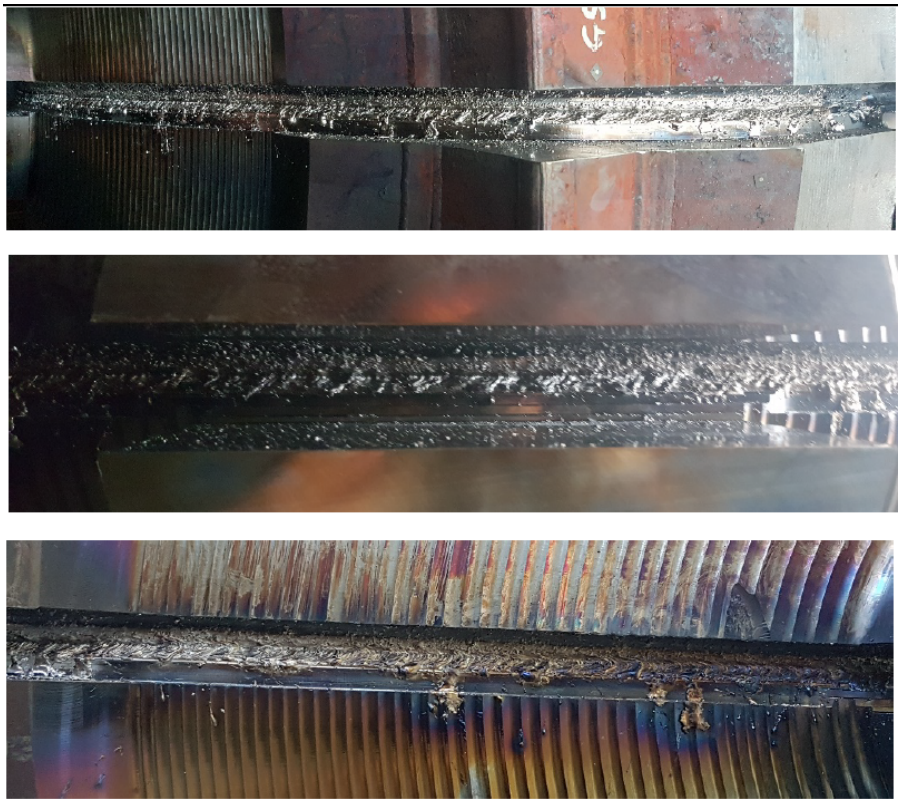

Figure 99. Two-piece lower head produced by PM-HIP: photos of outer diameter weld profile shown near start, middle, end at top, middle, and bottom respectively (From Gandy [2], reprinted with permission from Electric Power Research Institute).

Powder for the PM-HIP process was procured using the air melt inert gas atomized powder (AM-IGA) with nitrogen for the EBW samples evaluated through EPRI's first three yearly reports. Heats of vacuum induction melted inert gas atomized (VIM-IGA) using nitrogen have been procured to further reduce oxygen with lower silicon and higher nickel content for subsequent welds. The VIM-IGA material was sought to improve the toughness of the PM-HIP materials. Initial testing through a heat produced by Nuclear AMRC resulted in similar strength and ductility to other heats with improved toughness equally 110 ft-lb (150 J) [2]. The materials performance during EBW has not yet been reported.

2.8.2.5 Full Solution Heat Treatment of SA508 Grade 3 Steels

As part of the thick section EB development being done on SA508 Grade 3 Class 1 steels, EPRI is investigating the use of a heat treatment that will effectively remove the EB weld [2]. Because the EB weld does not add filler metal, the chemical composition of the weld is nearly identical to the base material minus small elemental losses during EBW. The heat treatment study being conducted by EPRI seeks to determine the minimum heat treatment temperature to remove evidence of the weld while obtaining superior mechanical properties. The baseline comparison for this study is a conventional arc weld with a PWHT. An example weld with heat treatment is provided in Figure 100. Vickers hardness traces are shown across the as-welded and homogenized samples, showing a reduction of hardness to base metal hardness after heat treatment.

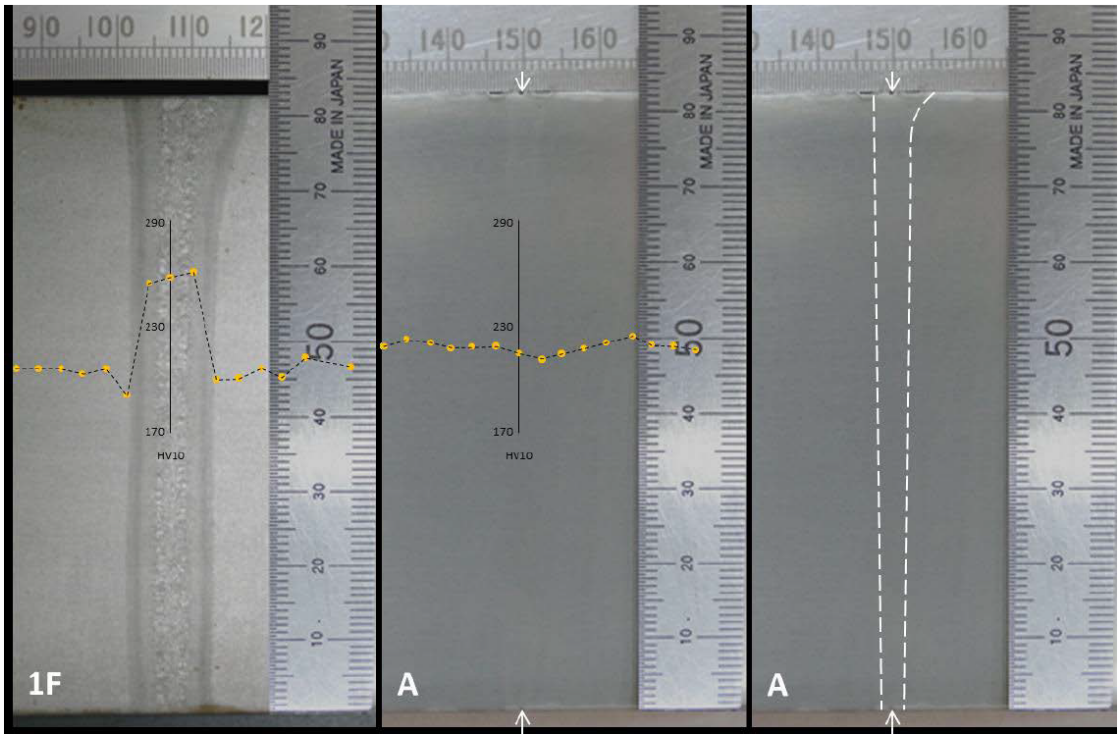

Figure 100. Homogenizing heat treatment of SA508 Grade 3 Class 1 material: as-welded (left), homogenized heat treatment (middle), and homogenized with previous weld outline (right). Vickers hardness traces are shown overlapping the images for the as-welded and post-heat-treated samples (From Gandy [2], reprinted with permission from Electric Power Research Institute).

Because the heat treatment would be completed on final assemblies after welding and machining, distortion caused by the heat treatment is a concern. A study of homogenizing temperatures was undertaken to determine the lowest temperature heat treatment that could be used and applicable to the full size components in the future [2]. Sheffield Forgemasters (SF) and Nuclear AMRC were contracted by EPRI to conduct the tests resulting in two plates EB welded by Nuclear AMRC and one non-welded plate provided to SF [2]. Five sections were removed: samples A–C from plate 1, samples D–E from plate 2, and sample P from the non-welded plate. A process of (1) homogenizing, (2) water quenching, (3) hardening heat treatment, (4) water quenching, and (5) final tempering was developed. The five different homogenizing temperatures started at 875°C and increased at increments of 25°C, with fixed hardening and tempering temperatures of 870°C for 3.5 hr and 640°C for 3.5 hr, respectively [2].

Mechanical test coupons were machined from the test samples according to Figure 101. ASTM A370-08A tensile bars were extracted from the test sample at ¼ T, ½ T, and ¾ T, as well as 6 ASTM E23 Charpy V-notch samples [2]. Three Charpy V-notch samples were positioned along the weld center line, with the remaining three in the HAZ of the EB weld. Fracture appearance transition temperature (FATT) samples were removed from sample block A with slices through the FZ.

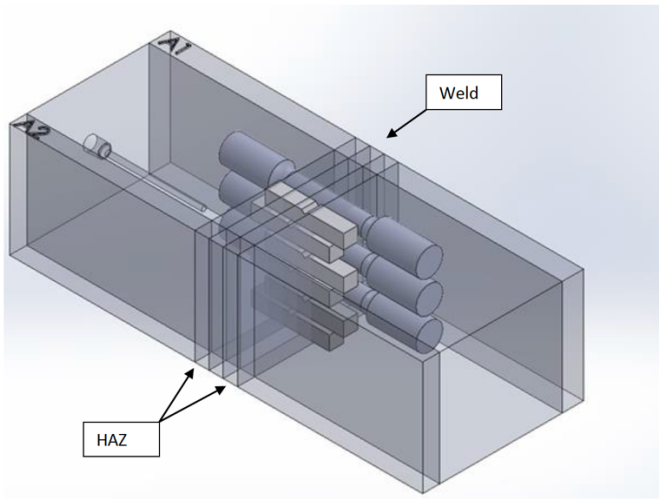

Figure 101. Mechanical test coupons removed from test samples (From Gandy [2], reprinted with permission from Sheffield Forgemasters.

Tensile tests conducted on the samples did not reveal any significant differences between heat treatments. All results were reported to have average values within 11 Mpa of each other, including the parent unwelded material [2]. The average YS, UTS, and elongation values are plotted in Figure 102 for comparison. Charpy impact testing was conducted at -20°C for samples in the FZ and HAZ. Results of the impact tests can be seen in Figure 103. A slight trend of decreasing toughness can be seen in the FZ samples, with increasing homogenizing temperature with all values exceeding the parent material except at the 975°C homogenizing temperature. A more significant change can be seen in the HAZ samples, in which the impact energy drops with increasing temperature above 900°C.

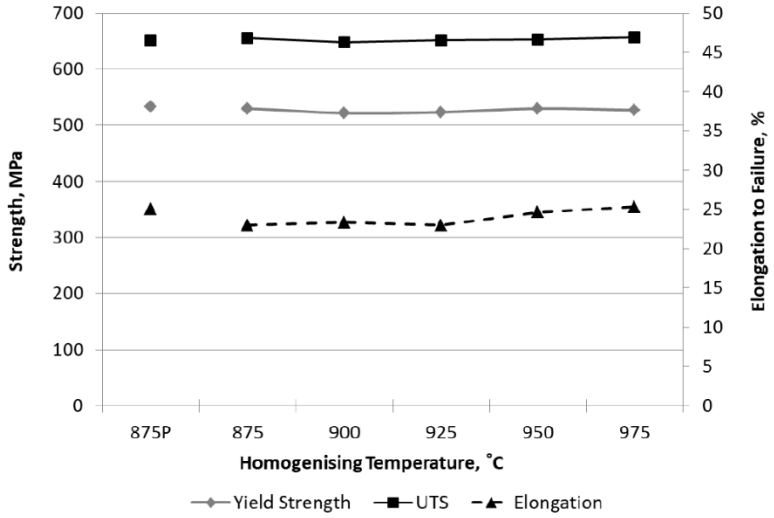

Figure 102. Tensile test results of homogenizing temperature tests (From Gandy [2], reprinted with permission from Sheffield Forgemasters.

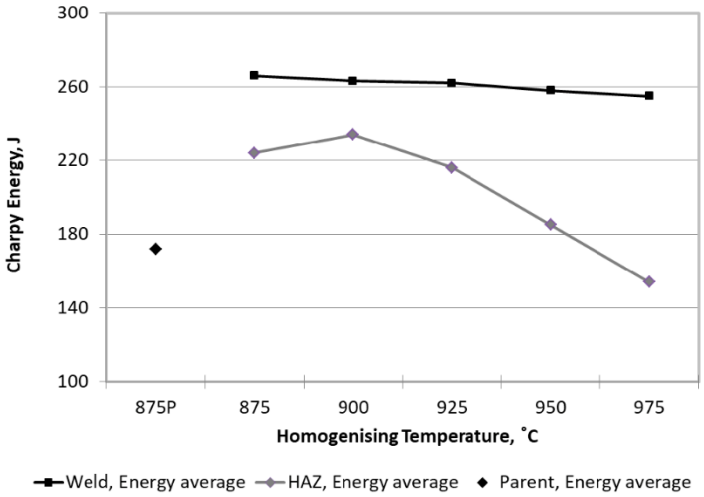

Figure 103. Impact test results for different homogenizing temperatures (From Gandy [2], reprinted with permission from Sheffield Forgemasters.

A review of the weld metal, HAZ, and base metal microstructure was completed by SF. The difference in HAZ impact toughness was theorized to be related to the growth of the prior austenite grains in the HAZ. A comparison between the low (875°C) and high (975°C) homogenizing temperatures can be helpful to explain the drop in toughness. Starting with the same HAZ microstructure for all samples, the difference must be related to the homogenizing temperature. Sample A shown in Figure 104 has smaller prior austenite grains than sample E. The higher homogenizing temperature resulted in larger prior austenite grains, which may be partly responsible for the lower toughness. SF theorized that the higher temperature allowed for dissolution of grain pinning particles, allowing for a larger volume fraction of dissolved phases that allows for further redistribution upon cooling [2].

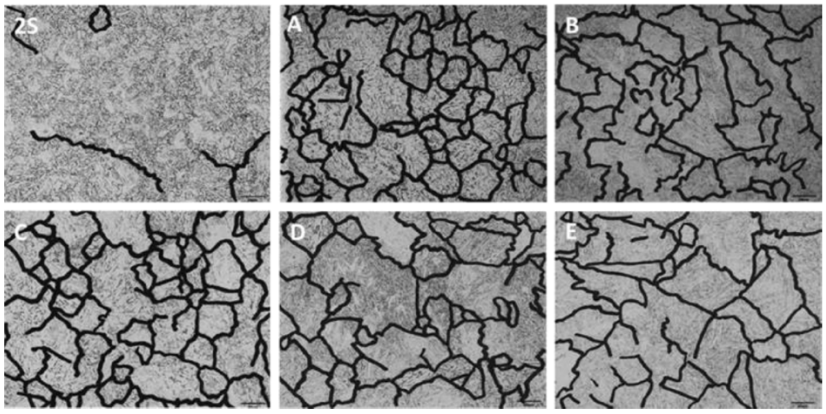

Figure 104. 500× micrographs with prior austenite grain boundaries traced: 2S (as welded), A (875°C), B (900°C), C (925°C) D (950°C), and E (975°C) (From Gandy [2], reprinted with permission from Sheffield Forgemasters.

Larger micrographs of the parent (base metal) and HAZ microstructures for samples A and E are shown in Figure 105. A more in-depth microstructural evaluation based on the provided metallographs is difficult. A difference in morphology is evident between sample A and E HAZ metallographs. Additional evaluation through SEM microscopy to determine phase balance, lathe spacing, and morphology could help identify the trend in lower toughness with homogenization temperature.

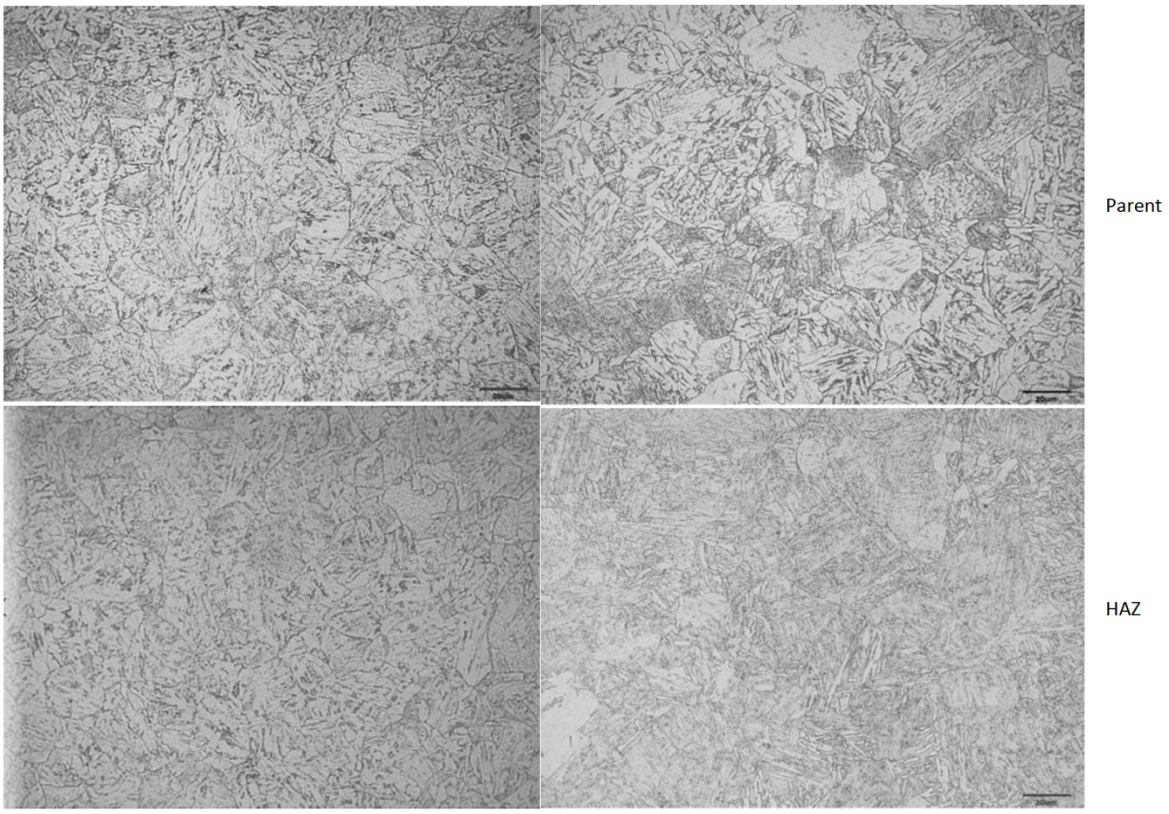

Figure 105. HAZ microstructures of sample A, 875°C (left) and sample E, 975°C (right), parent material (top row), and HAZ (bottom row) (From Gandy [2], reprinted with permission from Sheffield Forgemasters.

The generation of a FATT curve was completed using the 875°C homogenizing temperature. Four additional temperatures were selected for testing to complete the transition temperature curve: 0, -60, -100, and -140°C. The temperature at 50% shear was determined to be at -80 °C. Data from the tests are shown and plotted in Figure 106. Some scatter exists in the data, particularly at -60°C, where one sample was 106 J less than the other two samples at the same temperature. The parent material FATT was reported to be -60°C, with more consistent results as would be expected [2]. Because of the narrow EB weld, it would be useful to validate the location of the failures to the FZ or HAZ. This information may explain the scatter in the reported toughness of the EB-welded samples.

Impact Test Temp, °C	Energy, J,	% Shear
0	236	100
	176	75
	212	100
-20	268	100
	259	100
	270	100
-60	64	10
	173	60
	170	60
-100	71	10
	147	40
	171	50
-140	8	0
	32	0
	12	0

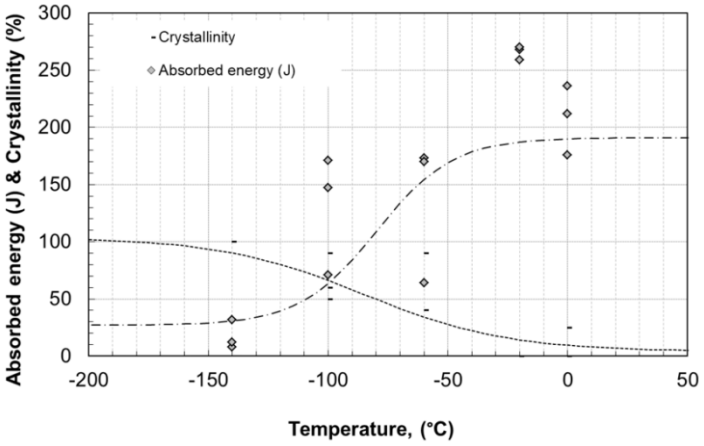

Figure 106. Charpy impact toughness data of welded and homogenized (875°C) to generate FATT curve (From Gandy [2], reprinted with permission from Sheffield Forgemasters.

Impact Test Temp, °C	Energy, J,	% Shear
20	216	100
	221	100
-20	162	65
	139	60
	215	100
-60	111	40
	89	30
	85	30
-80	111	35
	83	20
	71	20
-100	74	20
	33	5
	11	0
-140	34	0
	25	5
	8	0
-160	3	0
	10	0
	15	0

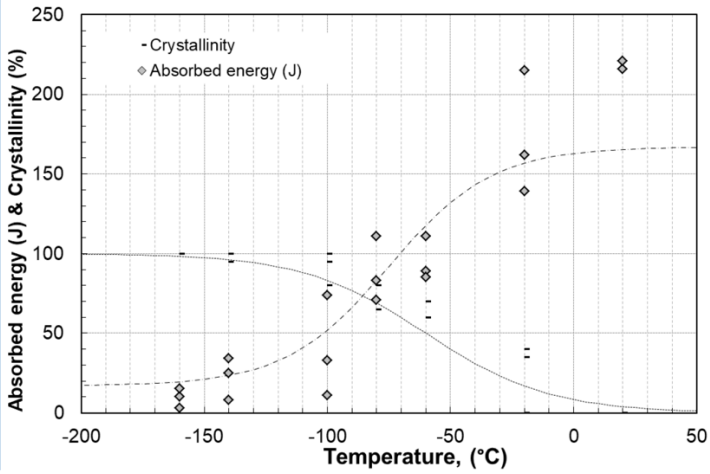

Figure 107. Charpy impact toughness data from non- welded parent material to generate FATT curve (From Gandy [2], reprinted with permission from Sheffield Forgemasters..

Hardness measurements were taken in the 7 samples as part of this study: a parent material sample (parent), an as-welded sample (1S), and 5 heat-treat conditions (A1, 875°C; B1, 900°C; C1, 925°C; D1, 950°C; and E1 975°C). Hardness measurements were taken at the ¼ T, ½ T, and ¾ T positions at intervals of 3 mm. In the as-welded specimen, the hardness values can be seen increasing to peaks >260 HV. All heat-treated samples had measured hardness values roughly equivalent to their base metal measurements. The spacing of 3 mm is not small enough to resolve the differences in FZ and HAZ hardness and may have resulted in missed areas of peak hardness in the HAZ. A microhardness test of finer spacing was conducted at 1 mm spacing, which showed peak as welded hardness approaching 290 HV, and in sample A (875°C), the hardness was shown to be reduced to slightly below that of the base material.

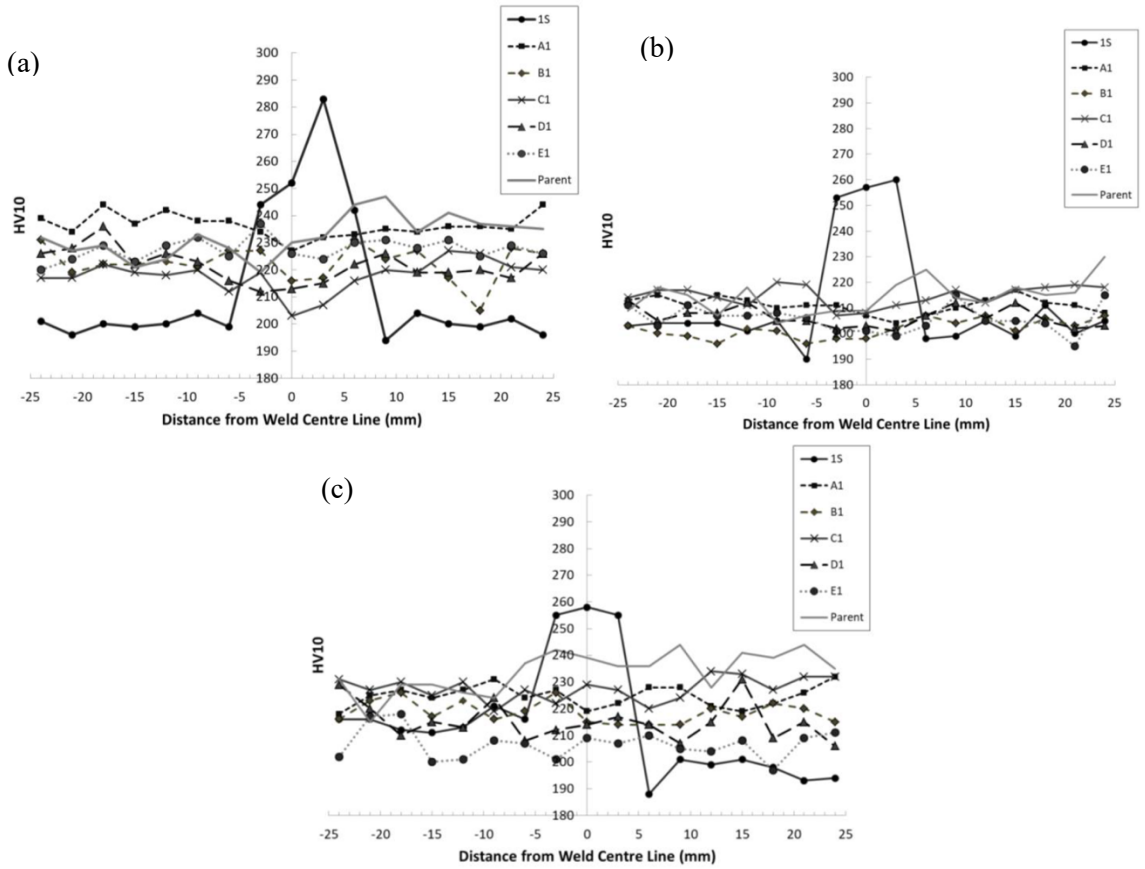

Figure 108. Hardness traces of parent material, as-welded (1S), and heat treat conditions A–E at ¼ thickness (a), ½ thickness (b), and ¾ thickness (c) (From Gandy [2], reprinted with permission from Sheffield Forgemasters.

2.8.2.6 MIC-EBW Weld Development

EPRI and Nuclear AMRC initiated a project to develop a new system for the welding of large diameter components. Existing technologies, including the traditional high vacuum chamber, would necessitate a system 35 feet in length by 13 feet in diameter [8]. The gun placement along the 35 feet in height/length would need to be installed at multiple locations, potentially causing issues with misalignment, damage to the high voltage cabling, and shielding [8]. Other technologies, such as the reduced-pressure EBW system, were determined to need further development to overcome the complexities of preventing failure if the vacuum fails during movement along the joint [8]. A MIC-EBW system was an alternative developed by EPRI and Nuclear AMRC to enable efficient welding of SMR components [8].

The system being built by PTR utilizes a different gun design, as discussed in Section 2.3.4. This system operates at a maximum voltage level of 150 kV with a beam current of 400 mA. This correlates to a maximum power output of 60 kW. The previous development covered in Years 1 and 2 of the EPRI reports utilized a ProBeam K2000 system with a maximum of 80 kV. Because of the change in voltage, PTR was asked to demonstrate the weld on 1.2 m × 127 mm thick (4 ft × 5 in.) SA508 rings [8]. Two rings were stacked upon one another to form a weld joint that could be welded in the 2G horizontal position. The ring diameter was separated into four quadrants for the parameter study, and the quadrants were labeled A, B, C and D. Welds were completed according to Table 17. Inspection of the welds was completed by EPRI NDE staff using UT. Photographs of the exterior and interior weld surfaces can be seen in Figure 109 through Figure 112.

Table 17. MIC-EBW weld demonstration at 150 kV (From Gandy [8])

Quadrant	Accelerating voltage (kv)	Beam current (mA)	Beam power (kW)
A	150	230	34.5
B	150	250	37.5
C	150	200	30
D	150	185	27

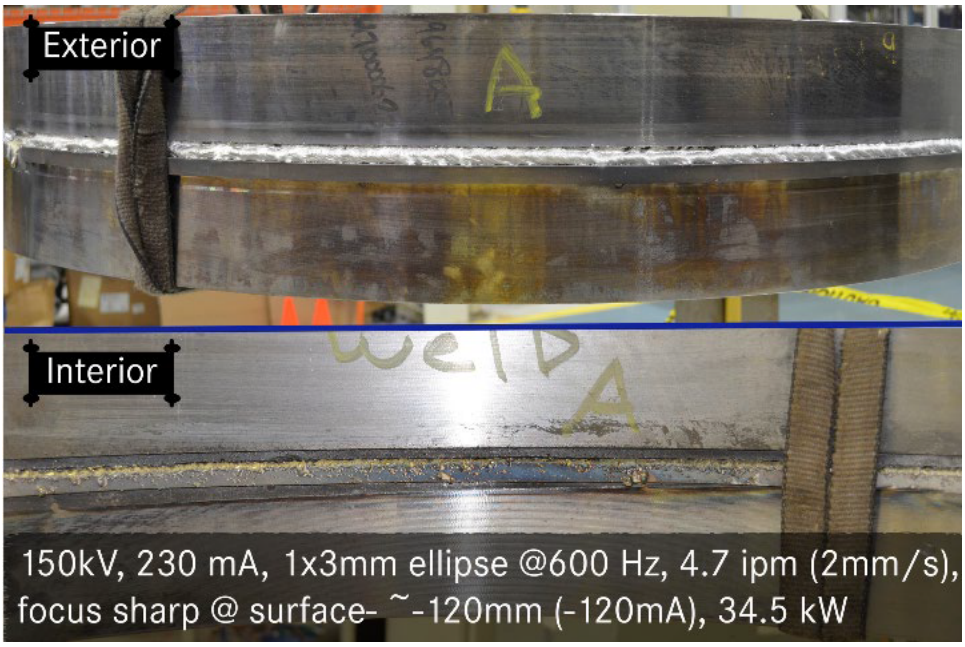

Figure 109. Quadrant A - 150 kV, 230 mA, 34.5 kW (From Gandy [8], reprinted with permission from Electric Power Research Institute).

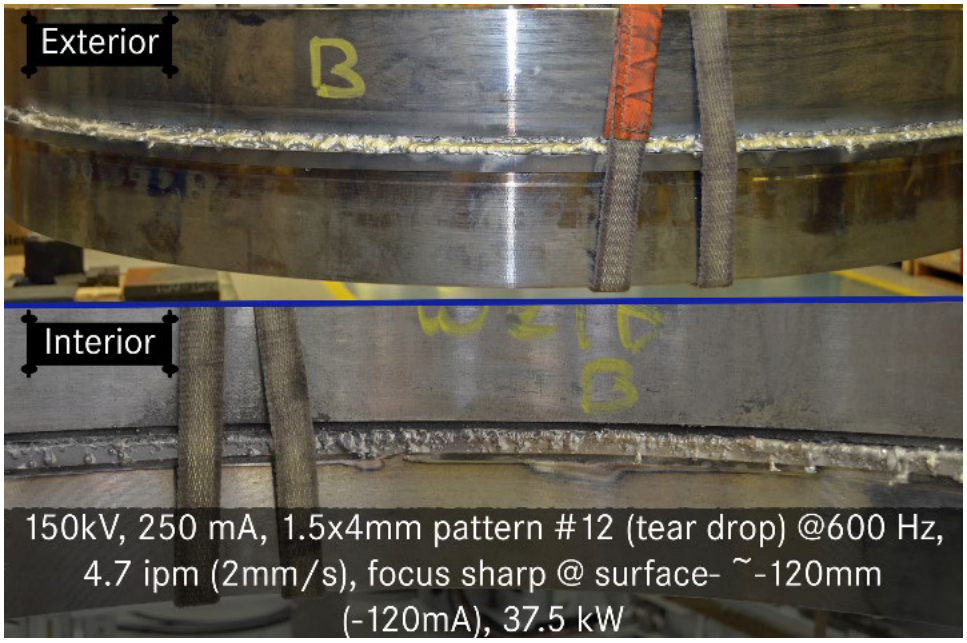

Figure 110. Quadrant B - 150 kV, 250 mA, 37.5 kW (From Gandy [8], reprinted with permission from Electric Power Research Institute).

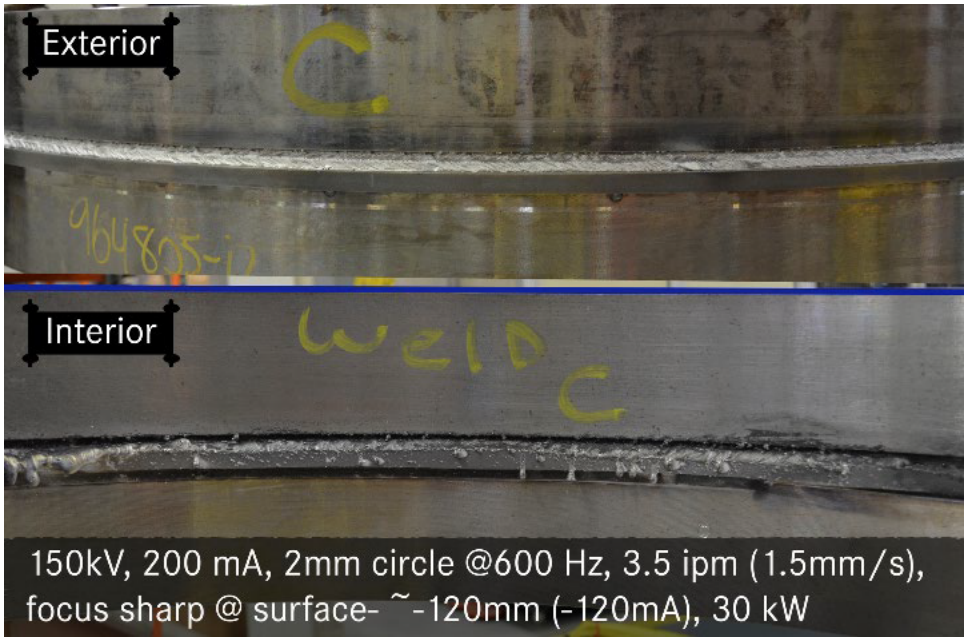

Figure 111. Quadrant C - 150 kV, 200 mA, 30 kW (From Gandy [8], reprinted with permission from Electric Power Research Institute).

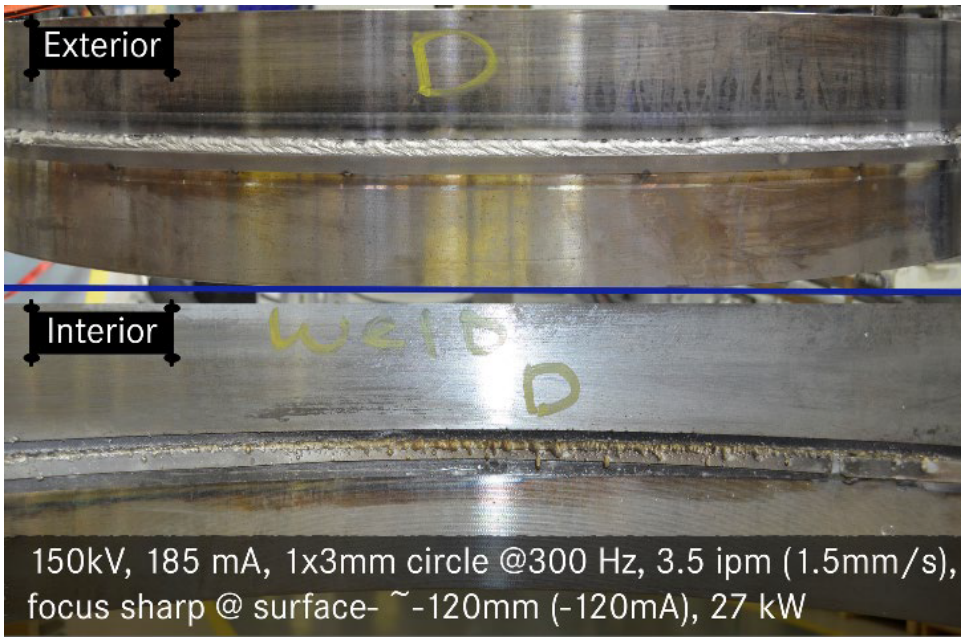

Figure 112. Quadrant - 150 kV, 185 mA, 27 kW (From Gandy [8], reprinted with permission from Electric Power Research Institute).

Quadrant D was determined to have the best weldability and NDE results, having no indications throughout the weld except for the start and stop, which were expected. No ramp in or out was performed in these tests to determine the steady-state welding parameters. UT was performed by EPRI NDE staff from the outer face of the ring, perpendicular to the through-thickness weld. The UT results for all four quadrants can be seen in Figure 113. The abrupt starts and stops can be seen in the UT scan, segmenting the scan into the four quadrants. Indications are readily seen in quadrants A and B. The NDE staff highlighted areas of concern using the red boxes shown in the figure. Quadrants A, B, and C contained areas of concern within the weld. Quadrant D, shown on the far right of Figure 113 was free of UT indications. Quadrant D parameters were 150 kV, 185 mA, 1.5 mm/sec travel speed, elliptical beam oscillation of 1 × 3 mm @ 300 Hz and focused on the OD joint surface. This parameter set results in a beam power of 27 kW. Although the beam power is equal to that seen in previous work at Nuclear AMRC, the joint thickness was significantly greater (127 mm vs. 80 mm) with a slower travel speed (1.5 mm/s vs 2.0 mm/s) [8].

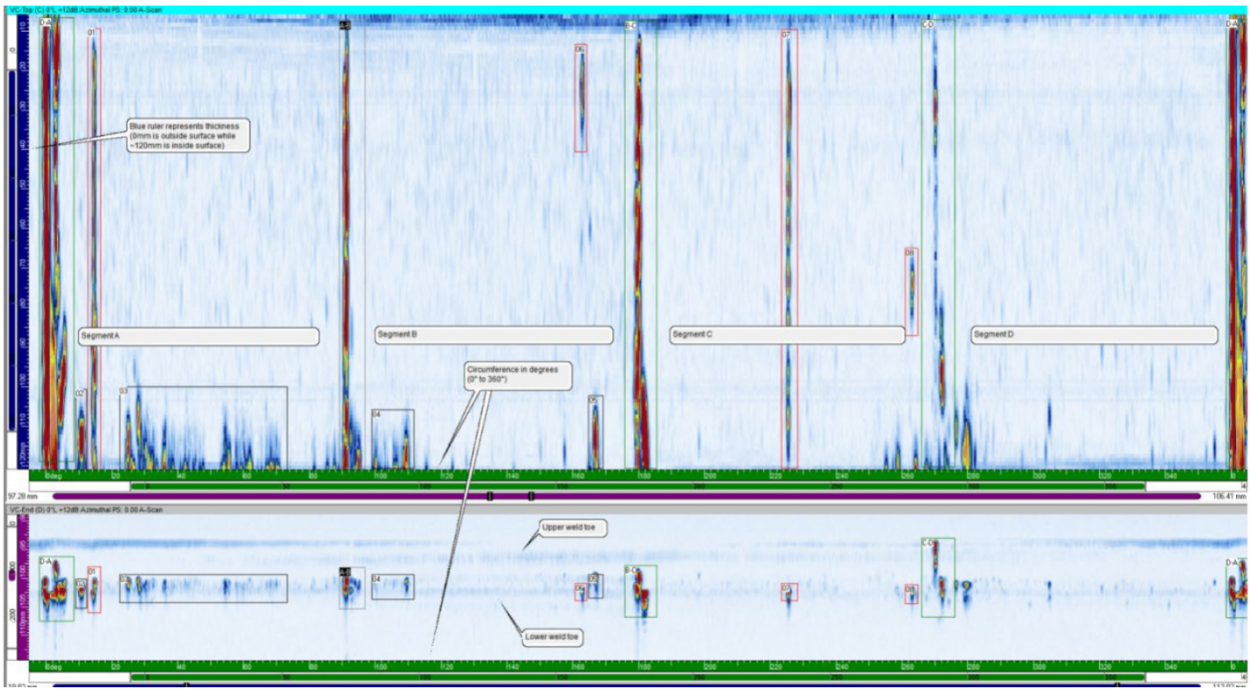

Figure 113. UT results, Quadrants A, B, C, and D (From Gandy [8], reprinted with permission from Electric Power Research Institute).

A full diameter ring was then completed using the Quadrant D parameters. This was completed on a replicate SA508, 1.2 m diameter ring used for the quadrant parameter development. A drip tray was tacked in place to support the weld. Photos of the outer diameter weld can be seen in Figure 114 and Figure 115, with a close-up of the weld in Figure 116.

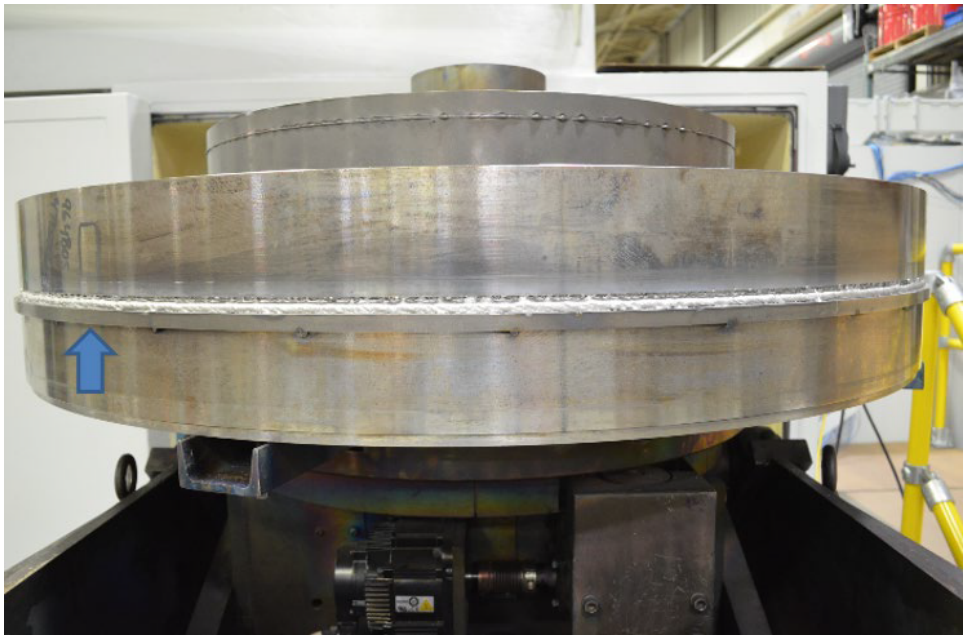

Figure 114. Full diameter demonstration ring using 150 kV, photo 1.
Blue arrow used to reference a location in all photos (From Gandy [8], reprinted with permission from Electric Power Research Institute).

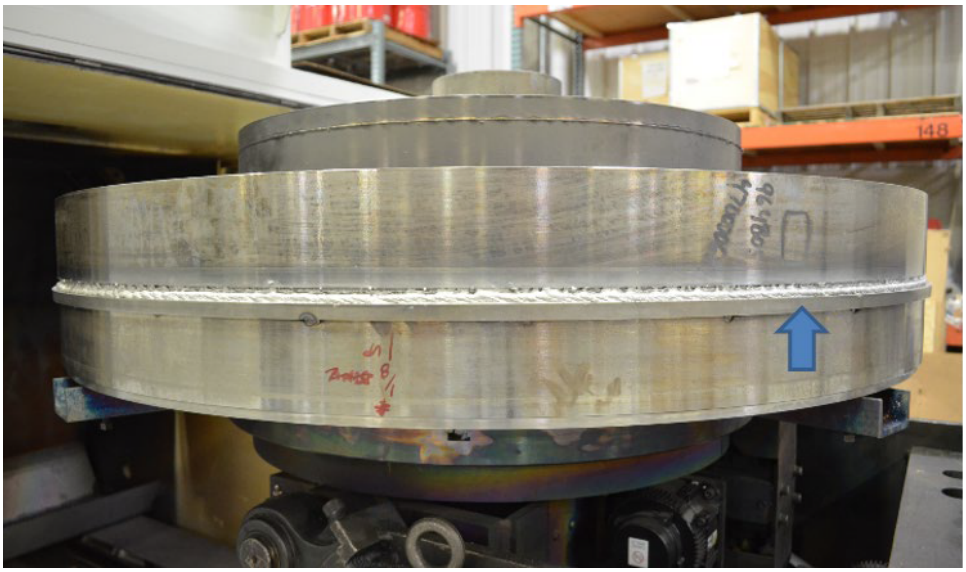

Figure 115. Full diameter demonstration ring using 150 kV, photo 2.
Blue arrow used to reference a location in all photos(From Gandy [8], reprinted with permission from Electric Power Research Institute).

Figure 116. Full diameter demonstration ring close-up of weld on OD (From Gandy [8], reprinted with permission from Electric Power Research Institute).

An electrical fault was noted during welding of the full diameter ring. The fault caused a gun shutdown which interrupted the beam and weld mid process. The weld was restarted to complete the process. Phased array UT was conducted on the full diameter of the ring to ascertain its quality. The phased array UT results are shown in Figure 117 for the full 360° of weldment. Indications were present from 0° to 200°, and were reported as partial through-wall occurring only on the inside surface region of the weld [8]. From 104° to 200°, there are indications within 50 mm of the internal surface [8]. The remainder of the weld was free of indications. The EPRI report indicates that results were reported within days of the closing out of Phase 1 of the project. Phase 2 will finalize the welding parameters. The indications for the first 200° are the results of a beam instability which is not discussed in the report. Because the remaining 160° was free of UT indications without any mentioned changes to the procedure, it is probable that there was some contamination either on the part or in the EB gun that led to the instability. Phase 2 aims at further development and finalization of the welding parameters [8].

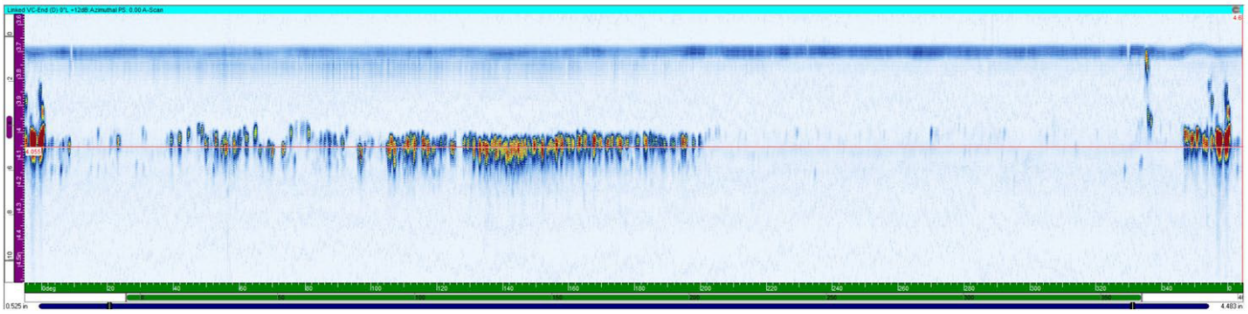

Figure 117. Full diameter demonstration ring UT results welded using quadrant D parameters (From Gandy [8], reprinted with permission from Electric Power Research Institute).

The MIC-EBW system being built by PTR will be installed at the BWXT facility in Barberton, Ohio [8]. Welding development will continue using this equipment to produce the 3.05 m diameter SA508 Class 2 rings. The project aims to demonstrate the successful welding of three full diameter shell girth welds to ASME BPV-IX acceptance criteria [8]. Welds will then be benchmarked against the existing traditional high vacuum chamber welds produced at Nuclear AMRC using the K2000 system [8].

3. GAP ANALYSIS

A gap analysis was conducted as part of the review of advanced manufacturing techniques and qualification processes for light-water reactors. The gap analysis includes the fabrication technologies and potential material property, or it addresses performance needs, as well as a review of existing codes and standards.

3.1 TECHNICAL GAP ANALYSIS

The following technical gap analysis is written with a focus on the performance of a welded assembly for a nuclear application. The importance of each topic is rated according to its potential impact on material properties and does not correspond to a specific material property or failure mode.

Table 18. EB fabrication gaps

Importance	Topic	
High	Weld Repairs	
	Related in-document sections	2.2.5, 2.4.9, 2.4.16, 2.4.17, 2.8.2.6
	Ranking rationale	Weld repairs are often difficult for EBW.
	Discussion	EBW is often used for its highly penetrating capability with low heat input. Because the welding process is typically used for deep single pass welds, the defect is typically not near the surface of the weld when discovered. This may require additional machining and/or grinding to reach the defect depth. When a defect is found below the surface, a repair is more difficult to successfully complete. The best-case weld repair is referred to as a *re-weld*, consisting of the repeat use of the fusion pass weld schedule over the previously welded section. This is often done in its entirety, re-welding the entire weld joint, not just the section with the defect. Because of the autogenous weld created using EBW, an arc fault such as that which occurred during the MIC-EBW full ring demonstration may result in a loss of material that cannot be suitably filled due to the lack of filler material. In such cases, welding on both sides of the

Importance	Topic	
		affected area may flow enough material for repair, but success is not certain. The amount of concavity or material loss at the joint will greatly affect the potential for repair through EBW. A more difficult repair may require the use of a qualified repair procedure. Arc welding is typically used in similar cases to repair the weld in a typical groove repair. Weld repairs were rated with high importance because they have not been discussed in the reports by EPRI or Nuclear AMRC. The use of conventional arc welding processes with filler metal will affect the desired normalizing heat treatment sought to reduce in-service inspection.
High	Unexpected Arc Shut Down / Faults During Welding	
	Related In-Document Sections	2.4.9, 2.4.9, 2.4.17, 2.8.2.6
	Ranking Rationale	The EBW process is highly reliable, but arc faults or shutdowns do occur for various reasons. Arc faults are known to scrap small components as a result of the runaway energy that is sometimes produced. Welding amperage can spike suddenly, causing a large increase in heat input locally to the weld. This is often followed by a fault and termination of the weld, which may leave a hole in the weld.
	Discussion	A repair of the area can be attempted in large components. However, a loss of material at the joint through expulsion at the weld's top surface or forced through the root of the weld may be problematic. Insufficient material may remain to satisfy weld profile requirements. The addition of filler metal can easily rectify the situation either by being added by EB or through traditional arc welding practices. A weld repair as discussed above may be required.
High	Addition of filler metal using conventional or electron beam methods	
	Related in-document sections	2.3.5, 2.6.3, 2.6.4, 2.6.5, 2.4.18
	Ranking rationale	A weld repair using conventional arc welding methods or use of wire fed into the EB or preplaced onto the joint may affect mechanical properties as a result of material mismatch.
	Discussion	EBW with filler metal additions has had limited historical use. Advanced beam controls and additive manufacturing have revitalized the use of wire for EBW to the point of practical use for certain applications. The use of wire will result in a FZ chemistry that does not match the base material chemistry. This may impact plans for a full solution heat treatment. The addition of wire through conventional arc welding or using the EB welder to repair a localized concavity is likely to be needed and should be considered early in the process.
High	Vendor / Equipment Capability	
	Related In-document sections	2.2.2, 2.3.1, 2.3.4, 2.3.4
	Ranking rationale	Large EBW systems capable of performing the girth welds of a full size RPV do not exist in the United States.
	Discussion	Currently there is no vendor with the capability to perform all the EB welds of a fully assembled RPV. A system is currently being fabricated with plans to install such a system at BWXT Barberton [8]. Many of the high-consequence components of the EB gun and power supply are shared, with smaller EB systems allowing for use of existing spare parts. The single point of failure of the system and chamber components are a risk to the manufacture of RPV systems.

Medium	Electron beam–specific material specifications	
	Related in-document sections	2.4.14, 2.6.3, 2.7, 2.8.2.4
	Ranking rationale	EB welds may benefit from specifying limits of tramp elements and other elements not traditionally captured as a result of the limiting nature of existing processing methods.
	Discussion	The application of EBW to pressure vessel girth welds may benefit from the use of supplemental chemistry requirements within existing specification limits. Material selections for EBW are typically cleaner of impurities and selected for their fast-cooling rate morphology upon welding. New material processing techniques such as PM-HIP introduce higher levels of argon, oxygen, and/or nitrogen, depending on the technique used. In the case of PM-HIP, it may be beneficial to place limits on the amount of oxygen and nitrogen in the material. EBW of alloys with high gas content can result in excessive porosity and reduction in fracture toughness. Oxygen and nitrogen are not required to be reported in many material specifications. Supplemental material requirements may be needed for EB welded materials. PM-HIP materials should be evaluated for oxygen and nitrogen content, with suitable limits set. As discussed in Section 2.4.16 oxygen and nitrogen contents were recommended to be restricted below 150 ppm to avoid porosity [65].
Medium	Magnetism	
	Related In-document sections	2.4.13, 2.8.2.3,
	Ranking rationale	Magnetism is a property that is usually not measured or noticed until it is a problem.
	Discussion	Magnetism is often found in pre-weld checks before or during welding. Welders must be cognizant about the effects of magnetism, which can vary according to the material chemistry effects, installed ferritic components, or the magnetization of tooling components. For instances in which the parts are known to have a magnetic influence on the weld, the path of the beam can be programmed to work with the magnetic deflection to maintain the path. Systems using the beam to scan the joint ahead of time using the electron optics can use the information during scanning to program an adjustment. The most common source of magnetism, however, is the part or tooling to be welded. In some cases, the use of a demagnetizer will eliminate induced magnetism of parts and tooling such as that described in Section 2.8.2.3. Steels are generally avoided in tooling for EBW because of the eventual magnetization of the tooling. Aluminum, stainless steel, and copper/brass are often used to avoid magnetization. Tooling with bearings may eventually be magnetized. Therefore, for cases in which the tooling is known to have the potential to be magnetized, it can be written in the procedure to measure the magnetization during setup to determine if the levels need to be addressed. This can be done outside the chamber during assembly of the part/tooling on the EB carriage or positioner. Magnetism of ferritic alloys to be welded, or magnetism of a part of the fixture should be checked prior to each setup. Gauss limits can then be set related to the proximity of the magnetism to the weld joint.
Low	Porosity	
	Related in-document sections	2.4.4, 2.4.5, 3.1.3, 3.2.4
	Ranking rationale	When discussing porosity in EB welds, they are almost entirely sub-surface porosity. A subsurface pore that does not meet NDE requirements will need to be repaired.

	Discussion	The most common repair is a re-weld. This is typically done using the exact same weld parameters that were used in the primary weld, although an alternately qualified weld schedule can be used. The success rate of this process is low. The pore often moves and/or changes in size, but it does not tend to be eliminated. The best means of repairing a pore is to grind or machine it out of the weld and proceed with a repair procedure. Welds conducted so far have not shown deleterious levels of porosity in the steady-state or slope-out regions of the weld. Pores are acceptable within the limits of the ASME BPVC, so the importance was rated as low.
Low	Undercut	
	Related In-Document Sections	2.2.4
	Ranking Rationale	Undercutting of EB welds can be an issue. In particular, deep welds commonly have issues with undercutting on the top surface.
	Discussion	The undercut area acts as a stress concentrator. Failures caused by loading or fatigue are commonly found to initiate at the undercut area of the welds. Locally to the undercut area, the material is under higher solidification stresses and can initiate solidification cracks in sensitive materials. The undercutting of the top surface can be remedied through a cosmetic/defocused weld pass placed on top of the penetrating pass such as that described in Section 2.8.2.3. Alternately, a wire-fed process can be used as a qualified weld repair process to fill in the undercut locations.
Low	Reduced pressure electron beam welding	
	Related in-document Sections	2.2.5, 2.2.2
	Ranking rationale	The sizes of some RPVs necessitate a large chamber or an advanced process to allow for EBW. Minimal information is available about the reliability of these systems. This process has not been widely used in industry.
	Discussion	The specialized local vacuum process needed for RPV girth welds are not commonly available in the United States. Existing systems are in the UK for fabrication of wind power monopiles at Dogger Bank [118] and the EBManPower program [41]. The RPEB process summarized in Section 2.8.1 is not currently being pursued for use in the United States, so the importance is commensurate. Current efforts in the United States are focused on large-chamber EBW.
Low	Weld appearance, including spatter and blow-through	
	Related in-document sections	2.2.4, 2.4.8, 2.4.9, 2.8.2.3
	Ranking rationale	During full penetration, EBW spatter can solidify on the inner and outer surfaces, requiring mechanically assisted tools to remove. The weld root in particular can have large amounts of spatter present.
	Discussion	The visual appearance of an EB weld will be narrower and more rough than a typical arc weld and may include spatter, particularly on the interior of the component. Welds as proposed by EPRI include machining of the weld outer diameter for NDE, with little spatter occurring on the beam side of the joint. The excess beam power and droplets of material are expelled out the root of the weld and adhere strongly to the opposite side of a vessel. When possible, as in the welding of rings by EPRI, a beam impingement device can be inserted on the backside of the weld (Section 2.8.2.3). This absorbs excess energy from the EB and captures spatter from the root. Final closure welds of the lower or upper assembly may not be able to use the same impingement device, and this aspect was not discussed in the reports. An alternate beam

		impingement device may be used for this weld, and/or mechanical removal of the spatter could be completed if needed.
Low	Slope-Out	
	Related In-Document Sections	2.4.1, 2.4.9, 2.5.1, 2.8.2.2
	Ranking Rationale	The slope-out portion of a keyhole mode weld may be more prone to porosity and other defects.
	Discussion	The slope-out of a weld occurs in the transition period between steady-state welding and termination of the weld. During welding, the beam current is ramped to the welding current to achieve the desired penetration. In the case of full penetration welds, the beam power is typically overpowered to ensure full penetration and stability of the puddle. The slope-out consists of the start of weld termination, during which the beam current, lens current, travel speed, and/or accelerating voltage may be adjusted to reduce the beam power to a suitable level prior to turning off the beam. As reported by EPRI in section 2.8.2.2, maintaining weld puddle stability during the slope-out region requires experimentation and weld development. During the transition from keyhole mode welding to conduction mode, the puddle and beam instabilities primarily result in the formation of root porosity. The slope-out region must be carefully developed to avoid defects.
Low	Joint Preparation, Fit up, and Gaps	
	Related In-Document Sections	2.2.4, 2.2.5, 2.4.7, 2.4.11, 2.4.12, 2.4.14, 2.4.15, 2.5.1
	Ranking Rationale	The joint prep for EBW and tolerancing of mating components is critical for EBW without wire additions.
	Discussion	The machining of weld joints is simplified for EBW; however, tolerancing of the mating components is critical to achieve success. Simple butt welds can be welded by EBW in a single pass, whereas a traditional arc weld may require a bevel in one or both parts to allow for the multiple passes required to fill the joint. Most EB welds are completed without the addition of filler material. This requires that the mating components are tight fitting with minimal gaps. Small gaps can be overcome using EBW, because the expansive and contracting forces of the weld will typically result in a slightly convex weld reinforcement. Larger gaps reduce the amount of weld reinforcement and may result in a concave weld surface. The concavity of the weld reinforcement also increases the solidification cracking susceptibility of the weld and should be avoided.
Low	Fluidity of the Molten Pool	
	Related In-Document Sections	2.4.2, 2.8.2.4
	Ranking Rationale	Changes in weld pool fluidity were found during parameter development when welded occurred at different accelerating voltages, as well as between forging materials and PM-HIP.
	Discussion	The fluidity of the material to flow away from the weld joint should be evaluated during the procedure development and is not likely to occur spontaneously. Drip trays, support bars, and run on/off tabs, are tack welded to support the molten weld bead during welding. Loss of material in terms of a fluid flow is usually more severe on the beam side or hot end of the weld; therefore, support structures are typically used on the beam side and not the root side of the weld. Very hot, deep, or high-energy welds may require support at the root side as well. During development of welds using SA508 Grade 3 Class 2 steel a change in accelerating voltage corresponded to a change in fluidity of the joint [10]. Welds were successfully developed on forgings. The PM-HIP welds have not been evaluated to the extent of forgings.

		A change in FZ width was seen in the EPRI Year 1 tests, as well as increased spatter and fluidity in Year 3 when joining of the lower head assembly (see Section 2.8.2.4). EPRI has not reported on the inspection results of the lower head assembly completed at the end of the Year 3 effort [2].

The following material property and performance gap analysis is written with the conventionally welded pressure vessel steel as a baseline. Ranking is assessed on whether the EB-welded assembly exceeds the conventionally arc welded material properties and the likelihood of a given failure mode.

Table 19. Material property and performance gaps

Importance	Topic	
High	Welding of forgings to PM-HIP and PM-HIP to PM-HIP	
	Related in-document sections	2.6, 2.8.2.4
	Ranking rationale	Components are being fabricated by PM-HIP and are being EB welded to form sections of the RPV. Some differences have been highlighted between the combinations of welded forged and PM-HIP materials.
	Discussion	Differences have been seen in the few tests completed on deep penetrating EB welds on RPV steels when using PM-HIP base materials. During the Year 1 investigation, a forged plate to PM-HIP plate weld behaved comparatively to the wrought product, with no significant difference in weld FZ or HAZ width. For comparison, a PM-HIP–to–PM-HIP plate weld joint was also completed in Year 1, with notable differences in the FZ and HAZ width. No mechanical testing or microstructure characterization was reported on the weldments in Year 1. Additional evaluation of PM-HIP material continued in Year 3 with the fabrication of lower head assemblies. The development of the large assemblies needed for the RPV using PM-HIP has been a significant ongoing effort. Year 3 continued the work with welding of PM-HIP material initially utilizing the article 1 lower head assembly. The gas content of article 1 exceeded detection limits in argon content and demonstrated the release of entrapped gasses through EB or arc welding. Articles 2 and 3 were improved with little argon entrapment (<8 ppm) [2]. However, they did have high levels of the nitrogen and oxygen, (370 and 450 ppm) [2]. For comparison, Tomita recommended a product value of less than 150 ppm for steels [65]. The Year 3 results did not report on the weld quality of the article 2 and 3 weldment because of the need for additional machining to allow for UT inspection. The welds evaluated to date on PM-HIP material have had high gas contents. Ongoing efforts are being made to reduce the residual gas levels and to improve material toughness to near wrought. Microstructure and mechanical properties of the welds and the associated residual stress distribution must be determined as development of the PM-HIP material compositions are optimized.
High	Aging and irradiation degradation	
	Related in-document sections	2.4.19
	Ranking rationale	The effects of neutron irradiation on EBW PM-HIP A508 material were not found in published sources.

Importance	Topic	
	Discussion	Irradiation embrittlement, and particularly loss of fracture toughness, is a concern in NPP applications. Copper has been directly attributed to radiation effects in welds on NPP applications. EBW removes a source of the copper from the filler materials added through arc welding, providing a cleaner weld with less impurities. No published studies could be found discussing the neutron irradiation of deep penetrating EB welds in SA508 steels. The reconstitution of Charpy test specimens by EBW as reported by Bokuchava may provide a data set for irradiated EBW [130]. Because of the matching base material chemistry, the irradiation embrittlement of EBWs may be able to leverage the extensive knowledge on irradiation embrittlement of RPV plate and forging materials. PM-HIP materials have not been subjected to the same amount of testing and analysis as wrought materials. Because PM-HIP materials are still being developed, additional analysis of the irradiation effects will need to be completed. EPRI has made several PM-HIP components that meet the A508 PM-HIP specification out of AM-IGA powder; however, these builds have had lower toughness than wrought SA508. A more costly process of producing powder through VIM-IGA is being investigated with lower silicon and higher nickel content up to the maximum allowable limit (exceeded nickel content in heat #181) [2]. This process has increased toughness as desired to 110 ft-lb (150 J). Irradiation effects of the PM-HIP material for AM-IGA and VIM-IGA material were not found in published literature.
High	Residual Stress	
	Related In-Document Sections	2.3.5, 2.4.10, 2.4.12, 2.4.18, 2.6.3, 2.8.1
	Ranking Rationale	Residual stress is known to affect important properties of the weld.
	Discussion	Residual stress is a factor in the mechanical properties of materials, including crack susceptibility and irradiation behavior. The measured residual stresses in deep-penetrating EB-welded RPV materials have shown peak stresses matching the parent material yield stress [24, 125]. These levels are also reached when materials are welded using traditional arc processes. PWHT of the EB welds reduces peak residual stress levels significantly to approximately 100 MPa [24, 125]. Unlike traditional arc welding processes in which the peak stress is located within the fusion zone, the EB weld peak stresses are outside the weld region in a characteristic M-shaped profile. Residual stresses may be a concern in aging materials in which the ductile-to-brittle transition temperature has shifted [24]. No publications could be found that investigated the change in residual stress to the long-term ageing and irradiation behavior of deep EB-welded RPV materials. Therefore, the importance is considered high.
High	Fracture toughness	
	Related in-document sections	2.6.3, 2.8, 2.8.1, 2.8.2.1, 2.8.2.5, 2.4.19
	Ranking rationale	Fracture toughness of EB-welded LASs can be recovered through PWHT in wrought alloys. No information could be found on EB-welded PM-HIP A508 steel.
	Discussion	In the as-welded condition, EB-welded joints have poor fracture toughness requiring PWHT to recover base metal toughness. In fracture toughness tests

Importance	Topic	
		completed by Ayres and Gandy, the fracture toughness of SA508 Grade 3 Class 1 EB-welded steel was equal to that of the wrought alloy after PWHT [2, 22]. Fracture toughness of AM-IGA PM-HIP A508 steel alloys was reported to be low prior to heat treatment and after heat treating [2]. EB-welded AM-IGA PM-HIP A508 steel has not been evaluated in this study. Because of the low fracture toughness, EPRI decided to pursue the higher cost powder manufactured by VIM-IGA. The use of a vacuum reduces the oxygen uptake and drastically improves toughness after heat treatment [2]. EB-welded fracture toughness of VIM-IGA A508 steel has not been evaluated in the as-welded or PWHT conditions. As the PM-HIP process matures, fracture toughness tests of EB-welded material can be completed. These tests could be used to help determine limits for argon, nitrogen, and oxygen content.
Low	Stress corrosion cracking (SCC)	
	Related in-document sections	2.4.18
	Ranking rationale	SCC is not a common issue in ferritic low alloy RPV steels.
	Discussion	EB welds generally perform better than arc welding because of the inherent clean environment, lower overall heat input, and resulting refined grain structure of the weld. SCC susceptibility is more pronounced in austenitic stainless steels and nickel-based alloys than in LASs. Dissimilar metal EBW joints between the LASs and nickel / austenitic alloys have been investigated by Seiffert [79, 131]. Additional research is needed for the application of EBW of nozzle–to–pressure vessel connections to determine feasibility and performance because of the complex microstructures and thermal history of these components. SCC of EB-welded PM-HIP A508 steel has not been published.
Low	Fatigue	
	Related In-Document Sections	2.6.4, 2.7,
	Ranking Rationale	Fatigue information for EB welds on RPV steels is limited. Few publications were found discussing fatigue of EB welds.
	Discussion	Fatigue life is not expected to be detrimentally affected by EBW of the RPV steel. Publications for EBW have reported weld microstructures containing martensite and bainite. PWHT of the EB welds results in a primarily bainitic microstructure. Because fatigue is heavily reliant on the weld microstructure, a significant change is not expected if similar microstructures are achieved and undercut is kept below ASME BPVC allowable limits [117].
Low	Solidification cracking	
	Related In-Document Sections	2.6.2, 2.6.3
	Ranking Rationale	Solidification cracking is a result of the base metals selected, restraint conditions of the joint, and solidification rates. Base metals that are generally considered to be weldable by arc fusion processes may be susceptible to cracking during EBW because of the faster cooling / solidification rates.
	Discussion	Ferritic steels are not as susceptible to solidification cracking as stainless steels. Base metal chemistries are controlled to reduce the potential for SCC and solidification cracking, primarily by reducing sulfur and phosphorous contents in steels. Higher residual stresses, deep penetrating welds, and concavity at the

Importance	Topic	
		weld reinforcement increases the risk of solidification cracking, but this has not been seen in any of the EB weld development efforts.

3.2 CODES AND STANDARDS GAP ANALYSIS

This gap analysis was completed as an effort to identify gaps in the ASME code pertaining to EBW of nuclear pressure vessel components. Because of the many potential applications, it is not possible to anticipate every code issue. This review is limited to the existing 2021 ASME BPVC and potential applications identified through published research.

3.2.1 Codes and Standards

ASME BPVC Sections III, IX, and XI pertain to the nuclear power generation components. An emphasis was placed on the examination of these codes. ASME BPVC Section IX provides guidance for the qualification of welding procedures and welders, including EBW. A review of the code was completed with the intent to determine potential gaps for the implementation of advanced EBW techniques. In most cases, the code does not restrict the use of EBW. The gap analysis provided below discusses current code cases that have been applied to the BPVC and potential future code cases. A list of relevant codes and standards for EB is provided in Table 20.

Table 20. EB welding codes and standards

Type / Topic	Number	Title
Standard	AWS A2.4 : 2020	Standard symbols for welding, brazing, and non-destructive examination
Terminology	AWS A3.0 : 2020	Standard Welding Terms and Definitions Including Terms for Adhesive Bonding, Brazing, Soldering, Thermal Cutting, and Thermal Spraying - 12th Edition
Standard	AWS B1.10 : 2016	Guide for the Nondestructive Examination of Welds
Standard	AWS B2.1 : 2014	Specification for Welding Procedure and Performance Qualification
Standard	AWS C7.3 : 2016	Process Specification for Electron Beam Welding
Safety	ANSI Z49.1 : 2012	Safety in Welding, Cutting, and Allied Processes
Standard	ISEA Z87.1 : 2020	American National Standard Occupational and Educational Personal Eye and Face Protection Devices
ASME BPVC	Section III : 2021	Rules for Construction of Nuclear Facility Components
ASME BPVC	Section V : 2021	Nondestructive Examination
ASME BPVC	Section IX : 2021	Qualification Standard for Welding, Brazing, and Fusing Procedures; Welders; Brazers; and Welding, Brazing, and Fusing Operators
ASME BPVC	Section XI : 2021	Rules for In-service Inspection of Nuclear Power Plant Components
ASME BPVC	Code Cases	Nuclear Component Code Cases

EBW is an approved welding process according to the ASME BPVC. The use of EBW to weld the RPV sections is allowable per the existing ASME BPVC. The only clear restriction was found in ASME Section III, which restricts the welding of instrument tubing to GTAW only. Other limitations may be in the welding of structural attachments called out in Section III. The code does not specifically restrict EBW; however, the joint design requirements for attachments are suitable only for conventional arc welding processes. Joint designs could be improved for EBW use; however, the cost benefit of using EBW over conventional welding processes would have to be considered. As of the writing of this review the BPVC code allows for conventional EBW practices to be used to join pressure retaining components followed by PWHT.

An effort to eliminate in service inspection through use of a full solution heat treatment has been presented that is not currently allowable per the ASME BPVC. A full solution heat treatment as discussed in Section 2.8.2.5 seeks to demonstrate that a heat treatment can be applied to eliminate the weld [2]. This work is ongoing with the goal of eliminating in-service inspection. This was not identified as a gap because it is sought as an improvement, and the application of EBW is not contingent upon use of this heat treatment.

CONCLUSIONS

Advanced manufacturing technologies (AMTs) including electron beam welding (EBW), are being explored by academic, industrial, and regulatory entities for technical feasibility, cost effectiveness, and safety of fabricating components for nuclear power plant applications. EBW is being sought to replace traditional arc welding as the joining method used to make up the girth welds on nuclear power plant (NPP) reactor pressure vessels (RPVs). EBW has been around for over 50 years, with primary uses in the aerospace and automotive industries. EBW can complete thick section RPV weldments in a single pass without the need for filler metal, with lower total heat input than traditional arc welding methods currently used. This results in a significant savings of time and money if it can be realized in production. The Electric Power Research Institute (EPRI) estimated a reduction of 12 months with a corresponding cost savings greater than 40% if EBW can be applied [10]. However, applying EBW to the RPV girth welds is not trivial: the largest impediment to its use is the lack of equipment capable of performing all the welds. No vendors in the United States currently have the equipment necessary to complete all the welds on an NPP RPV. The deep penetration required for thick section RPV welds in steel requires a large vacuum chamber. A conventional EBW chamber exceeding 40 feet was estimated to be needed [12]. EPRI, The Welding Institute (TWI), Nuclear Advanced Manufacturing Research Center (AMRC), along with industrial, academic, and government partners, have sought novel solutions for applying EBW to RPV girth welding. TWI and Nuclear AMRC have been developing a reduced pressure electron beam system that eliminates the need for a large vacuum chamber. This system relies upon a series of pumps and vacuum dividers between the gun and component to supply the partial vacuum environment needed for thick section welding [15]. In the United States, EPRI, Nuclear AMRC, and NuScale power have launched a project to develop a modular in-chamber EBW system in which the chamber is assembled in sections as needed to form the vacuum chamber as the RPV is fabricated [8].

Publications for reduced pressure electron beam (RPEB) of RPV steels have focused on the hardness and residual stress of weldments to support the inclusion of EBW in the R6 (UK) and API 579-1/ASME FFS-1 fitness for service procedures [1, 24, 27, 43, 44, 82, 121-124]. SA508 Grade 3 and 4N steels have been used in the evaluation of RPEB welds. Welds were made in 30 and 130 mm steel weldments and evaluated for hardness, microstructure, and residual stress. Welds were successfully made in 130 mm thick RPV steel joints at 45 kW of energy, resulting in a total heat input of 27 kJ/mm [1]. Total heat input for NG-GTAW, and NG-SAW were 287 kJ/mm and 176 kJ/mm, respectively. Hardness in the completed RPEB welds were found to be higher throughout the fusion zone (FZ) in the as-welded condition when compared to the arc welding processes. This is because of the tempering nature of the sequential layering method used during arc welding. High hardness areas in the arc welds were limited to the coarse grain heat-affected zone (CGHAZ) consisting of bainite and martensite. Residual stress measurements completed through use of neutron diffraction and deep hole drilling revealed similar peak stresses in the arc-welded and RPEB samples before and after post-weld heat treatment (PWHT). Peak stresses nearing 600 MPa were measured in the as-welded state of all welds, with peaks near 100 MPa after PWHT. A difference in the distribution of residual stresses was seen. Arc welding methods produced two areas of high stress in the FZ. Residual stress was highest near the weld reinforcement and near the root of the weld. The RPEB weld did not have peak residual stresses within the FZ; instead, it contained two parallel regions just outside the weld area in the through-thickness direction on both sides of the weld. The maximum residual stress was concentrated near the mid-thickness position of the RPEB weld [44].

In collaboration with Nuclear AMRC, NuScale Power, and other industrial partners, EPRI is demonstrating the use of a modular in-chamber electron beam welder through fabrication of a ⅔ scale small modular reactor (SMR) pressure vessel. EPRI has produced three yearly reports to date

summarizing the activities completed as part of the program on technology innovation. EBW is part of the overall effort to develop advanced technologies, including powder metallurgy – hot isostatic pressing (PM-HIP and diode laser cladding (DLC). Feasibility weld tests were conducted in a traditional electron beam (EB) chamber at Nuclear AMRC using a ProBeam K2000 system. Initial weld development on 80 mm thick SA508 Grade 3 Class 1 steel was successfully welded. Charpy impact testing of as-welded samples were poor, with lowest absorbed energy results near 40 J at the weld center line and the heat-affected zone (HAZ) [10]. Absorbed energy increased dramatically after PWHT, with weld metal having a value near 150 J compared to the parent material slightly above 180 J [10]. Once steady-state parameters were developed, the slope-in and slope-out of parameters needed to be developed as part of Year 2. Along with linearly ramping the beam current to zero mA, the lens current (focal position) was adjusted from an under-focus position to over-focus by increasing the lens current by 970 mA [7]. Beam oscillation was also adjusted to increase the amount of vertical oscillation amplitude (normal to weld direction). These changes were made to slow the collapse of the keyhole to prevent spiking defects [7]. Several mockup welds with a 80 mm joint thickness were completed, including a flange-to-shell mockup, shell-to-dome, and lower head assembly [7].

Welding of PM-HIP components is also being evaluated as part of the work by EPRI. Limited information has been published because of the tandem development effort of the PM-HIP process for large components. Initial weld trials on the PM-HIP material demonstrated the need for lower gas contents in the material. Initial heats were produced using AM-IGA which contained gas contents of 370 and 450 ppm oxygen and nitrogen in two articles fabricated as two halves of the lower head assembly [2]. These values may not represent an optimized process, because as development is ongoing. A more expensive powder fabrication process using VIM-IGA is being investigated [2]. The two lower head assemblies—articles 2 and 3, fabricated by PM-HIP—were EB welded. Evaluation of the EB weld is in progress as the adjacent surface is being machined to allow ultrasonic testing (UT) [2].

Fabrication of the MIC-EBW system is underway with the EB gun being built by Precision Technologies Inc. (PTR). Demonstration rings were welded to transfer parameters from the 80 kV EB system at Nuclear AMRC to the 150 kV system built by PTR. The rings were 1.2 m × 127 mm thick SA508 rings provided by EPRI. A series of welds was made using the new gun, with final parameters of 150 kV, 185 mA, 1.5 mm/sec travel speed, with an elliptical oscillation of 1 × 3 mm @ 300 Hz, with focus set at the outer diameter of the ring. A full-diameter ring weld was completed. A beam instability occurred over the first 200° of the ring, with UT indications becoming more significant as the weld progressed. The first 200° was reported as partial penetration. The weld after a restart from 200° to 360° was free of UT indications [2].

As an additional enhancement and benefit to the use of EBW for of RPV steels, EPRI is investigating the use of a full solution heat treatment to eliminate the weld and to achieve mechanical properties consistent with that of the base metal [2]. Sheffield Forgemasters evaluated two plates of EB-welded SA508 Grade 3 Class 1 by using five homogenizing heat treatments from 875°C and fixed hardening and tempering temperatures of 870°C for 3.5 hr and 640°C for 3.5 hr [2]. Comparisons of the tensile properties and Charpy impact toughness of the full solution treated samples were made to the base material. HAZ properties were affected to a greater extent than the FZ. At temperatures above 900°C, the absorbed energy dropped linearly as homogenizing temperature increased [2]. The 875°C homogenizing temperature was determined to be the optimum setting [2].

The ASME BPVC currently permits EBW of RPVs with PWHT. Major gaps exist in the development of EBW of PM-HIP materials. Further development of reducing residual gas content by cleaner powder manufacturing methods such as VIM-IGA is needed. EBW of high residual gas containing PM-HIP materials has proven to be problematic because of unstable weld characteristics. Specification limits with regard to gas content and chemical composition are needed for EBW. The weldability of PM-HIP

materials produced by VIM-IGA will require evaluation and comparison to wrought material in terms of fracture toughness, residual stress, stress corrosion cracking (SCC), and irradiation damage. Weld repair techniques, including filler metal additions (if needed) by EBW or conventional arc processes have not been discussed. Weld repairs may be completed according to existing allowances of the ASME BPVC. The benefits of full solution heat treatment could be negatively affected by the repair method chosen and unmatched filler metals. If these issues are not addressed, they have the potential to adversely affect material properties.

EBW can significantly help reduce the cost and lead time to produce components for NPPs. The advantages of EBW suit the needs of thick section RPV weldments if the vendor and equipment capability can be developed in the United States. Further work in PM-HIP material development, including applicable residual gas content limits, chemistry limits, and residual stress, effects are needed. The irradiation behavior of thick section EB-welded wrought and PM-HIP materials would prove the viability of EBW for pressure vessels intended for use as RPVs.

REFERENCES

1. Rathod, D.W., et al., "Residual stresses in arc and electron-beam welds in 130 mm thick SA508 steel: Part 1-Manufacture". *International Journal of Pressure Vessels and Piping*, 2019. 172: p. 313-328.
2. Gandy, D.A., M., *Program on Technology Innovation: Small Modular Reactor Vessel Manufacture and Fabrication: Phase 1 Progress (Year 3)*. 2021.
3. Schultz, H., *Electron beam welding*. Vol. 93. 1993: Woodhead Publishing.
4. Volker Adam, U.C., H.C. Dietrich v. Dobeneck, Thomas Krussel, Thorsten Lower, *The Fundamentals of a Fascinating Technology*. Vol. 1 Basic Principles. 2011, Germany: pro-beam AG & Co. KGaA.
5. Węglowski, M.S., S. Błacha, and A. Phillips, "Electron beam welding–techniques and trends–review". *Vacuum*, 2016. 130: p. 72-92.
6. Gandy, D., *Factory Fabrication of Small Modular Reactor Vessel Assemblies*, in *NRC RIC: Use of Advanced Manufacturing Technology for Power Reactors*. 2019, EPRI. p. 16.
7. Gandy D., A.M., *Small Modular Reactor Vessel Manufacture and Fabrication - Phase 1 - Progress (Year 2)*. 2020, Electric Power Research Institute. p. 146.
8. Gandy D., A.M., *Program on Technology Innovation: Modular In Chamber Electron Beam Welding: Phase 1 - System Design and EBW Equipment Production*. 2020, Electric Power Research Institute. p. 98.
9. Gandy D., A.M., Bridger K., *Establishing Modular In-Chamber Electron Beam Welding Capability in the USA*, in *AMM Newsletter*. 2020. p. 3.
10. Gandy D., S.C., *Small Modular Reactor Vessel Manufacture and Fabrication - Phase 1 - Progress*. 2019, Electric Power Research Institute. p. 122.
11. Patterson, T., et al., "A review of high energy density beam processes for welding and additive manufacturing applications". *Welding in the World*, 2021. 65(7): p. 1235-1306.
12. Gandy, D. *Establishing Modular In-Chamber EB Welding (MIC-EBW) Capability in USA*. in *DOE AMM Technical Review Webinar*. 2019. energy.gov.
13. *PTR-EB-Welding-Sytems-Brochure-Set-2017*. 2017; Available from: https://www.ptreb.com/sites/default/files/papers/PTR-EB-Welding-Systems-Brochure-Set-2017.pdf.
14. Steigerwald, K., et al., *An international history of electron beam welding*. 2007: Pro-beam.

15. American Welding Society, *Recommended practices for electron beam welding and allied processes*. 2013, American National Standards Institute, Technical Activities Committee.
16. Blakeley, P., "Electron beam welding: some questions answered". *Welding Institute Research Bulletin*, 1983. 24(5): p. p145.
17. Olson, D.L., et al., *Welding, Brazing and Soldering*, ed. D.L. Olson, et al. 1993: ASM International.
18. del Pozo, S., C. Ribton, and D.R. Smith. *Characterisation of an RF excited argon plasma cathode electron beam gun*. in *2014 Tenth International Vacuum Electron Sources Conference (IVESC)*. 2014. IEEE.
19. *Plasma Cathode Electron Gun*. 2020 [cited 2020 2020-03-25]; TWI Core Research]. Available from: https://www.twi-global.com/what-we-do/research-and-technology/current-research-programmes/twi-core-research/plasma-cathode-electron-gun.
20. Accredited Standards Committee Z, S.i.W., Cutting, and S. American Welding, *Safety in welding, cutting, and allied processes*. 1994, Miami, Fla.: The Society.
21. American National Standards, I. and S. Health Physics, *American national standard for general radiation safety : installations using non-medical x-ray and sealed gamma-ray sources, energies up to 10 MeV*. 1993, New York: American National Standards Institute.
22. Ayres, K.R., et al. *Development of Reduced Pressure Electron Beam Welding Process for Thick Section Pressure Vessel Welds*. in *ASME 2010 Pressure Vessels and Piping Division/K-PVP Conference*. 2010.
23. Sanderson, A., "Four Decades of Electron Beam Development at TWI". *Welding in the World*, 2007. 51(1-2): p. 37-49.
24. Balakrishnan, J., et al., "Residual stress distributions in arc, laser and electron-beam welds in 30 mm thick SA508 steel: A cross-process comparison". *International Journal of Pressure Vessels and Piping*, 2018. 162: p. 59-70.
25. Schubert, D.G. *Electron Beam Welding–Process, Applications and Equipment*. in *Proceedings of the IIW International Conference on Advances in Welding and Allied Technologies*. 2009.
26. Cottrell, C., "Electron beam welding—a critical review". *Materials & design*, 1985. 6(6): p. 285-291.
27. Francis, J.A., et al., "Vacuum laser welding of SA508 steel". *Journal of Materials Processing Technology*, 2019. 274: p. 116269.
28. Rai, R., et al., "Heat Transfer and Fluid Flow during Electron Beam Welding of 304L Stainless Steel Alloy". *Welding Journal*, 2009. 88(3): p. 54s-61s.
29. Sun, Z. and R. Karppi, "The application of electron beam welding for the joining of dissimilar metals: An overview". *Journal of Materials Processing Technology*, 1996. 59(3): p. 257-267.
30. Mendez, P.F. and T.W. Eagar, "Welding processes for aeronautics". *Advanced Materials & Processes*, 2001. 159(5): p. 39-43.
31. Clauß, U. *Electron Beam Technology The Advanced Tool in Production*. in *7th International EWI/TWI Seminar on Joining Aerospace Materials*. 2014. Boeing Longacres Customer Center: Pro-Beam.
32. Powers, J., "Electron-Beam Welding - Application and Equipment Improvements". *Welding Journal*, 1984. 63(5): p. 39-40.
33. Kautz, D.H., PW; Milewski, JO; Powers, DE; Zacharias, KJ;, *Welding Handbook, Vol. 3, Welding Processes, Part 2 - Ninth Edition*. 9th ed. Vol. 3. 2007, Miami: AWS.
34. Powers, D.E., "Electron Beam Welding in the United States". *Welding Journal*, 2011. 90(1): p. 30-34.
35. Stecker, S., et al., "Advanced electron beam free form fabrication methods & technology". *AWS welding show', Atlanta, GA*, 2006: p. 35-46.
36. Galarraga, H., et al., "Effects of the microstructure and porosity on properties of Ti-6Al-4V ELI alloy fabricated by electron beam melting (EBM)". *Additive Manufacturing*, 2016. 10: p. 47-57.

37. Sames, W.J., et al., “The metallurgy and processing science of metal additive manufacturing”. *International Materials Reviews*, 2016. 61(5): p. 315-360.
38. Hershcovitch, A. and A. Team, “Air boring and nonvacuum electron beam welding with a plasma window”. *Physics of plasmas*, 2005. 12(5): p. 057102.
39. Hershcovitch, A., “High-Pressure Arcs as Vacuum-Atmosphere Interface and Plasma Lens for Nonvacuum Electron-Beam Welding Machines, Electron-Beam Melting, and Nonvacuum Ion Material Modification”. *Journal of Applied Physics*, 1995. 78(9): p. 5283-5288.
40. Hershcovitch, A. and M. Furey, *Non-Vacuum Electron Beam Welding*. 2007, Brookhaven National Laboratory (BNL), Upton, NY (United States).
41. *Electron Beam Welding in the Nuclear Industry - Cambridge Vacuum Engineering*. 2021; Available from: https://camvaceng.com/case-study/electron-beam-welding-in-the-nuclear-industry/.
42. *Ebflow - Cambridge Vacuum Engineering*. 2021; Available from: https://camvaceng.com/machine/ebflow/.
43. Vasileiou, A.N., et al., “The impact of transformation plasticity on the electron beam welding of thick-section ferritic steel components”. *Nuclear Engineering and Design*, 2017. 323: p. 309-316.
44. Vasileiou, A.N., et al., “Residual stresses in arc and electron-beam welds in 130 mm thick SA508 steel: Part 2-measurements”. *International Journal of Pressure Vessels and Piping*, 2019. 172: p. 379-390.
45. *Press release: £10m nuclear manufacturing project “road-tests” electron beam welding technology Ebflow*. 2021; Available from: https://www.agilitypr.news/Press-release-£10m-nuclear-manufacturin-12410.
46. Barreda, J., et al., “Electron beam welded high thickness Ti6Al4V plates using filler metal of similar and different composition to the base plate”. *Vacuum*, 2001. 62(2-3): p. 143-150.
47. Ruge, J., et al. *Welding of dissimilar metals by using the method of electron beam welding with filler wire*. in *Electron and laser beam welding. International Conference. 4*. 1986.
48. Jones, L.P., et al., “Towards advanced welding methods for the ITER vacuum vessel sectors”. *Fusion engineering and design*, 2003. 69(1-4): p. 215-220.
49. Schuchardt, T., S. Mueller, and K. Dilger, “Remanufacturing of die casting dies made of hot-work steels by using the wire-based electron-beam welding with an in situ heat treatment”. *Welding in the World*, 2019. 63(6): p. 1669-1679.
50. ASME, *ASME Boiler & Pressure Vessel Code*, in *Section IX Qualification Standard for Welding, Brazing, and Fusing Procedures*. 2021.
51. Kaur, A., C. Ribton, and W. Balachandaran, “Electron beam characterisation methods and devices for welding equipment”. *Journal of Materials Processing Technology*, 2015. 221: p. 225-232.
52. Elmer, J., T. Palmer, and A. Teruya, *An Overview of the Enhanced Modified Faraday Cup (EMFC) Electron Beam Power Density Distribution Diagnostic*. 2011, Lawrence Livermore National Lab.(LLNL), Livermore, CA (United States).
53. Faraone, K.M., *Electron Beam Welding of Stainless Steels*, in *Unpublished raw data*. 2012.
54. Elmer, J., et al., *Introduction to high energy density electron and laser beam welding*. 2009, Lawrence Livermore National Lab.(LLNL), Livermore, CA (United States).
55. Liebig, C., J. Fath, and T. Löwer, “Electron beam characterizing and its relevance for production”. *Electrotechnica & Electronica*, 2016. 51(5-6): p. 166-169.
56. Elmer, J.W., et al., *Transferring Electron Beam Welding Parameters Between Different Machines and Facilities Using Advanced Diagnostics*. Conference: Presented at: 57th Annual Assembly of the International Institute of Welding, Osaka, Japan, Jul 11 - Jul 16, 2004. 2004: ; Lawrence Livermore National Lab. (LLNL), Livermore, CA (United States). Medium: ED; Size: PDF-file: 33 pages; size: 2.9 Mbytes.

57. Elmer, J., *Characterization of defocused electron beams and welds in stainless steel and refractory metals using the enhanced modified faraday cup diagnostic*. 2009, Lawrence Livermore National Lab.(LLNL), Livermore, CA (United States).
58. Clauss, U., *Repeatable, precise and efficient - the Electron beam as universal tool for customized welding applications*, in *IIW International Conference*. 2008: India.
59. Wiednig, C., N. Enzinger, and C. Beal, *Considerations for sound parameter studies in electron beam welding of thick walled components*, in *Cracking Phenomena in Welds IV*. 2016, Springer. p. 87-99.
60. Kannengießer, T., et al., "The influence of local weld deformation on hot cracking susceptibility". 2002.
61. Blakeley, P.J. and A. Sanderson, "The Origin and Effects of Magnetic-Fields in Electron-Beam Welding". *Welding Journal*, 1984. 63(1): p. 42-49.
62. Rugh, J.L., G. *The use of Electron Beam Welding in Turbomachinery Manufacturing*. [cited 2019 November 19, 2019]; Available from: https://ptreb.com/electron-beam-welding-information/technical-papers/use-electron-beam-welding-turbomachinery-manufacturing.
63. "Evaluating EBW: A UK project is looking into electron beam welding in the nuclear industry.(MANUFACTURING)". *Nuclear Engineering International*, 2019. 64(774): p. 17.
64. Wei, P.S. and T.W. Lii, "Electron-Beam Deflection When Welding Dissimilar Metals". *Journal of Heat Transfer-Transactions of the Asme*, 1990. 112(3): p. 714-720.
65. Tomita, Y., H. Mabuchi, and K. Koyama, "Improving electron beam weldability of heavy steel plates for PWR-steam generator". *Journal of nuclear science and technology*, 1996. 33(11): p. 869-878.
66. Cross, C.E., *On the Origin of Weld Solidification Cracking*, in *Hot Cracking Phenomena in Welds*, T. Böllinghaus and H. Herold, Editors. 2005, Springer Berlin Heidelberg: Berlin, Heidelberg. p. 3-18.
67. Lacki, P., K. Adamus, and P. Wieczorek, "Theoretical and experimental analysis of thermo-mechanical phenomena during electron beam welding process". *Computational materials science*, 2014. 94: p. 17-26.
68. David, S.A. and J.M. Vitek, "Correlation between Solidification Parameters and Weld Microstructures". *International Materials Reviews*, 1989. 34(5): p. 213-245.
69. Zacharia, T., "Dynamic Stresses in Weld Metal Hot Cracking". *Welding Journal*, 1994. 73(7): p. S164-S172.
70. Herold, H. and T. Böllinghaus, *Hot Cracking Phenomena in Welds*. 2005: Springer.
71. Böllinghaus, T., et al., *Hot cracking phenomena in welds II*. 2008: Springer Science & Business Media.
72. Lippold, J., T. Böllinghaus, and C.E. Cross, *Hot cracking phenomena in welds III*. 2011: Springer Science & Business Media.
73. Kannengiesser, T. and T. Boellinghaus, "Hot cracking tests-an overview of present technologies and applications". *Welding in the World*, 2014. 58(3): p. 397-421.
74. Kou, S., "Solidification and liquation cracking issues in welding". *Jom-Journal of the Minerals Metals & Materials Society*, 2003. 55(6): p. 37-42.
75. Chen, F.R., et al., "Effects of electron beam local post-weld heat-treatment on the microstructure and properties of 30CrMnSiNi2A steel welded joints". *Journal of Materials Processing Technology*, 2002. 129(1-3): p. 412-417.
76. Sebastiano, T., N. Fabio, and D. Marcello, "Electron beam welding and post-weld treatments of steels". *Journal of materials science letters*, 1996. 15(10): p. 827-830.
77. Norris, J.T., et al., *Evaluation of weld porosity in laser beam seam welds: optimizing continuous wave and square wave modulated processes*. 2007, Sandia National Laboratories.
78. Seifert, H.P. and S. Ritter, "Stress corrosion cracking of low-alloy reactor pressure vessel steels under boiling water reactor conditions". *Journal of Nuclear Materials*, 2008. 372(1): p. 114-131.

79. Seifert, H.P., et al., "Environmentally-assisted cracking behaviour in the transition region of an Alloy182/SA 508 Cl.2 dissimilar metal weld joint in simulated boiling water reactor normal water chemistry environment". *Journal of Nuclear Materials*, 2008. 378(2): p. 197-210.
80. Odette, G.R. and G.E. Lucas, "Embrittlement of nuclear reactor pressure vessels". *Jom-Journal of the Minerals Metals & Materials Society*, 2001. 53(7): p. 18-22.
81. Odette, G.R., "On the Dominant Mechanism of Irradiation Embrittlement of Reactor Pressure-Vessel Steels". *Scripta metallurgica*, 1983. 17(10): p. 1183-1188.
82. Francis, J., et al., "Design and manufacture of industrially representative weld mock-ups for the quantification of residual stresses in a nuclear pressure vessel steel". *Mater Res Proc (ICRS-10)*, 2016. 2: p. 581-586.
83. Eason, E.D., J.E. Wright, and G. Odette, *Improved embrittlement correlations for reactor pressure vessel steels*. 1998: Division of Engineering Technology, Office of Nuclear Regulatory Research ….
84. Hawthorne, J. and L. Steele, *Metallurgical variables as possible factors controlling irradiation response of structural steels*, in *Effects of Radiation on Structural Metals*. 1967, ASTM International.
85. Canonico, D.A., *Significance of reheat cracks to the integrity of pressure vessels for light-water reactors(ORNL/NUREG-15)*. 1977.
86. ASME, *ASME Boiler & Pressure Vessel Code*, in *Section III Rules for Construction of Nuclear Facility Components*. 2021.
87. Lindgren, E., et al., "ASM Handbook, Volume 17, Nondestructive Evaluation of Materials". *ASM International*, 2018.
88. *Phased Array Tutorial - What are the advantages?* 2022; Available from: https://www.olympus-ims.com/en/ndt-tutorials/intro/advantages/.
89. *Introduction to Time-of-Flight Diffraction (TOFD) for Weld Inspection*. [cited 2022 3-9-2022]; Available from: https://www.olympus-ims.com/en/applications/introduction-to-time-of-flight-diffraction-for-weld-inspection/.
90. Boellinghaus, T., J.C. Lippold, and C.E. Cross, *Cracking phenomena in welds IV*. 2016: Springer.
91. Ueda, Y., Y.C. Kim, and A. Umekuni, "Measurement of Three-dimensional Welding Residual Stresses due to Electron Beam Welding (Welding Mechanics, Strength & Design)". *Transactions of JWRI*, 1986. 15(1): p. 125-131.
92. Kou, S., "Welding metallurgy". *New Jersey, USA*, 2003: p. 431-446.
93. Suutala, N., "Effect of Solidification Conditions on the Solidification Mode in Austenitic Stainless-Steels". *Metallurgical Transactions a-Physical Metallurgy and Materials Science*, 1983. 14(2): p. 191-197.
94. Lippold, J. and W. SAVAGE, "Solidification of Austenitic Stainless Steel Weldments: Part 1 A Proposed Mechanism". *Welding Journal*, 1979. 59: p. 362s-374s.
95. Lippold, J. and W. Savage, "Solidification of austenitic stainless steel weldments: Part 2—The effect of alloy composition on ferrite morphology". *Welding Journal*, 1980. 59(2): p. 48s-58s.
96. Lippold, J. and W. Savage, "Solidification of austenitic stainless steel weldments: Part III--the effect of solidification behavior on hot cracking susceptibility". *WELDING J.*, 1982. 61(12): p. 388.
97. Vitek, J.M., A. Dasgupta, and S.A. David, "Microstructural Modification of Austenitic Stainless-Steels by Rapid Solidification". *Metallurgical Transactions a-Physical Metallurgy and Materials Science*, 1983. 14(9): p. 1833-1841.
98. Lippold, J.C., "Centerline Cracking in Deep Penetration Electron-Beam Welds in Type-304l Stainless-Steel". *Welding Journal*, 1985. 64(5): p. S127-S136.
99. Elmer, J.W., S.M. Allen, and T.W. Eagar, "Microstructural Development during Solidification of Stainless-Steel Alloys". *Metallurgical Transactions a-Physical Metallurgy and Materials Science*, 1989. 20(10): p. 2117-2131.

100. Lippold, J. and D. Kotecki, *Welding metallurgy and weldability of stainless steels*. 2005, John Wiley & Sons, New York.
101. Lienert, T.J. and J.C. Lippold, "Improved weldability diagram for pulsed laser welded austenitic stainless steels". *Science and Technology of Welding and Joining*, 2003. 8(1): p. 1-9.
102. Rodelas, J., *Laser Welding for High Reliability High Consequence Applications*. 2018, Sandia National Lab.(SNL-NM), Albuquerque, NM (United States).
103. McCabe, D.E., *Initial Evaluation of the Heat-Affected Zone, Local Embrittlement Phenomenon as it Applies to Nuclear Reactor Vessels*. 1999, Oak Ridge National Lab., TN (US): United States. p. 30 pages, https://www.osti.gov/biblio/12551.
104. Suzuki, K., et al., "Application of high strength MnMoNi steel to pressure vessels for nuclear power plant". *Nuclear Engineering and Design*, 2001. 206(2-3): p. 261-277.
105. Lee, K.H., et al., "Effects of Tempering and Pwht on Microstructures and Mechanical Properties of Sa508 Gr.4n Steel". *Nuclear Engineering and Technology*, 2014. 46(3): p. 413-422.
106. Kim, M.-C., et al., "Comparison of fracture properties in SA508 Gr. 3 and Gr. 4N high strength low alloy steels for advanced pressure vessel materials". *International Journal of Pressure Vessels and Piping*, 2015. 131: p. 60-66.
107. Natesan, K., et al., *Preliminary materials selection issues for the next generation nuclear plant reactor pressure vessel*. 2007, Argonne National Lab.(ANL), Argonne, IL (United States).
108. ASME, *ASME Boiler & Pressure Vessel Code*, in *Section II A Ferrous Material Specifications (SA451 to End)*. 2021.
109. Bhadeshia, H. and R. Honeycombe, *Steels: microstructure and properties*. 2017: Butterworth-Heinemann.
110. Kim, S., et al., "Effects of alloying elements on mechanical and fracture properties of base metals and simulated heat-affected zones of SA 508 steels". *Metallurgical and Materials Transactions A*, 2001. 32(4): p. 903-911.
111. Lundin, C. and S. Mohammed, *Effect of welding conditions on transformation and properties of heat-affected zones in LWR (light-water reactor) vessel steels*. 1990, Nuclear Regulatory Commission, Washington, DC (USA). Div. of Engineering ….
112. Francis, J.A., H.K.D.H. Bhadeshia, and P.J. Withers, "Welding residual stresses in ferritic power plant steels". *Materials Science and Technology*, 2007. 23(9): p. 1009-1020.
113. Mark, A., et al., "On the evolution of local material properties and residual stress in a three-pass SA508 steel weld". *Acta Materialia*, 2012. 60(8): p. 3268-3278.
114. English, C.A., et al., *Comparison of Effects of Thermal Aging, Irradiation, and Thermal Annealing on the Propensity for Temper Embrittlement on an RPV Submerged-Arc Weld HAZ(ORNL/NRC/LTR-01/07)*. 2001.
115. Vasileiou, A.N., et al., "Development of microstructure and residual stresses in electron beam welds in low alloy pressure vessel steels". *Materials & design*, 2021: p. 109924.
116. Katsuyama, J., et al., "Mechanical and microstructural characterization of heat-affected zone materials of reactor pressure vessel". *Journal of pressure vessel technology*, 2012. 134(3).
117. Elliott, S., "Electron-Beam Welding of C/Mn-Steels - Toughness and Fatigue Properties". *Welding Journal*, 1984. 63(1): p. S8-S16.
118. Mercure, M. *RPEB Welding Technology to be Used at Dogger Bank*. Wind News 2021 [cited 2021 2021-07-28]; Available from: https://nawindpower.com/dogger-bank-looks-to-decrease-om-time-with-rpeb-welding-technology.
119. Sanderson, A., C.S. Punshon, and J.D. Russell, "Advanced welding processes for fusion reactor fabrication". *Fusion engineering and design*, 2000. 49-50: p. 77-87.
120. *The Canister Laboratory*. 2021; Available from: http://www.skb.com/research-and-technology/laboratories/the-canister-laboratory/.
121. Anis, M., et al., "Electron Beam Welding of Large Components for The Nuclear Industry". *MATEC Web of Conferences*, 2019. 269: p. 02009.

122. Baufeld, B., J. Priest, and T. Dutilleul, “EBW of nuclear pressure vessel steel”. *Elektronika ir Elektrotechnika*, 2018. 53: p. 136.
123. Yano, Y., et al., “Weldability of dissimilar joint between PNC-FMS and Type 316 steel under electron beam welding”. *Journal of nuclear science and technology*, 2015. 52(4): p. 568-579.
124. Abdolvand, H., et al. *On the stress development in SA508 autogenous weld*. in *Materials Science Forum*. 2014. Trans Tech Publ.
125. Smith, D., et al., “Measured and predicted residual stresses in thick section electron beam welded steels”. *International Journal of Pressure Vessels and Piping*, 2014. 120: p. 66-79.
126. Duffy, C.J., “Modelling the electron beam welding of nuclear reactor pressure vessel steel”. *University of Cambridge*, 2014.
127. Smith, M.C., et al. *A Review of Welding Research Within the New Nuclear Manufacturing (NNUMAN) Programme*. in *ASME 2017 Pressure Vessels and Piping Conference*. 2017.
128. Murakawa, H., et al., “Effect of low transformation temperature weld filler metal on welding residual stress”. *Science and Technology of Welding and Joining*, 2010. 15(5): p. 393-399.
129. Kim, S., et al., “Correlation of the microstructure and fracture toughness of the heat-affected zones of an SA 508 steel”. *Metallurgical and Materials Transactions a-Physical Metallurgy and Materials Science*, 2000. 31(4): p. 1107-1119.
130. Bokuchava, G. and P. Petrov, “Study of Residual Stresses and Microstructural Changes in Charpy Test Specimens Reconstituted by Various Welding Techniques”. *Metals*, 2020. 10(5): p. 632.
131. Seifert, H.P., et al., “Stress Corrosion Cracking Behavior in the Transition Region of Alloy 182/Low-Alloy Reactor Pressure Vessel Steel Dissimilar Metal Weld Joints in Light Water Reactor Environments”. *Corrosion*, 2015. 71(4): p. 433-454.

Impending Publication - Review of AMT and Qualification Processes for LWRs - EBW DATE May 25, 2022

DISTRIBUTION:
MYoo, RES/DE/CIB
MHiser, RES/DE/CMB
LLund, RES/DE
JMcKirgan, RES/DE

ADAMS Accession No.: 22143A927; ML22143A928

OFFICE	RES/DE/CIB	RES/DE/CMB	RES/DE	
NAME	MYoo *MY*	MHiser *MH*	LLund JMcKirgan for *JM*	
DATE	May 24, 2022	May 25, 2022	May 25, 2022	

OFFICIAL RECORD COPY